

## 13. SITE 1242<sup>1</sup>

Shipboard Scientific Party<sup>2</sup>

### INTRODUCTION

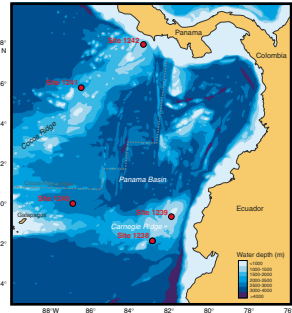
Site 1242 (proposed Site COC-4A) is located at 7°51.352'N, 83°36.418'W in a shallow basin (1364 m water depth) within the structurally complex intersection between Cocos Ridge and the Mesoamerican Trench (Fig. F1). The site is in a graben on the crest of the Cocos Ridge (Fig. F2), which is in turn crosscut by younger normal faults striking roughly east-northeast (von Huene et al., 2000). The crust underlying the site was probably formed at the Galapagos hotspot, roughly coeval with the formation of seafloor crust ~15–16 m.y. ago at the Cocos-Nazca Rise (Hey et al., 1977) (Fig. F3).

The seismic profile at Site 1242 (Fig. F4) documents the hemipelagic fill of a small subsiding basin ~460 m thick. Flat-lying reflectors mark the upper part of the sediment sequence. The geometry of seismic reflections is complex and is clearly affected by faulting in the lowermost part of the profile. At least one hiatus is likely in the deeper section. Because of this complexity, the drilling target here is limited to a penetration of 250 meters below seafloor (mbsf). Dominant sediments in the region are hemipelagic clay, with occasional ash layers that may record the history of volcanism in Central America (Ledbetter, 1985).

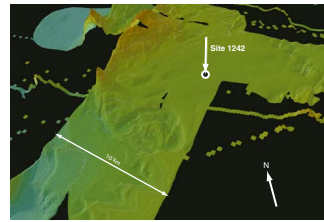
At present, Site 1242 is located under the warm, relatively low-salinity waters of the intertropical convergence in the Panama Basin (Ocean Climate Laboratory, 1999) (Fig. F5). Nutrients at the sea surface are low, and biological productivity is relatively low for a continental margin setting (Fig. F6).

A tectonic backtrack path on the Cocos plate (Pisias et al., 1995) moves Site 1242 southward and to the west relative to South America. The site was probably located close to the equator and at shallower depths early in its history, at a position near the Galapagos hotspot. Site 1242 is likely to record changes in the pool of warm and relatively low-salinity surface waters north of Panama Basin that are associated with

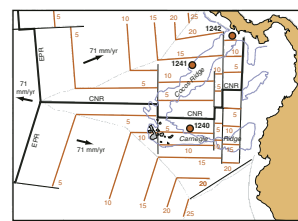
**F1.** Sites 1238–1242 and regional bathymetry, p. 19.



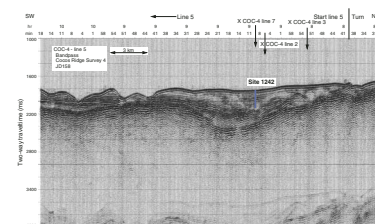
**F2.** High-resolution swath bathymetry, p. 20.



**F3.** Primary tectonic features of the Panama Basin, p. 21.



**F4.** Seismic profile at Site 1242, p. 22.



<sup>1</sup>Examples of how to reference the whole or part of this volume.

<sup>2</sup>Shipboard Scientific Party addresses.

the heavy rainfall under the intertropical convergence. The Pleistocene to Pliocene sediments will also provide evidence for variations in upwelling and biological production on the Costa Rica margin.

Plate tectonic backtrack locations (see Fig. F6, p. 80, in the “Leg 202 Summary” chapter) can be used to predict general features of oceanographic change at Site 1242, under the assumptions that overall conditions in the region remain constant and that the only change in the system is drift of the site location relative to this fixed oceanographic background (Fig. F7). In this analysis, we ignore changes in the position of the continental margin through time, which may be significant in the region of northern South America and the Central American Isthmus. Sampling of modern oceanographic atlas values at the paleosite locations suggests that from 13 m.y. ago, sea-surface temperatures at Site 1242 would have been significantly ( $\sim 5^{\circ}\text{C}$ ) cooler and saltier (by 2 units) than today, because at that time, the site was within the equatorial upwelling system and the South Equatorial Current. The pycnocline is relatively stable along the backtrack path. Silicate concentrations are substantially lower than present values in the interval representing 4–6 Ma but return to modern values as the backtrack path enters the equatorial upwelling system ( $>10$  Ma). The nutrients nitrate and phosphate are relatively stable along the backtrack path for the past  $\sim 6$ –8 m.y., suggesting that younger sediments may favor biogenic silica relative to older sediments, perhaps because of the recent proximity to the Mesoamerican coast. Significant deviations from these general trends, if detected in the sediment cores, would imply changes in regional oceanographic or climatic conditions, or errors in the tectonic backtrack or age models.

The bottom water chemistry at Site 1242 (Fig. F8) is influenced by the lower reaches of an anomalously thick oxygen minimum zone between North Pacific Deep Water and remnants of North Pacific Intermediate Water (Tsuchiya and Talley, 1998). These waters of North Pacific origin are relatively depleted in oxygen and  $\delta^{13}\text{C}$  and enriched in nutrients (Kroopnick, 1974). Moreover, the high organic carbon flux on the Central American margin and relatively little mixing with low-salinity surface waters, due to the formation of a strong pycnocline, lead to one of the deepest and strongest oxygen minimum zones in the world. Thus, this site offers an excellent opportunity to assess the relevance of nitrification vs. denitrification processes in a region that may have potentially contributed to global nutrient budgets (Ganeshram et al., 1995).

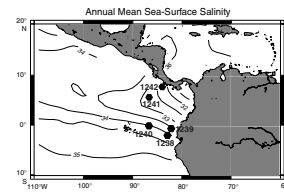
Given the relatively shallow depth of Site 1242 well above the regional lysocline, variations in carbonate dissolution are mainly controlled by rates of carbonate rain from surface waters and organic carbon degradation within the sediments.

The primary objective at Site 1242 is to provide a continuous Pliocene to Holocene sediment record to assess the variability of upper-ocean processes at high resolution, including biogeochemical cycles and biota as well as variations in the Atlantic to Pacific salinity contrast and dynamics of the intertropical convergence associated with late Neogene climate changes.

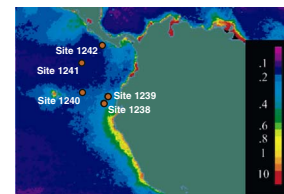
## OPERATIONS

The 209-nmi transit to Site 1242 (proposed Site COC-4A) required 18 hr at an average speed of 11.6 kt. The 3.5-kHz precision depth recorder

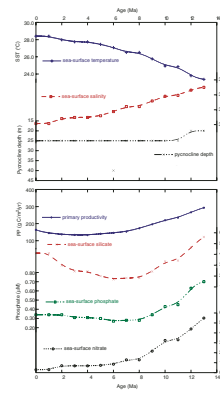
**F5.** Upper-ocean salinity, p. 23.



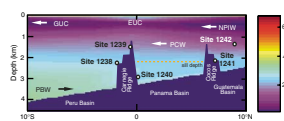
**F6.** Chlorophyll distributions in surface waters, p. 24.



**F7.** Modern ocean properties at backtrack locations of Site 1242, p. 25.



**F8.** Meridional cross section of water masses, p. 26.



(PDR) was used as a final check of site characteristics by comparison to precruise survey data. The vessel was positioning on the coordinates of Site COC-4A by 0230 hr on 26 May 2002.

### **Hole 1242A**

After the drill string was deployed and the bit placed at 1372 meters below rig floor (mbrf), Hole 1242A was initiated with the advanced piston corer (APC) at 0710 hr on 26 May. The seafloor depth estimated by the amount of recovery of the first core was 1374.8 mbrf. This was 5.6 m shallower than the corrected PDR depth of 1380.4 mbrf. Piston coring penetrated to 176.0 mbsf before it was necessary to switch to the extended core barrel (XCB). Piston coring in the hole was terminated when the Core 19H did not achieve a full stroke of the corer. No core barrels were drilled over.

The APC cores were oriented starting with Core 3H. The only operational tensor orientation tool was removed to download data during coring of Core 12H, and no orientation data are available for that core. Downhole temperature measurements were collected with the APC temperature (APCT) tool (Table T1). The nonmagnetic core barrel was deployed on even-numbered cores up to and including Core 18H. The APC cored 176.0 m and recovered 184.09 m.

XCB coring deepened the hole from 176.0 to 250.8 mbsf (the maximum allowed depth). The XCB cored 74.8 m and recovered 76.0 m. The APC/XCB cored interval was 250.8 m (recovery = 104%). The active heave compensator was online during XCB coring.

The bit was pulled free of the seafloor at 0415 hr on 27 May.

---

**T1. Operations summary, Site 1242, p. 54.**

---

### **Hole 1242B**

The vessel was offset 20 m west of Hole 1242A. Prior to coring operations in Hole 1242B, a bottom water temperature measurement was obtained with the APCT tool with the bit positioned just above the seafloor. To obtain a stratigraphic overlap with the first hole, the bit was placed at 1370 mbrf and Hole 1242B was initiated with the APC at 0548 hr. The seafloor depth derived from the recovery of the first core was 1376.6 mbrf. Piston coring combined with two 2-m drilled intervals (88.4–89.4 and 98.9–103.4 mbsf) deepened the hole to 169.9 mbsf. The temperature measurements indicate a high thermal gradient of ~20°C/100 m. Cores 4H through 17H were oriented. The nonmagnetic core barrel was deployed on odd-numbered cores up to and including Core 17H. The piston cored interval was 169.9 m with 171.96 m recovered.

Nine XCB cores deepened the hole from 169.9 to 256.0 mbsf. The XCB cored 86.1 m and recovered 87.3 m. The total cored APC/XCB interval was 250.5 m with an average recovery of 104%.

The bit was pulled free of the seafloor at 2315 hr on 27 May.

### **Hole 1242C**

The vessel was offset 20 m west of Hole 1242B. Hole 1242C was initiated with the APC at 0030 hr on 28 May. The bit was positioned at a depth of 1370 mbrf (same depth as for Hole 1242B). The seafloor depth calculated from the recovery of the mudline core was 1374.5 mbrf. Piston coring combined with drilling deepened the hole to 166.5 mbsf. Two intervals (24.0–27.5 and 46.5–48.5 mbsf) were drilled to maintain the proper overlap with the cores from the previous two holes. Cores

3H through 14H were oriented. The nonmagnetic core barrel was deployed on even-numbered cores. No core barrels were drilled over. The cored interval was 166.5 m with 171.0 m recovered (recovery = 103%).

The bit was pulled free of the seafloor at 1225 hr on 28 May.

### Hole 1242D

The vessel was offset 20 m west of Hole 1242C. Hole 1242D was initiated with the APC at 1305 hr on 28 May and drilled to 13.5 mbsf, where piston coring was started. Piston coring combined with drilling deepened the hole to 91.5 mbsf. Two intervals (0–13.5 and 51.5–53.5 mbsf) were drilled to maintain the proper overlap with the cores from the previous three holes. All cores were oriented. The nonmagnetic core barrel was deployed on odd-numbered cores. No core barrels were drilled over. The cored interval was 76.0 m with 80.2 m recovered (recovery = 106%).

The vessel was secured for transit and departed for the Balboa pilot station at 2230 hr on 28 May.

## COMPOSITE SECTION

We built a meters composite depth (mcd) scale to Section 202-1242B-27X-6 (0.00–287.38 mcd) and a splice (as defined in “**Composite Section**,” p. 4, in the “Explanatory Notes” chapter) that documents complete recovery for the upper 196.37 mcd. The splice ranges from the top of Core 202-1242A-1H to the bottom of Section 202-1242A-19H-6 (see Tables T2, T3). All APC cores can be correlated to the splice at Site 1242. One XCB core (202-1242B-19X) can also be correlated into the splice records of Site 1242. Below the splice, Cores 202-1242A-20X and 202-1242B-21X are correlated to each other. Below these cores, a floating splice exists to the bottom of the XCB section (205.68–287.38 mcd).

The mcd scale and the spliced interval (0–196.37 mcd) are based on the stratigraphic correlation of Oregon State University Fast Track magnetic susceptibility (OSUS-MS) measurements collected at 5-cm intervals (Fig. F9A, F9B, F9D, F9E, F9F, F9G; Tables T4, T5, T6, T7). The floating splice interval (205.68–287.38 mcd) is based on whole-core multisensor track magnetic susceptibility (MST-MS) data (Fig. F9H, F9I, F9J, F9K). Tie points (Table T3) were then used to construct representative spliced records for MST magnetic susceptibility, gamma ray attenuation (GRA) bulk density, and, where available, natural gamma radiation (NGR) data (Fig. F10) and for color reflectance ( $L^*$ ,  $a^*$ , and  $b^*$ ) data (Fig. F11).

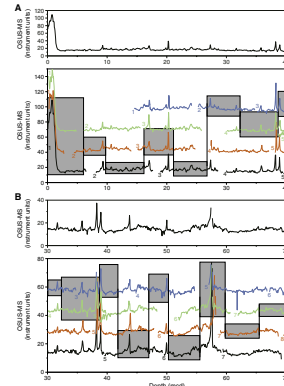
We assumed that the uppermost sediment (the “mudline”) in Core 202-1242A-1H was the sediment/water interface. A mudline was also recovered in Cores 202-1242B-1H and 202-1242C-1H. Core 202-1242A-1H is the “anchor” in the composite depth scale. From this anchor we worked downhole, correlating the stratigraphy on a core-by-core basis.

Correlation between holes in three areas of the composite section at Site 1242 is somewhat uncertain and should be confirmed by additional shore-based analyses. This also introduces uncertainty into the positioning of ties within the floating splice at Site 1242. The first problematic area is between 215 and 220 mcd and includes the tie between Section 202-1242B-21X-7, 70.0 cm, and Section 202-1242A-22X-2, 7.0 cm (Fig. F9, F9I). The second lies between 270 and 273 mcd and includes the tie between Sections 202-1242A-26X-6 and 202-1242B-26X-6 (Fig.

T2. Composite depth scale, p. 56.

T3. Splice tie points, p. 58.

F9. Magnetic susceptibility vs. mcd, p. 27.



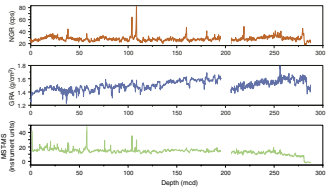
T4. OSUS-MS measurements, Hole 1242A, p. 59.

T5. OSUS-MS measurements, Hole 1242B, p. 60.

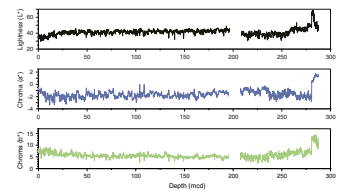
T6. OSUS-MS measurements, Hole 1242C, p. 61.

T7. OSUS-MS measurements, Hole 1242D, p. 62.

F10. Smoothed spliced records of NGR, GRA density, and MST-MS, p. 33.



F11. Smoothed spliced records of L\*, a\*, and b\*, p. 34.



**F9J, F9K).** The third area of uncertainty is from 278 to 282 mcd and includes the tie between Cores 202-1242A-27X and 202-1242B-27X (Fig. F9J, F9K).

A comparison of the mcd and mbsf depth scales (Fig. F12) shows that the mcd scale is on average 13% longer than the mbsf scale. To facilitate the calculation of mass accumulation rates (MARs), we provide corrected meters composite depth (cmcd) in Table T2 and in Table T3 for depths within the splice.

## LITHOSTRATIGRAPHY

A 287.74-mcd-thick sediment sequence was recovered at Site 1242, spanning the interval from the middle Miocene to the Holocene with a prominent hiatus from ~2.5 to 12.0 Ma that divides the sequence into two lithologic units (Table T8; Fig. F13). Unit I spans the upper Pliocene to Holocene and contains hemipelagic sediment that consists of nannofossil clays and clayey nannofossil oozes. Siliciclastic components are dominated by clay minerals with minor silt-sized minerals (Fig. F14), primarily feldspars and quartz, throughout the unit. Nannofossils are the dominant biogenic component (Fig. F15). Foraminifers are present in variable minor amounts, and the contribution of siliceous microfossils is generally low except for a distinct interval of diatom-bearing sediment between ~100 and 140 mcd. Authigenic components include micrite, dolomite, and pyrite. Volcanic glass is frequently present as a minor component of the dominant lithologies in Unit I. Forty-five ash layers are observed in Unit I, eighteen of which are correlative between holes.

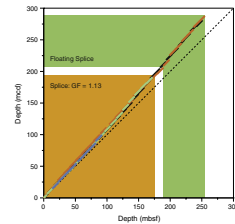
Physical properties measurements within Unit I are most strongly influenced by changes in calcium carbonate and siliciclastic content. GRA bulk density and lightness ( $L^*$ ) gradually increase downcore to ~200 mcd, consistent with gradually increasing calcium carbonate. Magnetic susceptibility (MS) shows slightly higher values in intervals containing higher siliciclastic content, and the broad pattern of NGR is similar to that of the siliciclastic content (Fig. F13).

A hiatus representing ~9.5 m.y. occurs at the base of Unit I, and an abrupt change in lithology accompanies the transition to Unit II. Lithologic Unit II contains a short sequence of middle Miocene pelagic sediment dominated by diatom-bearing nannofossil oozes. Except for minor abundances of clay minerals, Unit II lacks siliciclastic components. This interval is characterized by lower MS and higher GRA bulk density.

Site 1242 represents a homogeneous hemipelagic sedimentary record within an active continental margin setting spanning the upper Pliocene and the complete Quaternary (Unit I). Long-term decreasing biogenic contents throughout this interval may indicate increasing terrigenous supply, possibly related to the uplift of the Central American cordillera and/or long-term climate change. Rhythmic changes in MS are likely associated with relative variations in biogenic and terrigenous input, reflecting millennial- and orbital-scale changes in productivity, ocean circulation, and climate.

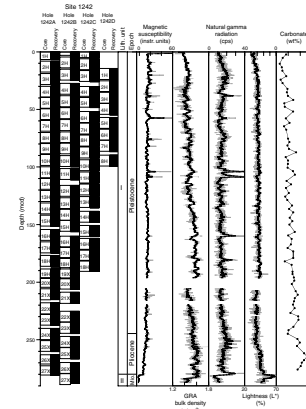
The Miocene sediments of Unit II represent pelagic conditions prior to the closure of the Isthmus of Panama. The ~9.5-m.y. hiatus between Units I and II, which spans the middle Miocene to upper Pliocene, is coeval with the closure of the Isthmus of Panama. Relatively high contents of siliceous microfossils may reflect higher Miocene productivity

**F12.** A comparison of the mbsf and mcd scales, p. 35.

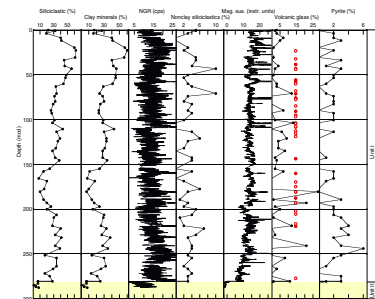


**T8.** Lithologic units, p. 63.

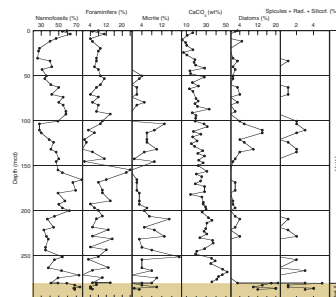
**F13.** Lithostratigraphic summary, p. 36.



**F14.** Nonbiogenic components vs. MS and NGR, Hole 1242A, p. 37.



**F15.** Biogenic components vs. CaCO<sub>3</sub>, Hole 1242A, p. 38.



associated with the tectonic backtrack of Site 1242 on the Cocos plate into the active equatorial upwelling zone.

### Description of Lithologic Units

Two lithologic units were defined at Site 1242 on the basis of visual core description, smear slide analysis, MS, color reflectance, NGR, moisture and density (MAD), and GRA bulk density measurements (Table T8; Fig. F13).

#### Unit I

Intervals: Core 202-1242A-1H through Section 27X-7; Core 202-1242B-1H through Section 27X-2, 33 cm; Cores 202-1242C-1H through 18H; and Cores 202-1242D-1H through 8H

Depths: 0–280.63 mcd; Hole 1242A: 0.00–250.71 mbsf (0.00–280.59 mcd); Hole 1242B: 0.00–247.75 mbsf (0.20–280.63 mcd); Hole 1242C: 0.00–172.19 mbsf (0.00–190.77 mcd); and Hole 1242D: 13.50–92.05 mbsf (14.55–99.75 mcd)

Age: Holocene to late Pliocene (0–2.5 Ma)

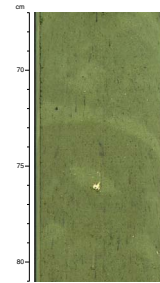
The major lithologies of Unit I are nannofossil clays and clayey nannofossil oozes. Siliciclastic components are dominated by clay minerals with minor silt-sized and rare sand-sized minerals throughout the unit (Fig. F14). Sediment color is homogeneous with only subtle gradational changes between different hues of grayish olive green. Moderate bioturbation is evidenced by the presence of mottles, burrow fills, and *Zoophycos* traces. Foraminifer fragments and spicule aggregates were commonly observed on the split core surface and sometimes as burrow infill (Fig. F16). Distinct dark layers of the pennate diatom *Ethmodiscus* are present from ~205 to 215 mcd (Fig. F17). Minor features in Unit I include wood fragments, microfaults, and a fold at ~142–143 mcd that may indicate a slump. Black coarse grains composed of pyrite-rich clay aggregates and glauconite are present toward the base of Unit I (~250 mcd).

Siliciclastic content ranges from ~20% to 60% throughout Unit I (Fig. F14). Abundance increases significantly from ~10 to 25 mcd, generally decreases downhole to ~180 mcd, and then remains comparatively low to the bottom of the unit. Coarser-grained siliciclastics, primarily feldspars and quartz, vary downcore with abundances between ~2% and 6% (Fig. F14).

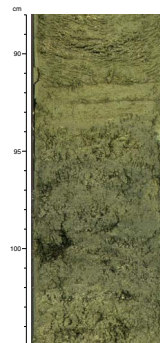
Nannofossils are the dominant biogenic component, ranging from ~30% to 70% (Fig. F15). A strong downhole decrease in the uppermost ~25 mcd corresponds to increasing siliciclastic content. Farther down-hole, nannofossil abundance generally increases, with broad minima paralleling the increases in micrite. Foraminifers are present in variable minor amounts, primarily in the range of ~4%–12%, except for maximum values of up to >20% near ~155 mcd. Diatom contents are generally only a few percent but reach ~10% between ~100 and 140 mcd. In this interval, radiolarians, silicoflagellates, and spicules also approach a maximum of ~2% but are present otherwise in very small amounts only (Fig. F15).

Authigenic components include micrite, dolomite, and pyrite. Micrite abundance generally increases downhole with two broad maxima, one between ~100 and 150 mcd and a second between ~210 and 250 mcd (Fig. F15). Dolomite is present as a minor component (~4%–9%) in a short interval from ~264 to 275 mcd. Pyrite abundance varies

F16. Unit I major lithology, p. 39.



F17. Pennate diatom *Ethmodiscus*, p. 40.



throughout the unit, with maximum values between ~200 and 250 mcd.

The only notable minor lithologies within Unit I are volcanic ash layers. Forty-five ash layers are observed in Unit I, eighteen of which are correlative between holes (Table T9). The ashes range from light gray to brownish gray and black and are usually characterized by sharp basal contacts and diffuse upper contacts (Fig. F18). Ashes at Site 1242 contain mostly silt- and sand-sized clear platy and vesicular glass, and accessory minerals include plagioclase feldspar, orthopyroxene, pyrite, quartz, hornblende, and biotite. Ash layers are present throughout the uppermost ~278 mcd, with high-frequency intervals between ~30 and 120 mcd and ~160 and 210 mcd. In addition to these discrete layers, volcanic glass often is present as a minor component (~2%–10%) of the dominant lithology throughout Unit I (Fig. F14).

Color reflectance measurements from Unit I plot in the “green” ( $a^* < 0$ ) domain of the  $a^*$ - $b^*$  color plane (Fig. F19). Lightness increases down-hole throughout the unit (Fig. F13), generally paralleling the decreasing siliciclastic and increasing calcium carbonate concentrations. Magnetic susceptibility is high at the top of Unit I (>40 instrument units). Below a sharp drop at ~1.5 mcd, MS averages ~10 to 15 instrument units, with pronounced variability on meter to decimeter scales (Fig. F13). Average values decrease below ~150 mcd, coinciding with increasing calcium carbonate concentrations (Fig. F15). Distinct maxima of >25 instrument units mostly reflect volcanic ash layers. Changes in NGR seem to parallel changes in siliciclastic content, particularly in the uppermost ~25 mcd (Fig. F13). GRA bulk density generally increases downhole (Fig. F13), reflecting the gradual increase in calcium carbonate and the simultaneous decrease in siliciclastic content. In addition, this increase may be related to compaction and lithification in the lower portion of the unit. A pronounced step change in GRA bulk density at ~200 mcd coincides with the change from APC to XCB coring. Throughout Unit I, GRA bulk density and MAD discrete bulk density are fairly well correlated to each other ( $r^2 = 0.70$ ). APC cores alone would probably yield a better correlation, but the XCB cores, which lie on a similar slope, introduce a constant offset, thus reducing the correlation. Porosity mirrors changes in bulk density ( $r^2 = 0.94$ ) (Fig. F20).

## Unit II

Intervals: Section 202-1242A-27X-CC and Section 202-1242B-27X-2, 33 cm, through Section 27X-CC

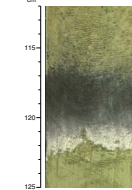
Depths: 280.63–287.74 mcd; Hole 1242A: 250.71–251.05 mbsf (280.59–280.93 mcd) and Hole 1242B: 247.75–254.86 mbsf (280.63–287.74 mcd)

Age: middle Miocene (12–13 Ma)

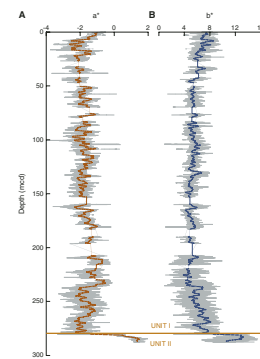
A prominent hiatus at ~280 mcd represents the transition to lithologic Unit II. The hiatus is characterized by a very sharp color change from grayish olive green to very pale brown (Fig. F21). Lithologic Unit II contains pelagic sediment composed of diatom-bearing nannofossil ooze with varying abundance of foraminifers, spicules, radiolarians, and silicoflagellates. Sediment color in Unit II varies from very pale brown to brown. *Zoophycos* traces and burrow structures are present throughout Unit II, indicating moderate bioturbation.

**T9. Ash layers, p. 64.**

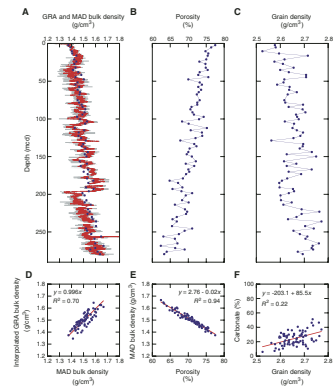
**F18. Sharp basal and diffuse upper contacts, p. 41.**



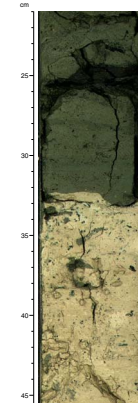
**F19. Color measurements, p. 42.**



**F20. Physical properties measurements, p. 44.**



**F21. Lithologic unit boundary, p. 45.**



The primary components of Unit II are nannofossils (~60%–70%) and diatoms (~10%–20%) (Fig. F15). Foraminifers and other siliceous microfossils (spicules, radiolarians, and silicoflagellates) represent minor biogenic components with abundances ranging from ~1% to 10%. Micrite abundance ranges from 0% to 10% in Unit II (Fig. F15). Siliciclastic content is much lower (<10%) than in Unit I (Fig. F14).

All physical properties measurements show an abrupt change at the beginning of Unit II (Fig. F13). MS and NGR decrease significantly, and lightness increases. These changes coincide with a significant decrease in siliciclastic content and an increase in biogenic content. GRA bulk density also decreases, which is consistent with the significant increase in biogenic silica content observed in Unit II. Color reflectance measurements from Unit II plot in the “reddish” ( $a^* > 0$ ) domain of the  $a^*-b^*$  color plane (Fig. F19).

### **Interpretation and Depositional History**

A 287.74-m-thick sediment sequence was recovered at Site 1242, spanning the interval from the middle Miocene to the Holocene with a prominent hiatus (~2.5–12 Ma) that divides the sequence into two lithologic units deposited within very different depositional environments. Today, this site is located within a tectonically active graben containing sediment of late Pliocene to Holocene age (lithologic Unit I). This graben overlies a sequence of Miocene and older sediment that represents lithologic Unit II.

The Miocene sediment of Unit II represents pelagic conditions before the closure of the Isthmus of Panama. The relatively high abundance of siliceous microfossils in Unit II suggests higher Miocene productivity that may be related to the southward tectonic backtrack of Site 1242 on the Cocos plate (Pisias et al., 1995) toward the equatorial upwelling zone. A comparison of the backtrack paths of Sites 1241 and 1242 shows that at ~12 Ma, Site 1242 was located in a setting similar to the Site 1241 Pliocene setting. This tectonic observation is further supported by the similar lithologies observed for these periods at the two sites (see “[Lithostratigraphy](#),” p. 5, in the “Site 1241” chapter).

The ~9.5-m.y. hiatus, which spans the middle Miocene to upper Pliocene, is coeval with the closure of the Isthmus of Panama, suggesting a plausible connection to this event. Additionally, during this interval, the Cocos Ridge at Site 1242 was approaching the Central American subduction zone, causing increasing tectonic extension, which probably formed the local graben structure that contains upper Pliocene to Holocene Unit I. Hence, both local tectonics and the large-scale isthmus closure might explain the possible lack of sediment accumulation or the tectonic “removal” of the missing upper Miocene to lower Pliocene sedimentary sequence.

Unit I contains a fine-grained, homogeneous hemipelagic sedimentary record with moderate to high sedimentation rates ranging from ~6 to 20 cm/k.y. (see “[Age Model and Mass Accumulation Rates](#),” p. 15) spanning the upper Pliocene to the Holocene. Aside from a possible slump observed at ~143 mcd in one hole, there is no widespread lithologic evidence for sediment redeposition at Site 1242, suggesting a complete and continuous sedimentary sequence representing the last 2.5 m.y.

The depositional environment was probably similar to the modern setting (i.e., the location of Site 1242 at a depth of ~1370 m on the northeastern Cocos Ridge), ~30 km off the Central American active

continental margin under relatively low salinity and nutrient-poor surface waters. The upper Pliocene is characterized by high calcium carbonate and relatively low siliciclastic content, followed by a gradual decrease in calcium carbonate and increase in siliciclastics into the upper Pleistocene–Holocene that may be attributed to one or more of the following:

1. The gradual movement of Site 1242 on the Cocos plate toward the continental margin and thus toward a terrigenous source;
2. The uplift of the Central American cordillera;
3. Long-term changes in pathways and syndepositional focusing of terrigenous material; or
4. Long-term environmental changes affecting both continental rainfall (amount of siliciclastic input) and marine productivity (carbonate production).

Preliminary sedimentation rate estimates (see “[Age Model and Mass Accumulation Rates](#),” p. 15) suggest relatively low values of ~6 cm/k.y. for the uppermost ~20 mcd, where carbonate content is lowest and siliciclastic content is highest. This may imply that terrigenous sediment input is affected by local synsedimentary processes.

Magnetic susceptibility displays significant variability on decimeter to meter scales throughout the upper Pliocene to Holocene sequence, suggesting changes in the relative supplies of terrigenous and biogenic material to Site 1242. These changes, in part, may reflect millennial- to orbital-scale changes in productivity and/or climate.

Increased ash layer frequency between ~30 and 120 mcd and ~160 and 210 mcd indicates increased volcanic activity from ~0.4 to 1.1 Ma and from ~1.3 to 1.6 Ma, respectively, which is consistent with high ash accumulation between ~0 and 2.5 Ma in the Caribbean Sea (Cadet et al., 1982; Sigurdsson et al., 2000). Clear platy and vesicular glass and intermediate accessory mineral compositions suggest an andesitic volcanic source, most likely in Central America.

## BIOSTRATIGRAPHY

Calcareous nannofossil, planktonic foraminifer, and diatom biostratigraphies indicate that the ~288-m sediment succession recovered at Site 1242 consists mainly of an expanded, continuous Pleistocene–upper Pliocene sequence (Table [T10](#); Figs. [F22](#), [F29](#)). A major unconformity spanning ~3 to 12 Ma and corresponding to a marked change in color and lithology is identified by all three microfossil groups between 280.6 and 284.1 mcd. Calcareous nannofossils and planktonic foraminifers at the base of the hole suggest an age between ~12 and 13 Ma.

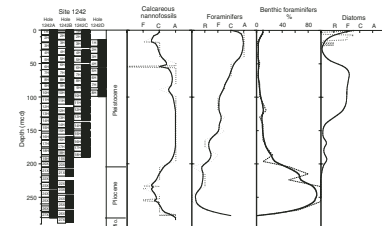
Calcareous nannofossils are less abundant than at Site 1241 and moderately well preserved with frequent indications of dissolution. Planktonic foraminifers are abundant to common and moderately well preserved down to ~70 mcd then become rarer and poorly preserved, except below the unconformity. The proportion of benthic foraminifers increases markedly below ~110 mcd. Marked changes in the relative proportions of benthic foraminiferal species within the Pleistocene–late Pliocene assemblage probably indicate variations in carbon fluxes at the seafloor. Diatoms are generally rare and moderately to poorly preserved. However, abundant *Ethmodiscus* fragments in Sections 202-1242A-21X-3 through 21X-7 (~208–215 mcd) form distinct thin, dark layers.

---

**T10.** Age-depth control points, p. 65.

---

**F22.** Nannofossil and planktonic foraminifer abundance, benthic foraminifer percentage of total foraminifers, and diatom abundance, p. 46.



## **Calcareous Nannofossils**

The abundance of calcareous nannofossils is notably lower at Site 1242 than at Site 1241, largely because of dilution by clay and some silt-sized detrital grains. Preservation of nannofossils is generally moderate, with frequent indications of dissolution but with minimal overgrowth (Table T11; Fig. F22).

*Emiliania huxleyi* was found from the mudline sample (Sample 202-1242A-1H-1, 0 cm) to Sample 2H-CC, 16 cm (Table T11). This documents the recovery of the 0- to 0.26-Ma interval at Site 1242. Most of the Pleistocene–late Pliocene nannofossil markers have been determined (Table T10). A few events, such as the last occurrences (LOs) of *Calcidiscus macintyrei* and *Discoaster pentaradiatus*, have not been located largely because of the lower abundance of these index species and/or inadequate shipboard sample resolution.

Calcareous nannofossil biostratigraphy documents a relatively continuous sequence that accumulated rapidly (~100 m/m.y.) down to ~2.5 Ma. A marked change in color and lithology occurs in Sample 202-1242B-27X-2, 33 cm (280.63 mcd) (see “**Lithostratigraphy**,” p. 5), where a hiatus representing ~3–12 Ma is detected between Samples 27X-CC, 1 cm (280.6 mcd), and 27X-4, 75 cm (284.1 mcd), based on the presence of a late Pliocene assemblage characterized by *D. pentaradiatus* and *Discoaster brouweri* in the upper sample and the presence of the late middle Miocene index species *Coccolithus miopelagicus* and *Coronocyclus nitescens* in the lower sample.

## **Planktonic Foraminifers**

Planktonic foraminifers are abundant to common in the upper part of Hole 1242A sediments (mudline to Sample 202-1242A-7H-CC; 0–69.28 mcd). Abundance decreases markedly downhole, and planktonic foraminifers are rare in samples from the lower part of Hole 1242A (Samples 202-1242A-16H-CC through 26X-CC; 164.3–272.5 mcd), except in Sample 27X-CC (280.9 mcd), which is below a major unconformity. Preservation is moderate to good down to Samples 202-1242A-10H-CC (99.2 mcd) but deteriorates markedly at greater depths, particularly between Samples 21X-CC and 26X-CC (215.2–272.5 mcd), where glauconite is commonly present in the >63-µm residue (Table T12).

The Pleistocene–late Pliocene assemblage is characterized by *Globorotalia menardii*, *Globorotalia tumida*, *Globigerinoides sacculifer*, *Globigerinoides ruber*, *Globigerinoides trilobus*, *Neogloboquadrina acostaensis*, *Neogloboquadrina dutertrei*, and *Orbulina universa*. A preliminary biostratigraphy was established for the Pleistocene–upper Pliocene interval. However, some of the standard marker species were not found during shipboard studies, and the biostratigraphy is not well constrained for the lower part of Hole 1242A (Samples 202-1242A-21X-CC and 26X-CC; 215.2–272.5 mcd) because of poor preservation and the scarcity of planktonic foraminifers.

The LO of *G. ruber* (pink), between Samples 202-1242A-1H-CC and 2H-CC (5.00–17.87 mcd), indicates an age younger than 0.12 Ma for the overlying interval. The first occurrence (FO) of *G. ruber* (pink) (0.40 Ma) can be placed between Samples 202-1242A-4H-CC and 5H-CC (40.00–49.52 mcd). However, the FO of *Globorotalia flexuosa* (0.40 Ma) appears to occur later, between Samples 202-1242A-3H-CC and 4H-CC (28.91–40.00 mcd), which probably reflects poor preservation, as severe dissolution damage was noted in particular for the species *G. tumida*.

---

**T11.** Distribution of calcareous nannofossils, p. 66.

---

**T12.** Distribution of planktonic foraminifers, p. 68.

and *G. flexuosa*. The standard marker *Globorotalia tosaensis* is extremely rare at Site 1242 and could not be used to define the boundary between the Subzones Pt1a and Pt1b of Berggren et al. (1995). The LO of representatives of the benthic genus *Stilostomella* (~0.65 Ma), which occurs between Samples 202-1242A-8H-CC and 9H-CC (80.13–88.94 mcd), provides an alternative datum to approximate this boundary. However, this extinction event was probably diachronous at low and high latitudes (Hayward, 2001), and detailed shore-based studies from Site 1242 and from more southerly Leg 202 sites are needed to clarify the timing of this event in the eastern Pacific. The species *Globigerinoides fistulosus*, which defines the base of the Pleistocene/Pliocene boundary, was not observed in our samples. The LO of *Globigerinoides extremus* (1.77 Ma), between Samples 202-1242A-21X-CC and 22X-CC (215.2–227.6 mcd), provides an alternative datum to approximate this boundary.

Planktonic foraminifers indicate a major unconformity (~3–12 Ma), which corresponds to an abrupt lithologic change (see “[Lithostratigraphy](#),” p. 5) in the core catcher of Core 202-1242A-27X. The presence of the typical middle Miocene species *Globorotalia fohsi* s.l., *Globorotalia panda*, and *Globorotalia praemenardii* in Sample 202-1242A-27X-CC (280.9 mcd), below the unconformity, indicates an age between 11.9 and 13.42 Ma for the base of Hole 1242A.

## Benthic Foraminifers

The percentage of benthic foraminifers relative to total foraminifers is, initially, relatively low (mainly ~10% or less) in samples from the upper part of Hole 1242A (mudline to Sample 202-1242A-11H-CC; 0–109.4 mcd) but increases markedly downhole, reaching ~99% between Samples 23X-CC and 25X-CC (237.5–260.4 mcd). Benthic foraminifers overall show better preservation than planktonic foraminifers, but preservation deteriorates downhole, particularly between Samples 202-1242A-21X-CC and 26X-CC (215.23–268.99 mcd).

The relatively diverse but sparse Pleistocene–late Pliocene assemblage in Samples 202-1242A-1H-CC through 21H-CC typically contains *Bolivina seminuda*, *Bulimina mexicana*, *Bulimina aculeata*, *Eggerrella bradyi*, *Eubulimina exilis*, *Globocassidulina subglobosa*, *Globobulimina affinis*, *Globobulimina pyrula*, *Gyroidinoides soldanii*, *Gyroidinoides orbicularis*, *Laticarinina pauperata*, *Melonis affinis*, *Melonis pompilioides*, *Planulina wuellerstorfi*, *Plectofrondicularia vaughani*, *Pleurostomella brevis*, *Pullenia bulloides*, *Stilostomella abyssorum*, *Stilostomella subspinosa*, and *Uvigerina proboscidea*. Marked variations in the proportions of *Bolivina*, *Bulimina*, *Globobulimina*, and *Uvigerina* may relate to changes in productivity, oxygenation, or circulation. However, it was not possible to evaluate from shipboard study to what extent these changes were affected by diagenesis.

## Diatoms

All core catcher samples from Hole 1242A and smear slides from some additional layers of the split cores were analyzed. Few to common diatoms of moderate preservation were found in the mudline sample (Sample 202-1242A-1H-1, 0 cm), Sample 1H-CC, and Samples 6H-CC to 14H-CC (59.5–141.2 mcd). Only traces of diatoms were observed in Samples 202-1242A-2H-CC through 5H-CC (17.9–49.5 mcd) and Sample 15H-CC (151.4 mcd). Abundant *Ethmodiscus* fragments were found in Sections 202-1242A-21X-3 through 21X-7 (~208–215 mcd), which

formed distinct thin dark layers (see “**Lithostratigraphy**,” p. 5). Below the obvious hiatus at 280.63 mcd, Sample 202-1242A-27X-CC (280.9 mcd) contained a middle-late Miocene diatom assemblage dominated by *Thalassiothrix* (Table T13).

Although diatoms are generally rare and poorly preserved at Site 1242, a total of three mid-Pleistocene diatom events were recognized (Table T10). In addition, the presence of middle Miocene diatoms *Craspedodiscus coscinodiscus* and *Actinocyclus ingens* and the absence of *Coscinodiscus lewisiensis* in Sample 202-1242A-27X-CC allow a tentative placement of this sample into the *Coscinodiscus gigas* var. *diorama* Zone (12.18–12.93 Ma), although *A. ingens* is rare and only fragments of *C. coscinodiscus* have been found.

**T13.** Distribution of diatoms, p. 69.

## PALEOMAGNETISM

### Natural Remanent Magnetization

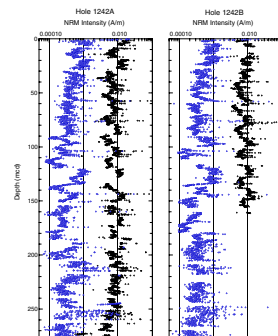
The natural remanent magnetization (NRM) of the archive half of each core section was either initially measured and remeasured after alternating field (AF) demagnetization or, because of time constraints, measured and only after demagnetization. Cores 202-1242A-1H through 12H were measured and then AF demagnetized at 10 and 20 mT. Additionally, Section 202-1242A-11H-2 was demagnetized at 30 and 40 mT. Cores 202-1242A-13H through 28X, 202-1242B-1H through 15H, and 202-1242C-1H through 8H were measured and then demagnetized at 20 mT. Cores 202-1242B-16H through 26H, 202-1242C-9H through 18H, and all cores from Hole 1242D were only measured after demagnetization at 20 mT. Sections obviously affected by drilling disturbance were not measured.

The NRM intensity before demagnetization at the top of Hole 1242A was in the range of ~0.01 A/m (Fig. F23). After 20-mT demagnetization, the NRM intensity is ~1 order of magnitude lower, varying around  $10^{-3}$  A/m (Fig. F23). The difference between demagnetized and nondemagnetized intensity increases downhole (~1.5 orders of magnitude lower at the base) because of a reduction in magnetic intensity after demagnetization with essentially no change in the intensity before (Fig. F23). This observation is consistent with a slight decrease in the finer-grained magnetic components downhole and could be a reflection of reduction diagenesis at Site 1242. Aside from the slight downhole trend, the intensity variations look promising for geomagnetic paleointensity studies. Because of time constraints, only a quick look at the susceptibility-normalized NRM intensity was possible. Such analysis suggests that through careful postcruise studies a detailed high-resolution paleointensity record may be forthcoming from Site 1242.

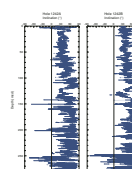
### Directional Variability

Steep positive inclinations observed prior to demagnetization and resulting from the drill string magnetic overprint are at least partially removed after 20-mT AF demagnetization (Fig. F24). The expected inclination at Site 1242 is ~15°, but the observed inclination after demagnetization for the upper 90 mcd, the interval that should correspond to the Brunhes Chron according to the biostratigraphic datums (see “**Biostratigraphy**,” p. 9), averages ~35°. The inclinations are more steeply positive in sediment cored with the normal steel core barrel,

**F23.** NRM intensity before and after AF demagnetization, p. 47.



**F24.** NRM inclination after demagnetization, p. 48.



whereas shallower inclinations closer to the expected values are present in sediment cored with the nonmagnetic core barrel. The overprint still remains after demagnetization but is apparently easier to clean when cored with the nonmagnetic core barrel. No reversed inclinations are observed even in sediments that should be clearly Matuyama in age, and therefore higher levels of demagnetization may be required to remove the overprint from these sediments.

The declinations within individual cores at Site 1242 are generally consistent (show similar directions) in most of the APC-cored part of Holes 1242A and 1242B (Fig. F25). This suggests that the drill string overprint is not pervasive and that geomagnetic information is preserved at Site 1242. Tensor tool measurements will be used to help decipher the polarity stratigraphy. Postcruise studies should allow us to successfully remove the overprint and isolate the geomagnetic record.

## GEOCHEMISTRY

### Sediment Gases

Concentrations of headspace gases were routinely monitored in Hole 1242A sediments according to shipboard safety and pollution prevention considerations. Methane increased from ambient concentrations at 1.5 mcd to >20,000 ppmv at 23.4 mcd (Table T14; Fig. F26). Methane concentrations were high at greater depth (average = 40,000 ppmv). Small amounts of ethane were detected, varying between 1.4 and 14.8 ppmv. High methane/ethane ratios, representative of microbial gases, indicate that the gases are of biogenic origin. This is supported by the disappearance of interstitial sulfate at approximately the same depth where methane contents begin to increase. The presence of interstitial sulfate inhibits methanogenesis in marine sediments (Claypool and Kvenvolden, 1983).

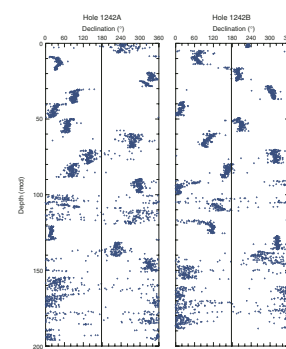
### Interstitial Water Geochemistry

We collected 19 interstitial water samples from Hole 1242A for shipboard analyses. All of these samples were taken from Unit I (see “[Lithostratigraphy](#),” p. 5). Chemical gradients at this site (Table T15; Fig. F27) reflect the influence of organic matter oxidation by sulfate reduction, authigenic mineralization, the dissolution of biogenic silica, and the diffusive influence of basalt alteration reactions at greater depth.

Chlorinity generally increases with depth, from 552 mM at 1.5 mcd to 564 mM at 275.5 mcd (Fig. F27). Salinity, measured refractively as total dissolved solids, ranges between 32–35 (Table T15). Sodium concentrations measured by inductively coupled plasma-atomic emission spectrophotometry averaged 2.0% lower than those estimated by charge balance reported here (Table T15). Sodium concentrations show a small increase from 478 mM at 1.5 mcd to >490 mM from 34.3 to 74.6 mcd then decrease substantially to 363 mM at 275.5 mcd. The lack of decrease in salinity or chlorinity is because the decrease in sodium is counterbalanced by a substantial increase in calcium.

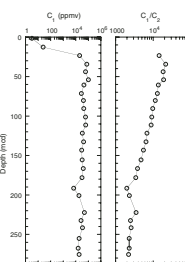
Dissolved manganese concentrations have a near-surface maximum of 5.8  $\mu\text{M}$  at 1.5 mcd, decrease to low values from 23.4 to 169.5 mcd, then increase to >10  $\mu\text{M}$  from 232.3 to 275.5 mcd. Dissolved iron has a small maximum of >15  $\mu\text{M}$  from 83.5 to 104.3 mcd. At greater depth,

**F25.** NRM declination after demagnetization, p. 49.



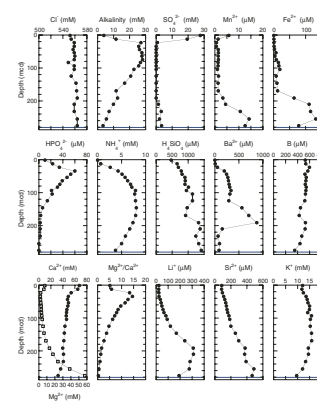
**T14.** Headspace gases concentrations and  $\text{C}_1/\text{C}_2$  ratio in sediments, p. 70.

**F26.** Headspace methane vs. depth, p. 50.



**T15.** Interstitial water geochemical data, p. 71.

**F27.** Interstitial water geochemical data, p. 51.



the iron profile resembles that of manganese, with a significant increase from 12.4  $\mu\text{M}$  at 169.5 mcd to  $>110 \mu\text{M}$  from 210.1 to 255.1 mcd. These deep maxima of iron and manganese may indicate the persistence of suboxic diagenesis of organic carbon at depths greater than  $\sim 180$  mcd, consistent with the presence of measurable sulfate at depth. Organic matter diagenesis, driven by microbially mediated oxidation reactions, significantly influences the interstitial water chemistry. Sulfate decreases to nearly nondetectable levels by 23.4 mcd and remains at that level to 191.5 mcd. The disappearance of sulfate coincides with the increase in methane. Interstitial water samples from 210.1 to 275.5 mcd, taken from XCB cores, have detectable sulfate concentrations (1.4–3.4 mM). This is often interpreted as reflecting seawater contamination in the XCB whole rounds, but the evidence from barium concentrations indicates that these may in fact represent in situ sulfate concentrations. Alkalinity rapidly increases from 3.9 mM at 1.5 mcd to  $>25$  mM from 23.4 to 93.6 mcd then decreases to 3.3 mM at 275.5 mcd.

Phosphate concentrations increase from 10  $\mu\text{M}$  at 1.5 mcd to 60  $\mu\text{M}$  at 34.4 mcd, decline steeply to 6  $\mu\text{M}$  at 146.2 mcd, then decrease more slowly with depth to values below the detection limit (1  $\mu\text{M}$ ). Ammonium concentrations increase from below the detection limit (0.4 mM) at 1.5 mcd to  $>7.5$  mM from 93.6 to 169.5 mcd then decline steadily to 3.7 mM at 275.5 mcd.

Dissolved silicate increases from 468  $\mu\text{M}$  at 1.5 mcd to  $>1400 \mu\text{M}$  at 275.5 mcd, indicating that interstitial waters could be at equilibrium with biogenic opal solubility. Despite the high thermal gradient at this site, dissolved silicate concentrations do not reach the extremely high values ( $>1800 \mu\text{M}$ ) seen at Sites 1238 and 1239.

Barium concentrations increase significantly with the disappearance of sulfate to values of  $>200 \mu\text{M}$  from 44.0 to 124.9 mcd then increase sharply to 872  $\mu\text{M}$  at 191.5 mcd. The increase in barium with the disappearance of dissolved sulfate is consistent with the dissolution of barite from sediments with sulfate reduction. In the deeper samples with small but measurable sulfate concentrations, barium concentrations return to low values,  $\leq 150 \mu\text{M}$  from 210.1 to 275.5 mcd. Boron concentrations decrease overall from 529  $\mu\text{M}$  at 1.5 mcd to 351  $\mu\text{M}$  at 275.5 mcd.

Calcium decreases from 9.9 mM at 1.5 mcd to 2.5 mM at 34.4 mcd then increases to 5.5 mM at 104.3 mcd and to 76.6 mM at 275.5 mcd. The deeper calcium gradient is equivalent to a 48 mM/100 m change in calcium concentration, the largest observed during this leg and a factor of 10 larger than the average oceanic gradient. Magnesium concentrations decrease overall, with the decrease in the deeper section linearly correlated to the calcium increase, indicating that these profiles are diffusively controlled from a reaction source/sink at depth such as basalt alteration reactions. Magnesium/calcium ratios increase from 5.1 at 1.5 mcd to  $>10$  from 23.4 to 54.0 mcd (Fig. F27). The decrease in calcium can result from authigenic calcite precipitation and drive magnesium/calcium ratios higher. High magnesium/calcium ratios, along with the disappearance of sulfate, can subsequently result in dolomite formation, and observations indicate the presence of dolomite in this site (see “**Lithostratigraphy**,” p. 5).

Lithium concentrations increase from 23  $\mu\text{M}$  at 1.5 mcd to 310  $\mu\text{M}$  from 191.5 to 210.1 mcd then decrease to 191  $\mu\text{M}$  at 275.5 mcd. Strontium concentrations increase with depth from 85  $\mu\text{M}$  at 1.5 mcd to  $>450 \mu\text{M}$  from 255.1 to 275.5 mcd. Potassium concentrations increase

from 12 mM at 1.5 mcd to >15 mM from 93.6 to 210.1 mcd then decrease to 9.6 mM at 275.5 mcd.

### Sedimentary Inorganic Carbon, Organic Carbon, and Nitrogen Concentrations

Inorganic carbon (IC), total carbon (TC), and total nitrogen (TN) concentrations were determined on sediment samples from Hole 1242A (Table T16). Organic matter carbon/nitrogen ratios were employed to characterize the organic matter contained within the sediments.

Calcium carbonate concentrations range between 5.7 and 51.2 wt% (average = 24.4 wt%) (Table T16; Fig. F28). Calcium carbonate concentrations generally increase with increasing depth, with fluctuations of ~10 to ~20 wt% around this trend.

Total organic carbon (TOC) concentrations range between 0.9 and 3.5 wt% from 2.2 to 238.8 mcd (average = 1.6 wt%) (Table T16; Fig. F28). TOC concentrations decrease from 3.5 wt% at 2.2 mcd to typically <1.5 wt% at depths >~90 mcd.

TOC/TN ratios range between 4.9 and 8.8 (average = 7.2), indicating that the sedimentary organic matter is dominantly of marine origin (Bordovskiy, 1965; Emerson and Hedges, 1988; Meyers, 1997). In the uppermost ~50 mcd, TOC/TN ratios average 8.2 (Fig. F28). TOC/TN ratios decrease to a minimum of 4.9 at 122.7 mcd.

## AGE MODEL AND MASS ACCUMULATION RATES

A 288.9-mcd-thick (256.0 mbsf) middle Miocene to Holocene sequence was recovered at Site 1242. A major hiatus near the base of the sequence (281 mcd) spans the tie from ~12 to ~2.5 Ma. Biostratigraphic datums (see “[Biostratigraphy](#),” p. 9) from the upper 280 mcd were used to construct an age-depth model for this site (Table T17; Fig. F29). Linear sedimentation rates (LSRs), total MARs, and carbonate MARs were calculated at 0.4-m.y. intervals (see “[Age Models and Mass Accumulation Rates](#),” p. 41, in the “Explanatory Notes” chapter).

### Age-Depth Model

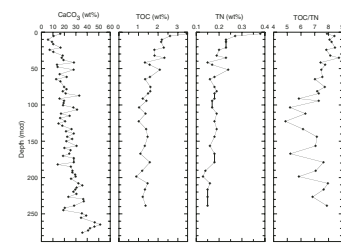
We relied primarily, although not exclusively, on calcareous nannofossil datums to define the age-depth model for Site 1242 (Fig. F29). The abundance of calcareous nannofossils was low, planktonic foraminifers were poorly preserved and rare in the lower part of the record, and diatoms were generally rare and poorly preserved (see “[Biostratigraphy](#),” p. 9). The age-depth profile shows no major inflections, reflecting the rather homogeneous lithology in this sediment sequence (see “[Lithostratigraphy](#),” p. 5).

### Linear Sedimentation and Mass Accumulation Rates

LSRs range between ~0 and 138 m/m.y., and total MARs range between 0 and 11 g/cm<sup>2</sup>/k.y. The rates all show the same general pattern of a broad peak characterized by an initial, rapid increase in values from 2.8 to 1.6 Ma, maximum values between 1.6 and 1.2 Ma, and a gradual decline in the values after 1.2 Ma. LSRs deviate from the MARs by a gradual relative increase with time, reflecting the general trend of increasing porosity with decreasing overburden combined with a general

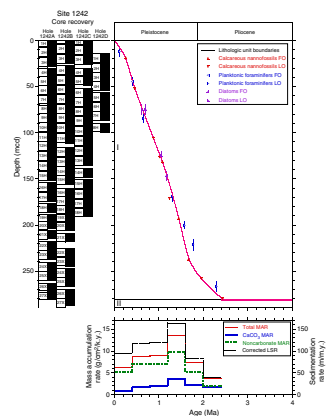
**T16.** IC, CaCO<sub>3</sub>, TC, TOC, and TN concentrations, and TOC/TN ratios in sediments, p. 72.

**F28.** CaCO<sub>3</sub>, TOC, TN, and TOC/TN vs. depth, p. 52.



**T17.** Age-depth model, LSRs, and MARs, p. 74.

**F29.** Biostratigraphic and magnetostratigraphic datums and age-depth model, p. 53.



trend of decreasing carbonate concentrations (decreasing grain density). The interval 100–150 mcd (0.8–1.2 Ma) has a significantly higher relative diatom abundance and reduced relative nannofossil abundance (see “[Lithostratigraphy](#),” p. 5), but this lithologic change has no apparent effect on the MARs.

Although total MARs and carbonate MARs show the same general trend, carbonate MARs are significantly lower than total MARs because of the high terrigenous content of this sediment.

## **REFERENCES**

- Behrenfeld, M.J., Randerson, J.T., McClain, C.R., Feldman, G.C., Los, S.O., Tucker, C.J., Falkowski, P.G., Field, C.B., Frouin, R., Esaias, W.E., Kolber, D.D., and Pollack, N.H., 2001. Biospheric primary production during and ENSO transition. *Science*, 291:2594–2597.
- Berggren, W.A., Kent, D.V., Swisher, C.C., III, and Aubry, M.-P., 1995. A revised Cenozoic geochronology and chronostratigraphy. In Berggren, W.A., Kent, D.V., Aubry, M.-P., and Hardenbol, J. (Eds.), *Geochronology, Time Scales and Global Stratigraphic Correlation*. Spec. Publ.—SEPM, 54:129–212.
- Bordovskiy, O.K., 1965. Accumulation and transformation of organic substances in marine sediment, 2. Sources of organic matter in marine basins. *Mar. Geol.*, 3:5–31.
- Cadet, J.-P., Pouclet, A., Thisse, Y., Bardintzeff, J.M., and Azéma, J., 1982. Middle America Neogene explosive volcanism and ash layers: evidence from the Middle America trench transect, Deep Sea Drilling Project Leg 67. In Aubouin, J., von Huene, R., et al., *Init. Repts. DSDP*, 67: Washington (U.S. Govt. Printing Office), 475–491.
- Claypool, G.E., and Kvenvolden, K.A., 1983. Methane and other hydrocarbon gases in marine sediment. *Annu. Rev. Earth Planet. Sci.*, 11:299–327.
- Emerson, S., and Hedges, J.I., 1988. Processes controlling the organic carbon content of open ocean sediments. *Paleoceanography*, 3:621–634.
- Ganeshram, R.S., Pedersen, T.F., Calvert, S.E., and Murray, J.W., 1995. Large changes in oceanic nutrient inventories from glacial to interglacial periods. *Nature*, 376:755–758.
- Hayward, B.W., 2001. Global deep-sea extinctions during the Pleistocene ice-ages. *Geology*, 29:599–602.
- Hey, R., Johnson, G.L., and Lowrie, A., 1977. Recent plate motions in the Galapagos area. *Geol. Soc. Am. Bull.*, 88:1385–1403.
- Kroopnick, P., 1974. The dissolved  $O_2$ - $CO_2$ - $^{13}C$  system in the eastern equatorial Pacific. *Deep-Sea Res. Part A*, 21:211–227.
- Ledbetter, M.T., 1985. Tephrochronology of marine tephra adjacent to Central America. *Geol. Soc. Am. Bull.*, 96:77–82.
- Levitus, S., Conkright, M.E., Reid, J.L., Najjar, R.G., and Mantyla, N.A., 1993. Distribution of nitrate, phosphate, and silicate in the world oceans. *Prog. Oceanogr.*, 31:245–273.
- Lyle, M., Liberty, L., Mix, A., Pisias, N., Goldfinger, C., Hulett, D., and Janik, A., 2000. *Site Survey Data Package 5: Site Surveys for ODP Leg 201 from the NEMO-3 Cruise, in Support of Proposal 465: Southeast Pacific Paleceanographic Transects*. CGISS Tech. Rpt. 2000-06, Boise State University.
- Meyers, P.A., 1997. Organic geochemical proxies of paleceanographic, paleolimnologic, and paleoclimatic processes. *Org. Geochem.*, 27:213–250.
- Mix, A.C., Pisias, N.G., Goldfinger, C., Lyle, M., Liberty, L., Janik, A., Hebbeln, D., Wefer, G., and Lamy, F., 2000. *Southeast Pacific Paleceanographic Transects, Site Survey Data Package 4: NEMO Expedition, Leg III, R/V Melville, May–June 2000*: Corvallis (Oregon State Univ.).
- Ocean Climate Laboratory, 1999. *World Ocean Atlas 1998 (WOA98)* [CD-ROM]. Available from: National Climatic Data Center, Asheville NC 28801-5001, USA.
- Pisias, N.G., Mayer, L.A., and Mix, A.C., 1995. Paleceanography of the eastern equatorial Pacific during the Neogene: synthesis of Leg 138 drilling results. In Pisias, N.G., Mayer, L.A., Janecek, T.R., Palmer-Julson, A., and van Andel, T.H. (Eds.), *Proc. ODP, Sci. Results*, 138: College Station, TX (Ocean Drilling Program), 5–21.
- Sigurdsson, H., Kelley, S., Leckie, R.M., Carey, S., Bralower, T., and King, J., 2000. History of circum-Caribbean explosive volcanism:  $^{40}Ar/^{39}Ar$  dating of tephra layers. In Leckie, R.M., Sigurdsson, H., Acton, G.D., and Draper, G. (Eds.), *Proc. ODP, Sci. Results*, 165: College Station, TX (Ocean Drilling Program), 299–314.

- Tsuchiya, M., and Talley, L.D., 1998. A Pacific hydrographic section at 88°W: water-property distribution. *J. Geophys. Res.*, 103:12899–12918.
- von Huene, R., Ranero, C.R., Weinrebe, W., and Hinz, K., 2000. Quaternary convergent margin tectonics of Costa Rica, segmentation of the Cocos plate, and Central American volcanism. *Tectonics*, 19:314–334.

**Figure F1.** Locations of Sites 1238–1242 and regional bathymetry of the Panama and Guatemala Basins, which are separated by Cocos Ridge. To the south is Carnegie Ridge. The Panama Basin is split by the Cocos-Nazca spreading center.

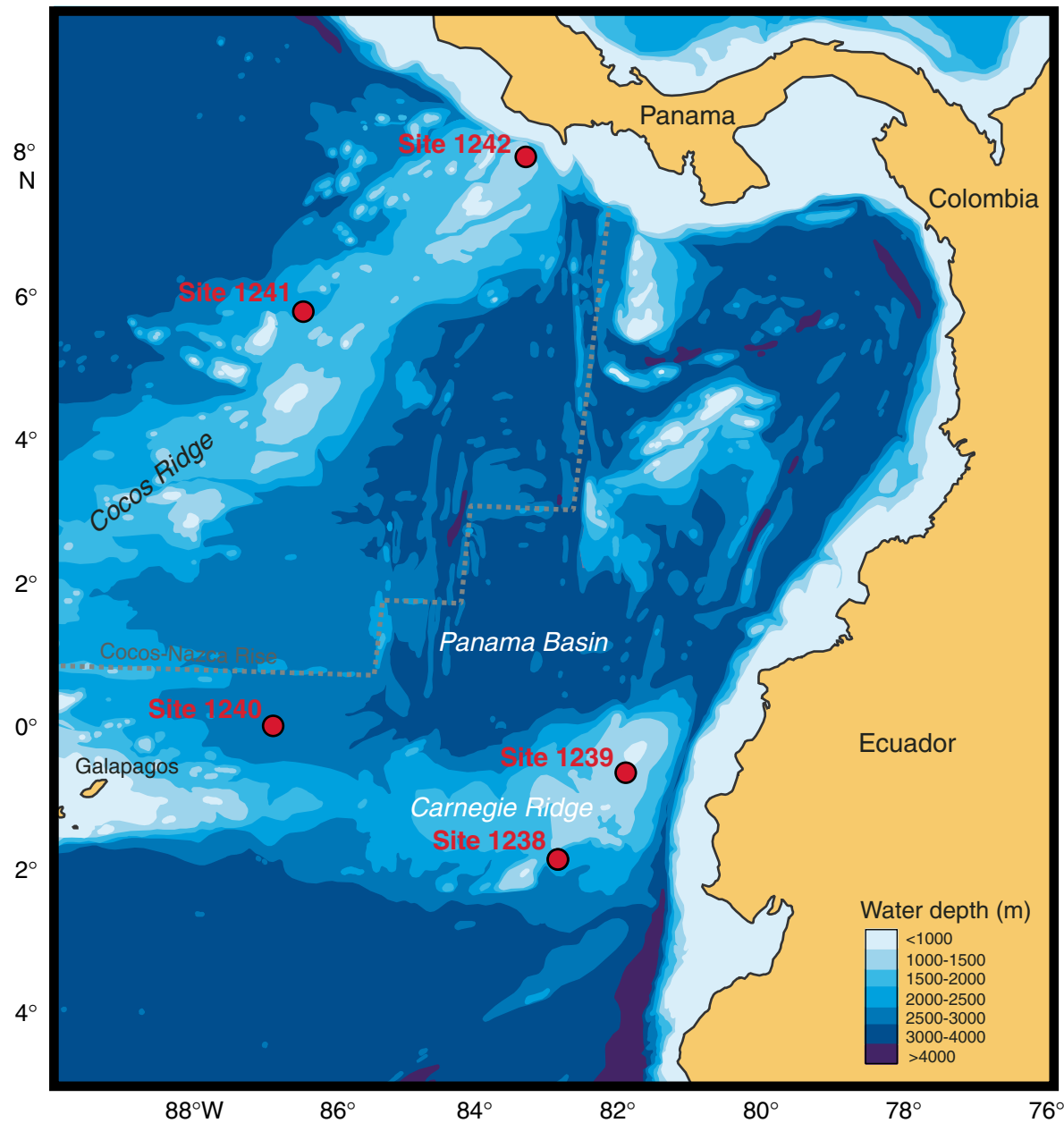


**Figure F2.** High-resolution swath bathymetry, illustrated in an oblique view (Mix et al., 2000). The graben occupied by Site 1242 lies atop Cocos Ridge, near its intersection with the Mesoamerica Trench. The oblate structure to the southwest of Site 1242 reflects slumping and erosion in this tectonically active region.

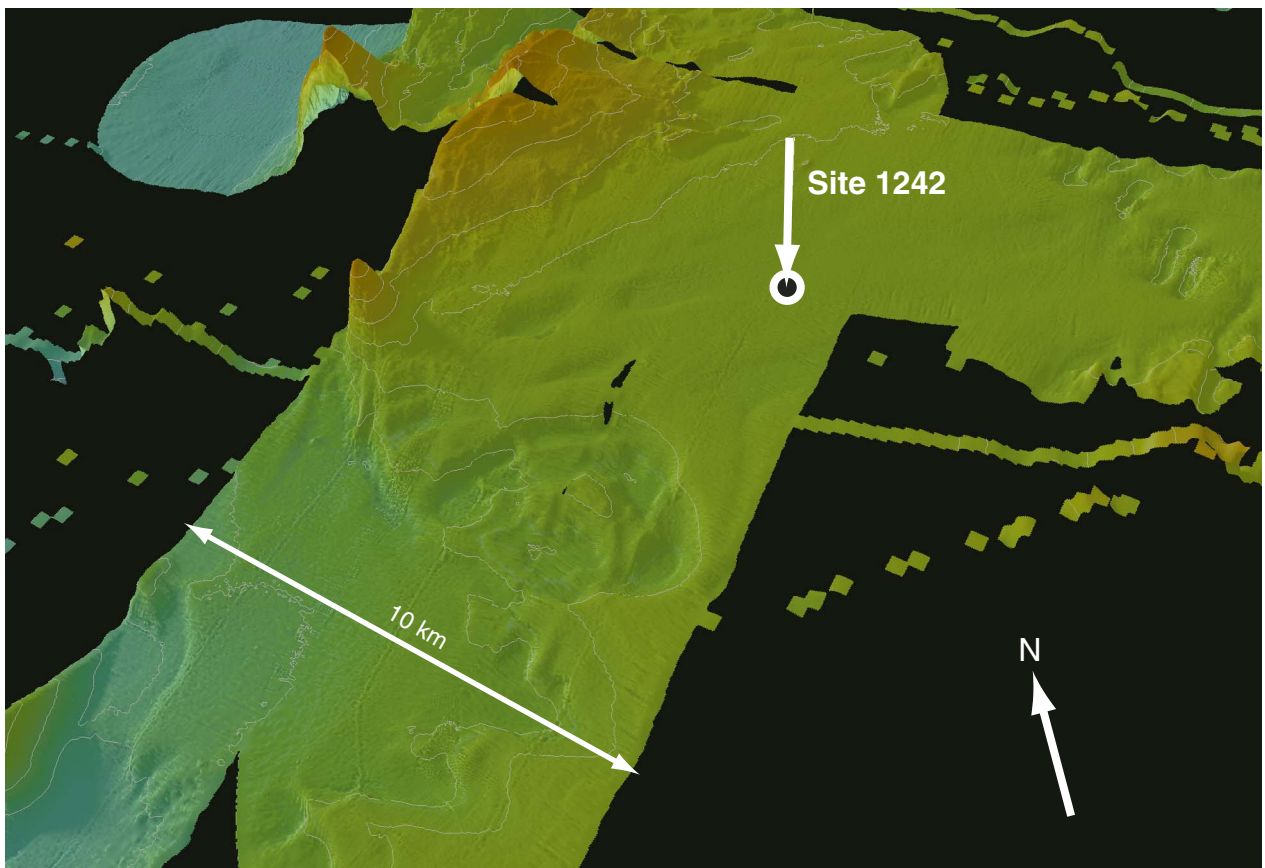


**Figure F3.** Primary tectonic features of the Panama Basin and surroundings (after Hey et al., 1977). Bold black lines = active oceanic spreading centers, red lines = age (in millions of years) of oceanic crust. CNR = Cocos-Nazca Rift, EPR = East Pacific Rise.

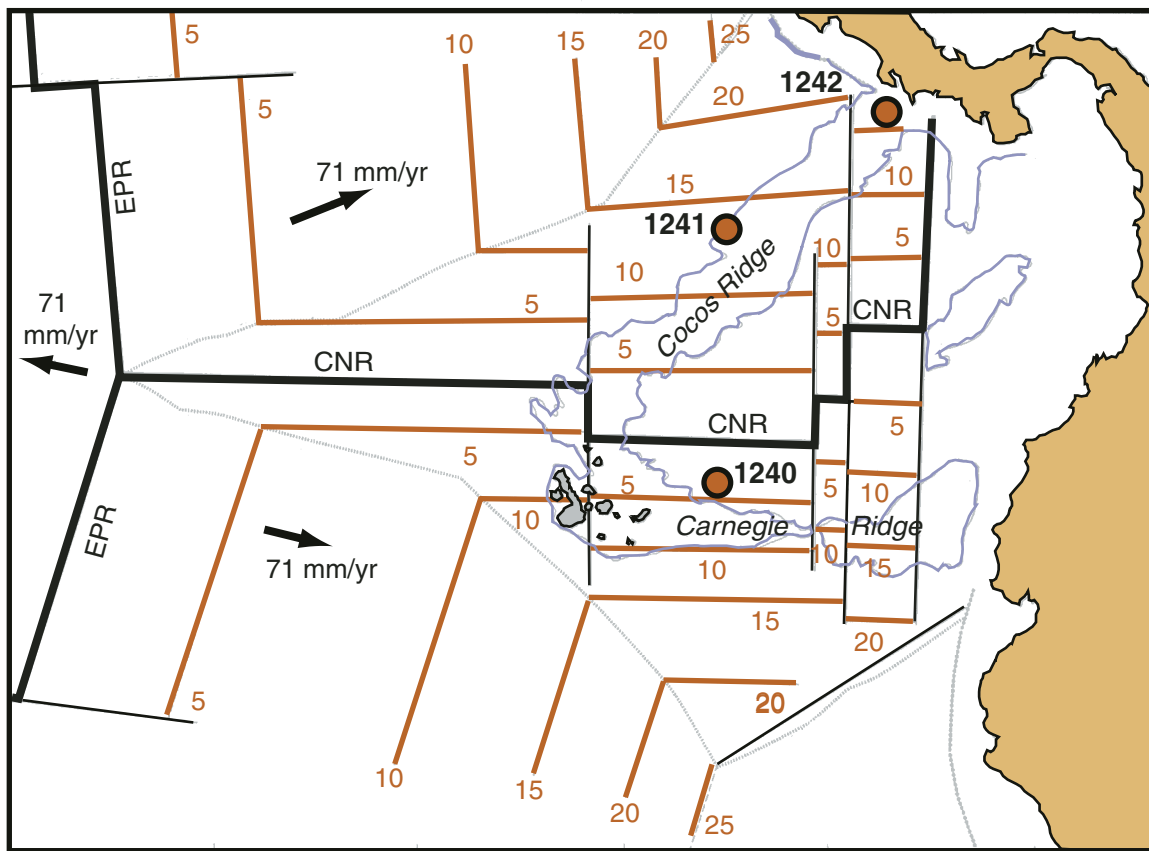
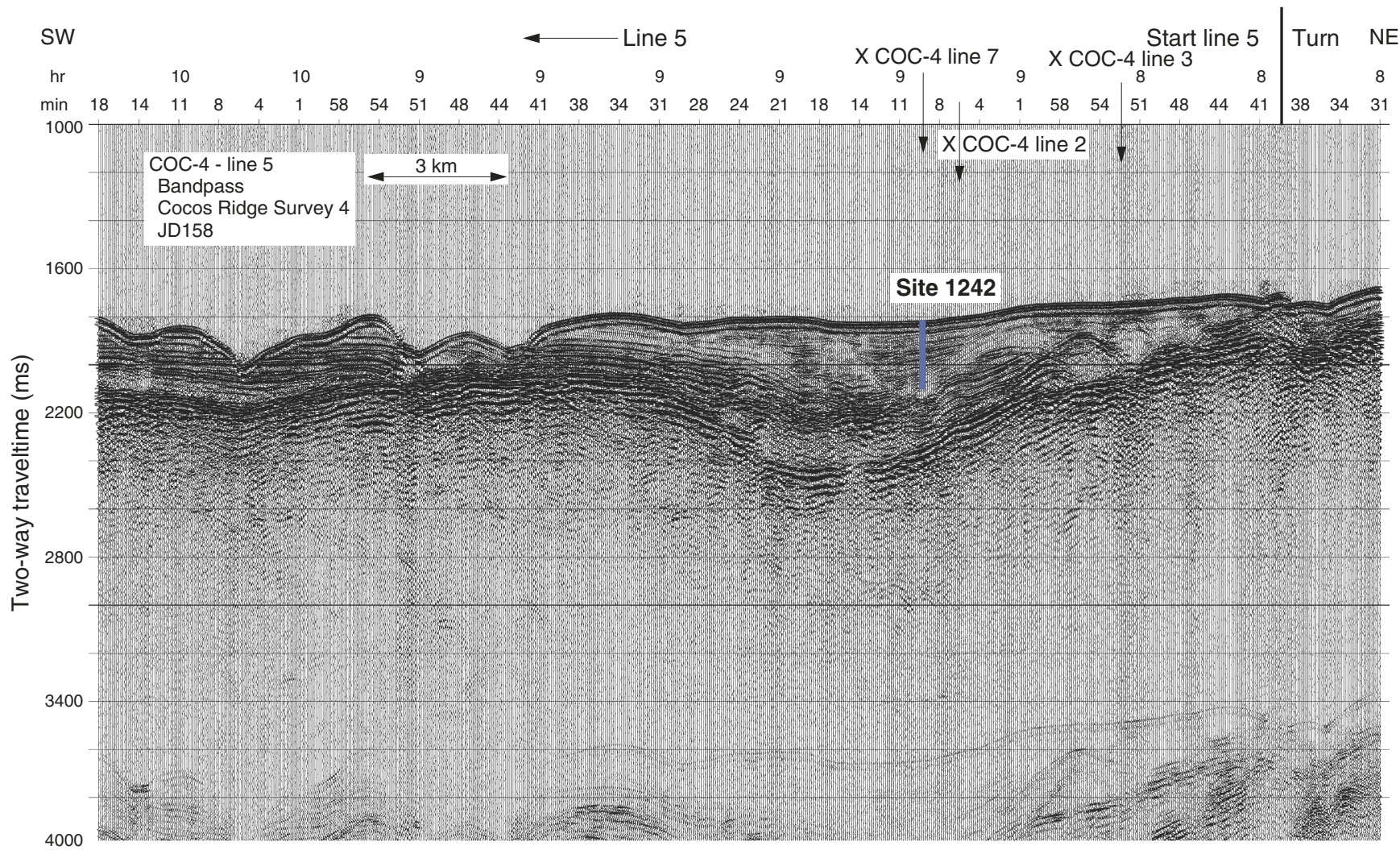
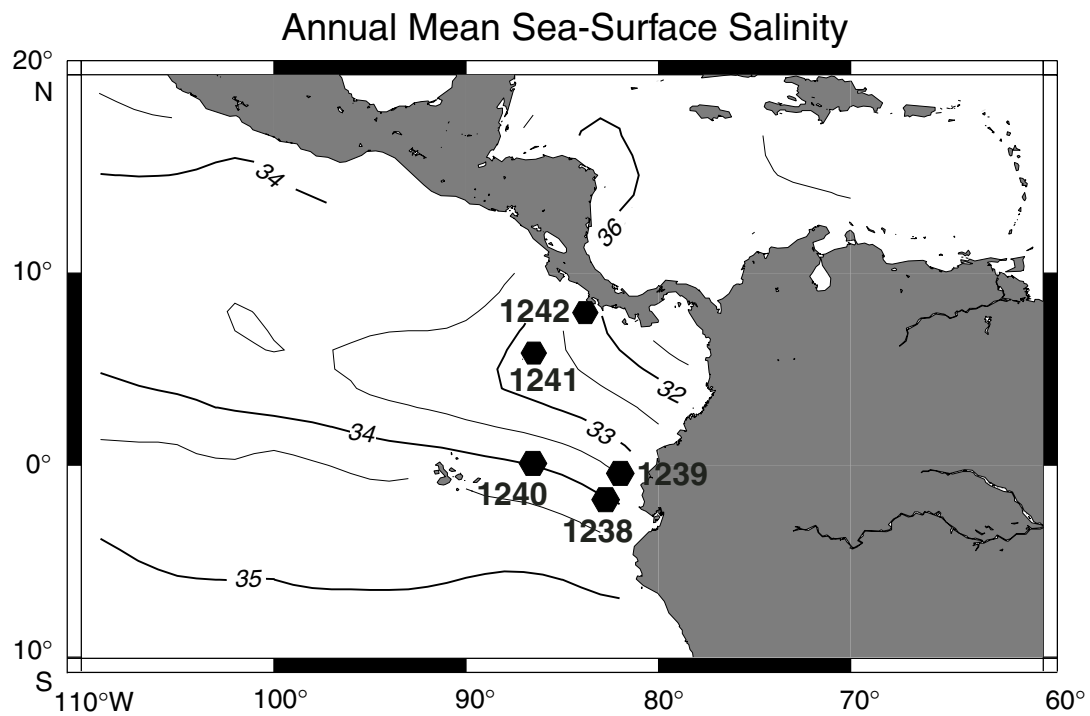


Figure F4. Seismic profile at Site 1242 (*Melville*, NEMO-3, COC-4, line 5, JD158, 6 June 2000; two 150-in<sup>3</sup> gas injection guns; Lyle et al., 2000).



**Figure F5.** Upper-ocean salinity of the eastern tropical Pacific (annual average) (data from Ocean Climate Laboratory, 1999).



**Figure F6.** Chlorophyll distributions in surface waters of the equatorial Pacific, based on satellite color data, reveal that Site 1242 is now within the relatively low production regime associated with termination of the North Equatorial Counter Current near Central America.

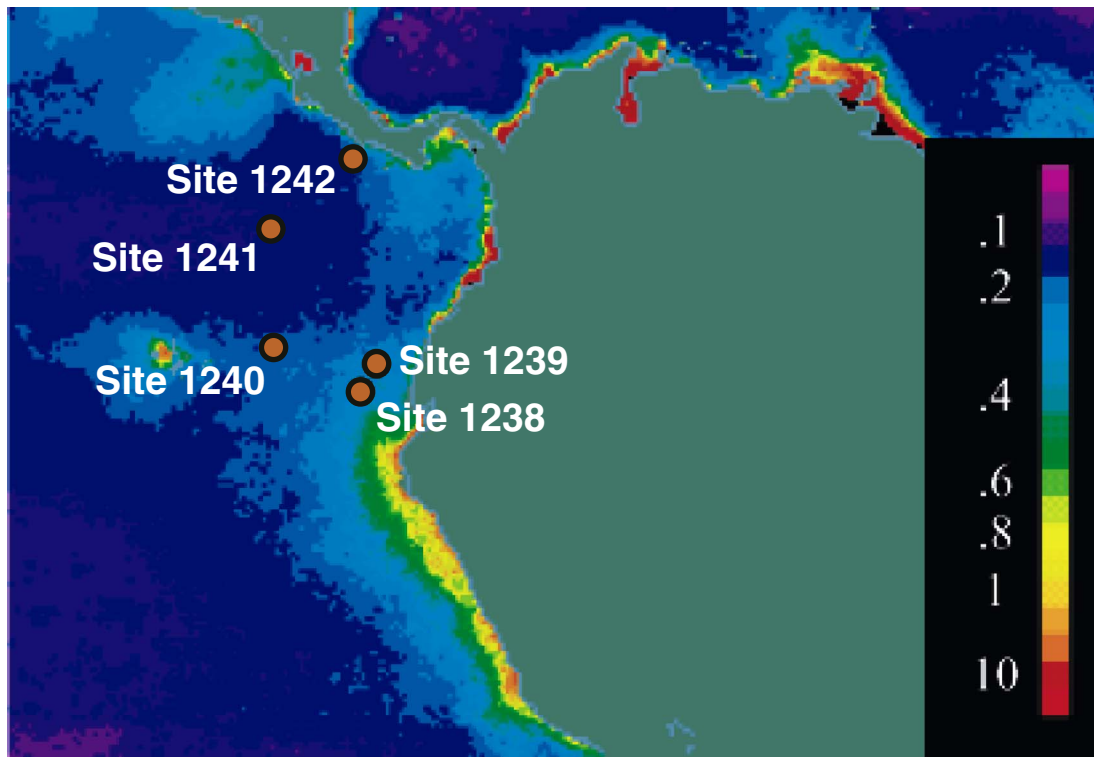


**Figure F7.** Modern annual-average properties of the upper ocean at paleolocations of Site 1242, based on plate tectonic backtracking and an assumption of no temporal changes in regional oceanic properties. Atlas data on physical and chemical properties are from WOA98 (Ocean Climate Laboratory, 1999). Primary productivity (PP) is from satellite measurements of sea-surface color (Behrenfeld et al., 2001). Pycnocline depth is calculated to the nearest 5 m, based on the shallowest maximum in the vertical density gradient. Symbols are average values extracted from the nearest  $1^{\circ}$  latitude-longitude box in each atlas. Lines = smoothed trends of each property along the backtrack path. SST = sea-surface temperature, SSS = sea-surface salinity.

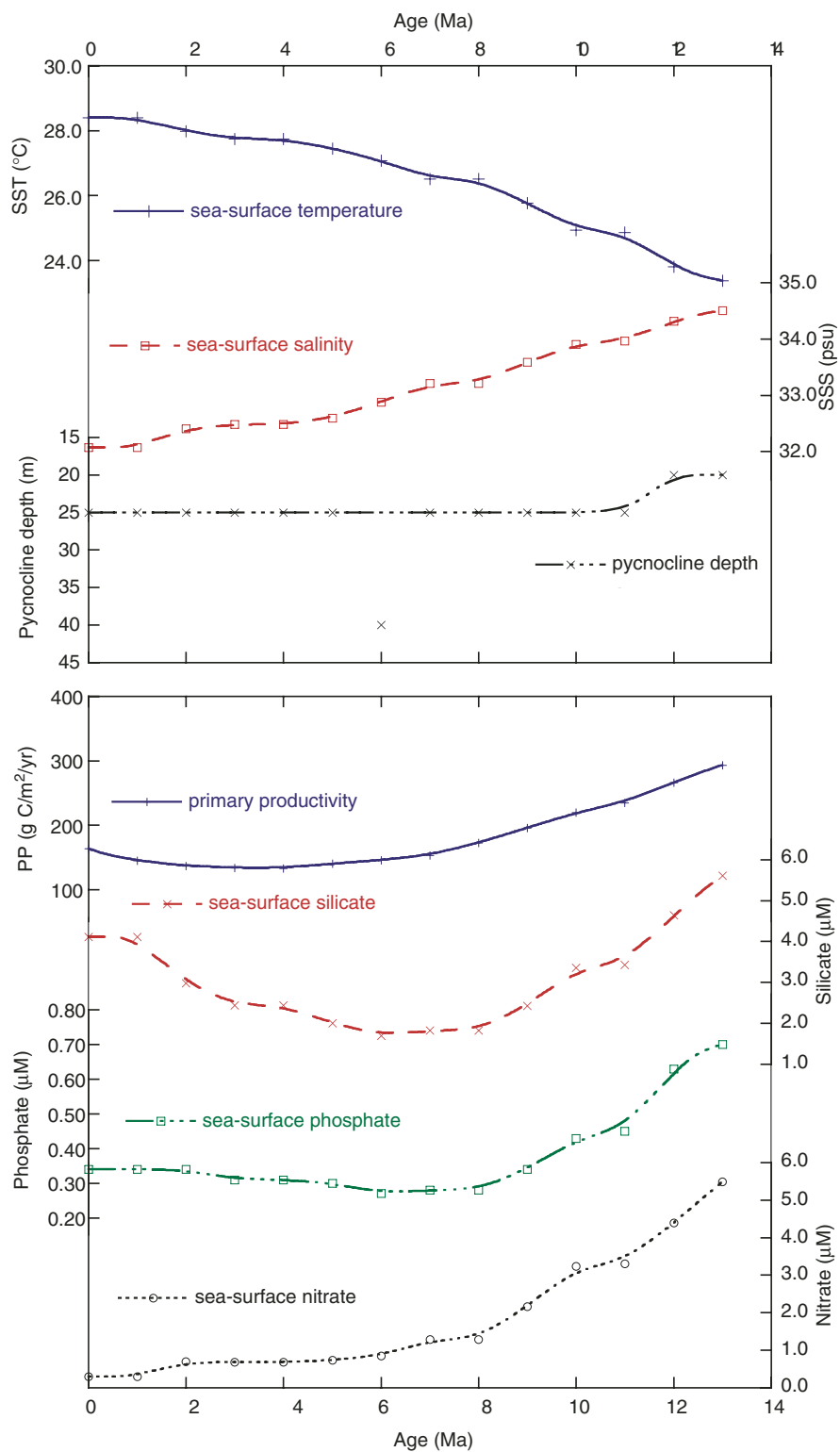


**Figure F8.** Meridional cross section of water masses, characterized by dissolved oxygen concentrations in the tropical East Pacific (Levitus et al., 1993) and Leg 202 site locations. GUC = Gunther Undercurrent, EUC = Equatorial Undercurrent, NPIW = North Pacific Intermediate Water, PCW = Pacific Central Water, PBW = Peru Basin Water. The relatively low oxygen content of water in the Guatemala Basin reflects the water's sources in PCW, relative isolation of water masses within the deep Guatemala Basin, and high organic rain on the Central American margin.

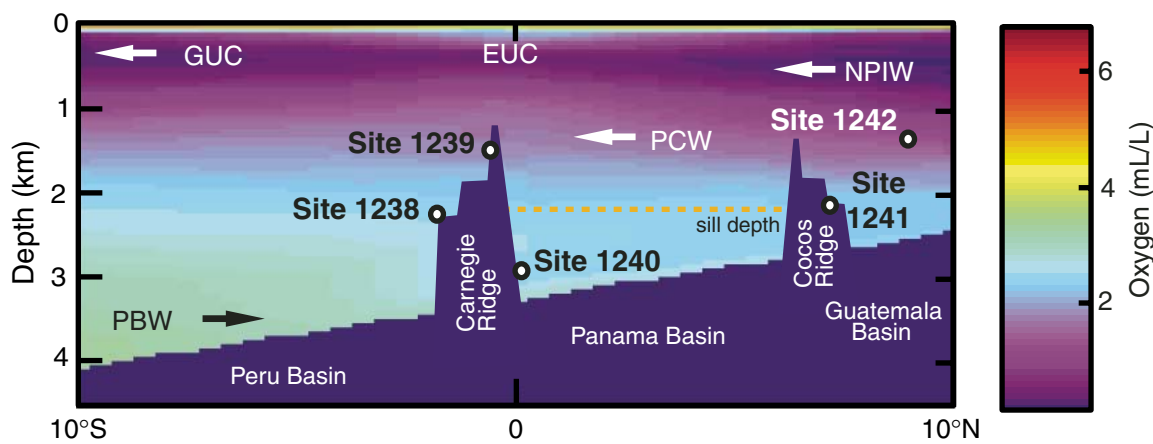


**Figure F9.** OSU Fast Track magnetic susceptibility data (OSUS-MS) or whole-core multisensor track magnetic susceptibility data (MST-MS) vs. mcd for the spliced record and Holes 1242A (black), 1242B (red), and 1242C (green). OSUS-MS are linearly adjusted approximately to the scale of the MST track by multiplying by a factor of 1.6. Gray boxes indicate the portions of cores that are in the splice. Pink boxes indicate areas of uncertainty in the composite section and the splice. A. 0–40 mcd. B. 30–70 mcd. (Continued on next five pages.)

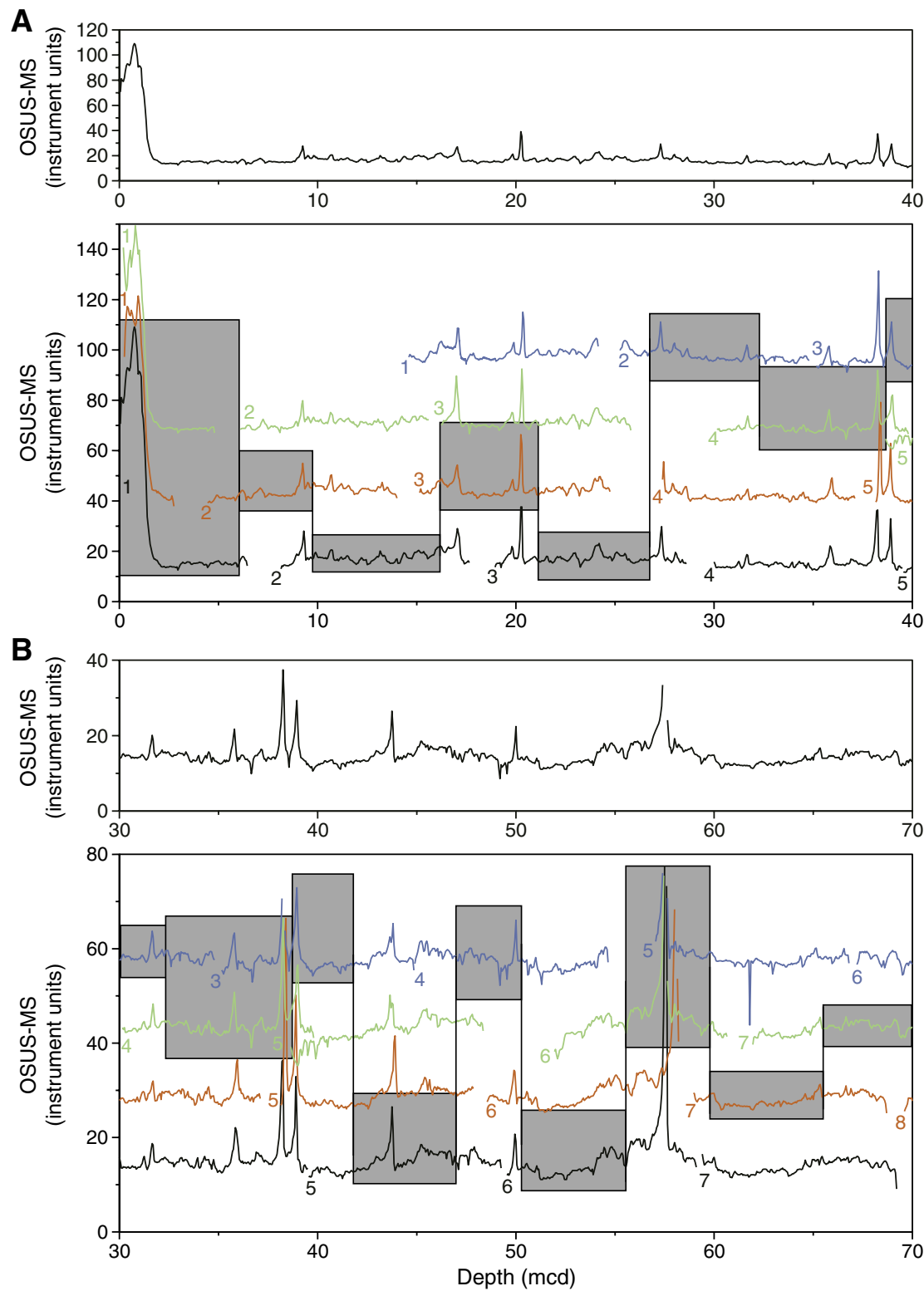


Figure F9 (continued). C. 60–100 mcd. D. 90–130 mcd.

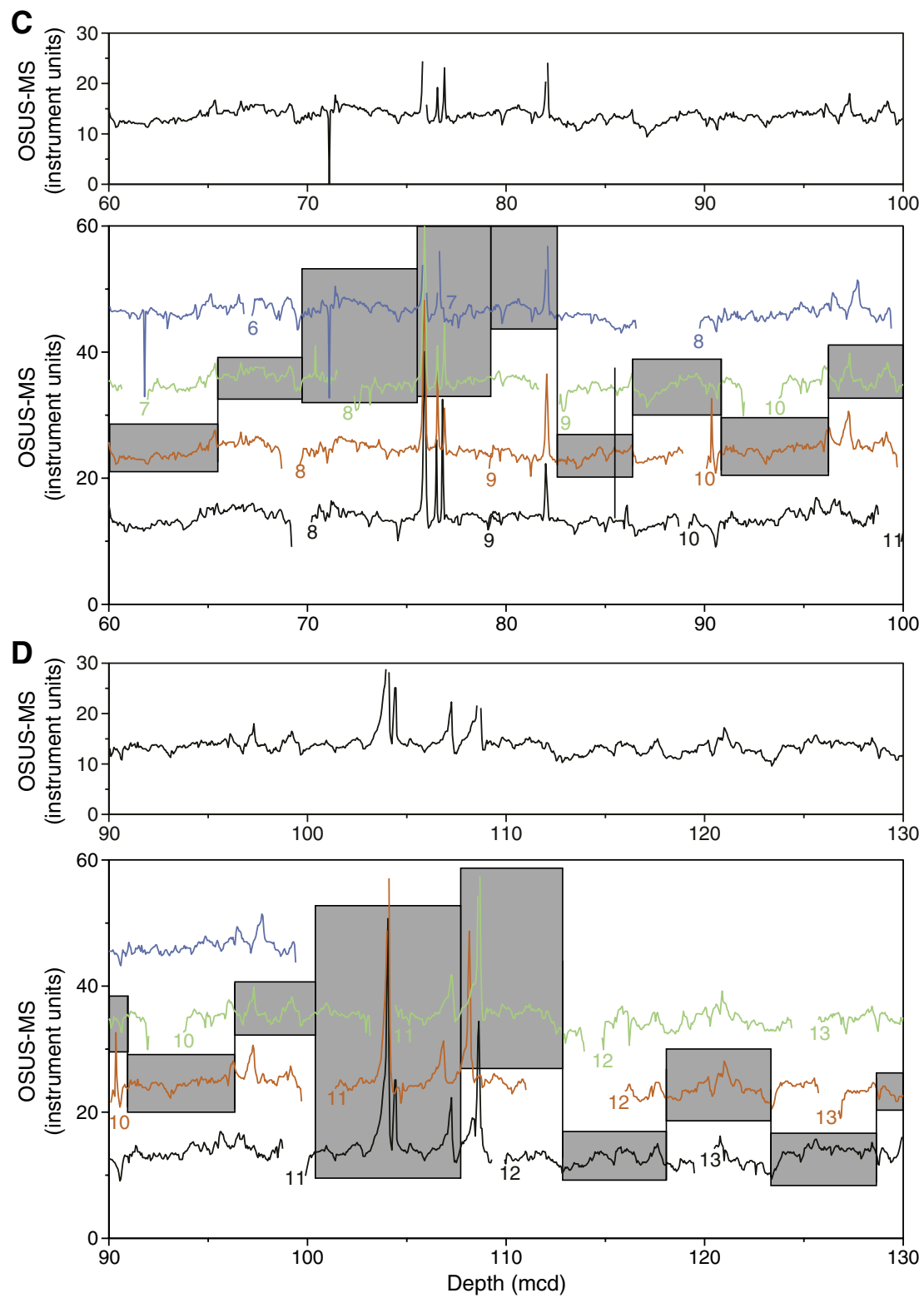


Figure F9 (continued). E. 120–160 mcd. F. 150–190 mcd.

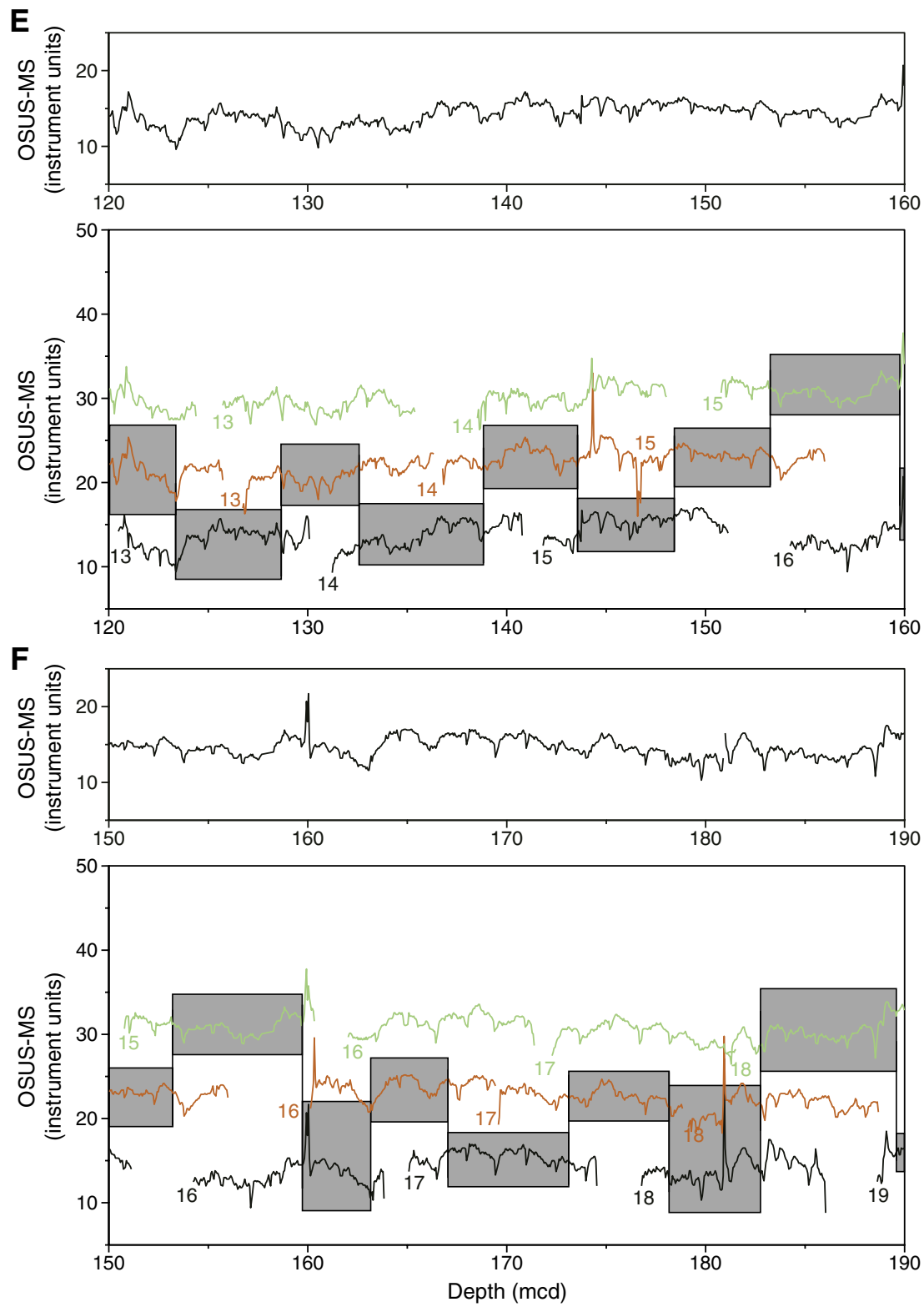
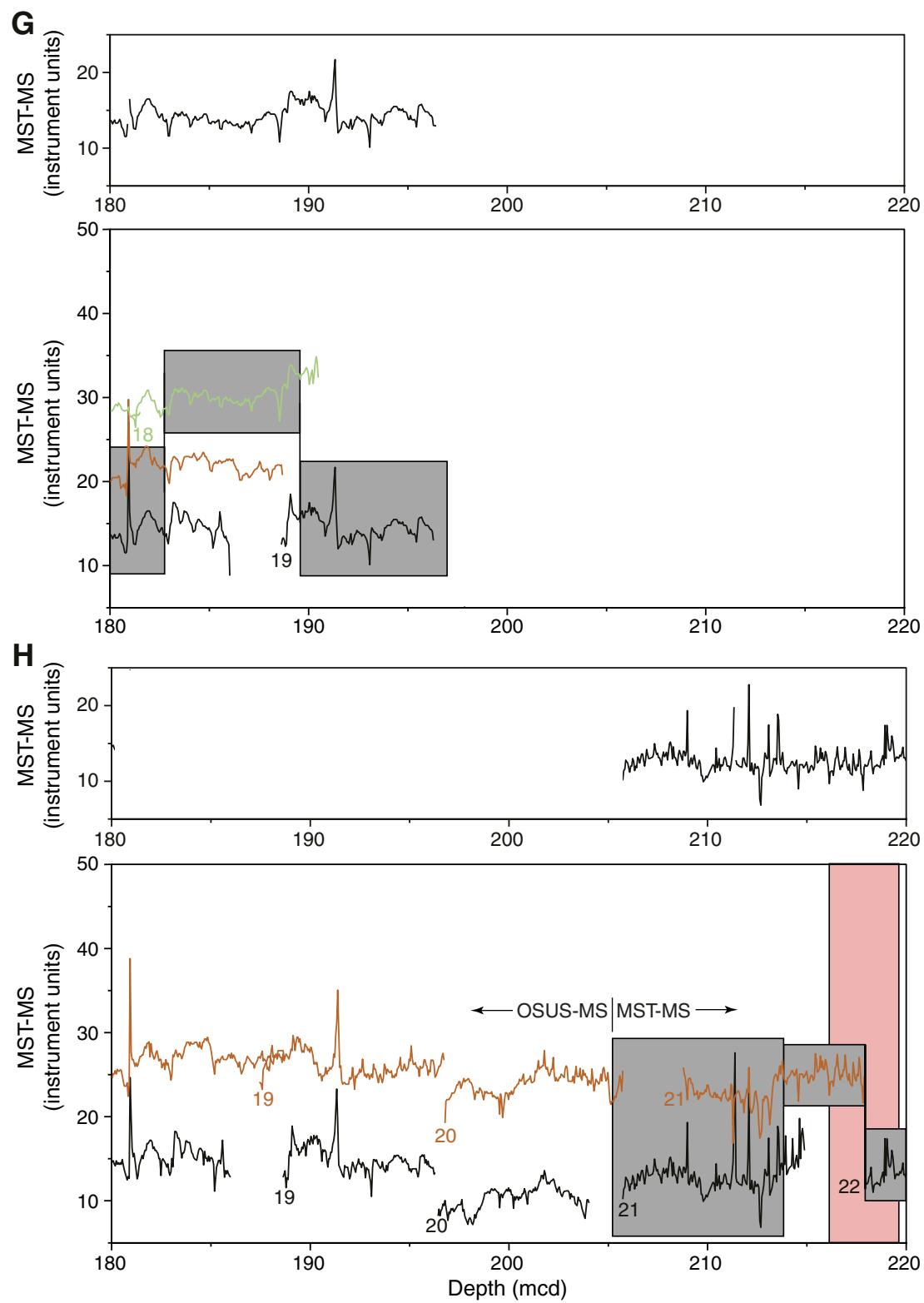
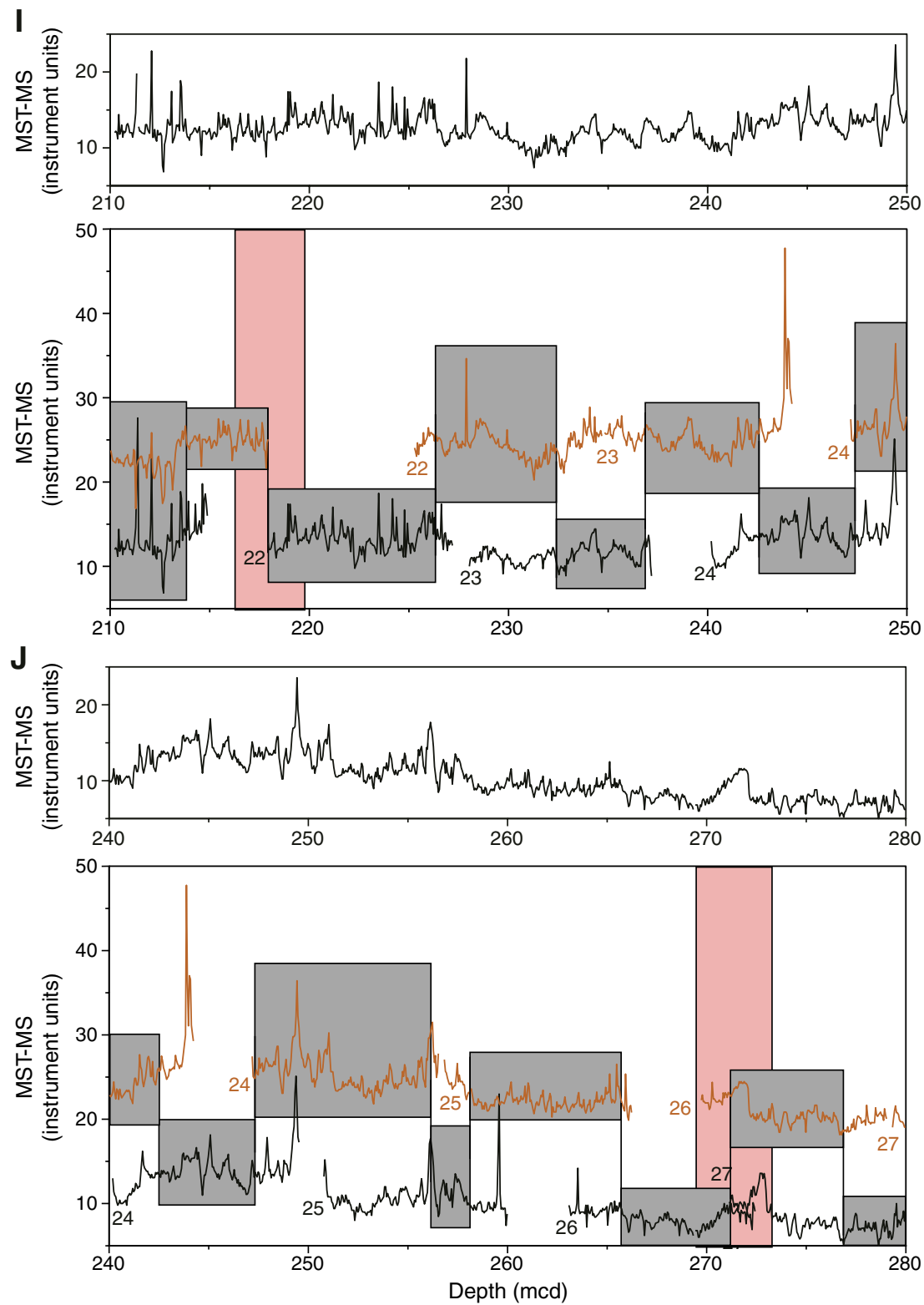


Figure F9 (continued). G. 180–220 mcd. H. 180–220 mcd.



**Figure F9 (continued). I. 210–250 mcd. J. 240–280 mcd.**



**Figure F9 (continued). K.** 270–310 mcd.

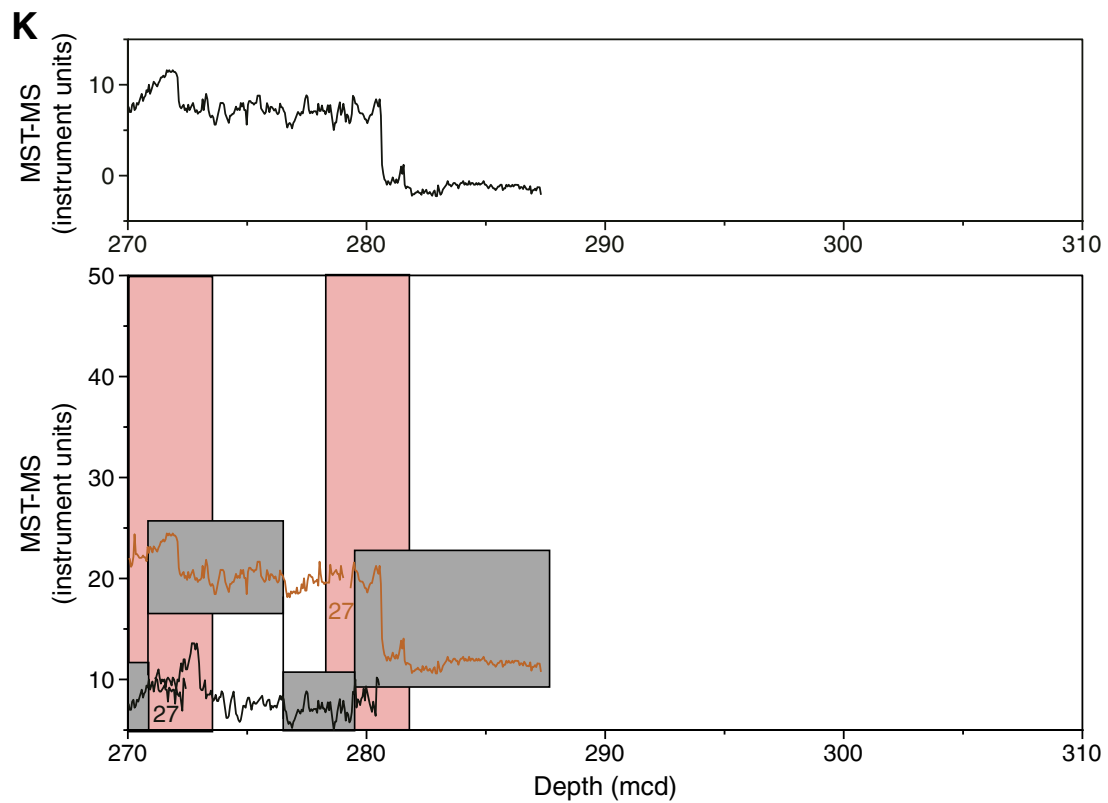


**Figure F10.** Smoothed (9-point Gaussian) records of natural gamma radiation (NGR), gamma ray attenuation (GRA) bulk density, and magnetic susceptibility (MST-MS) from the splice and floating splice for Site 1242.

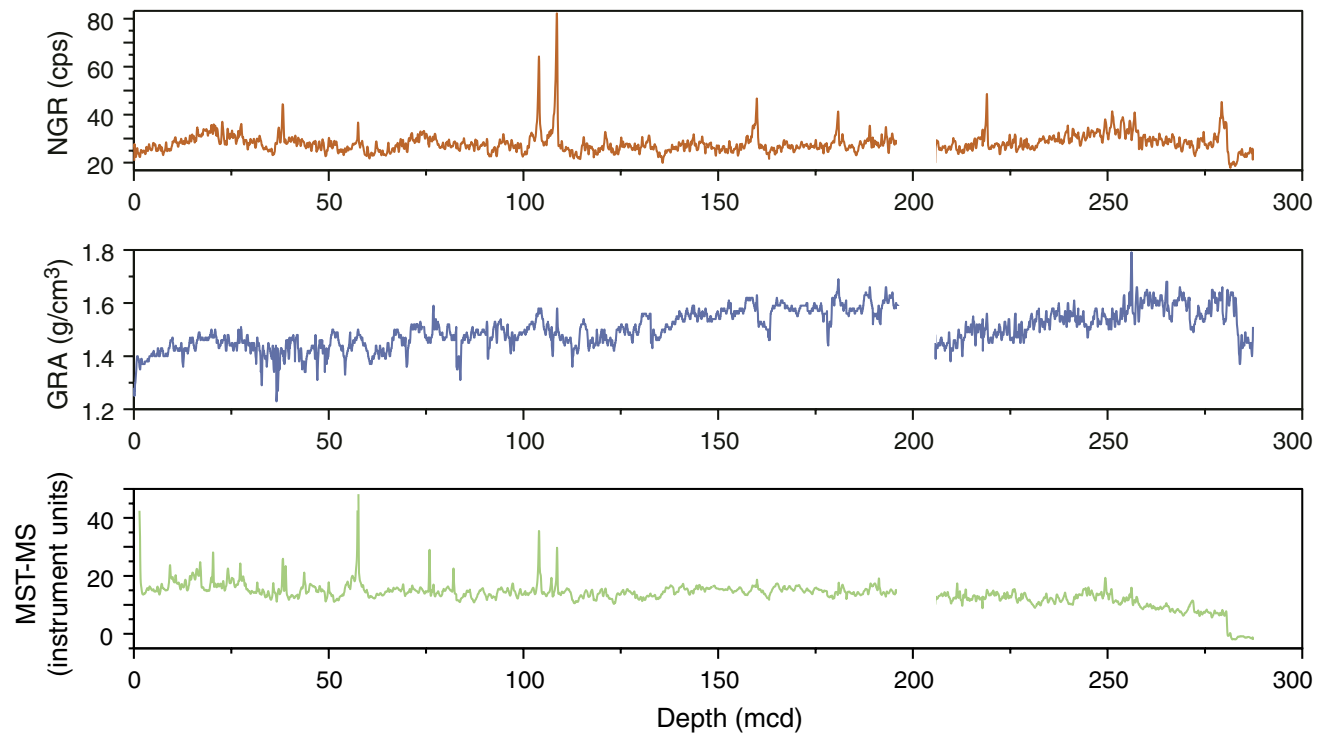
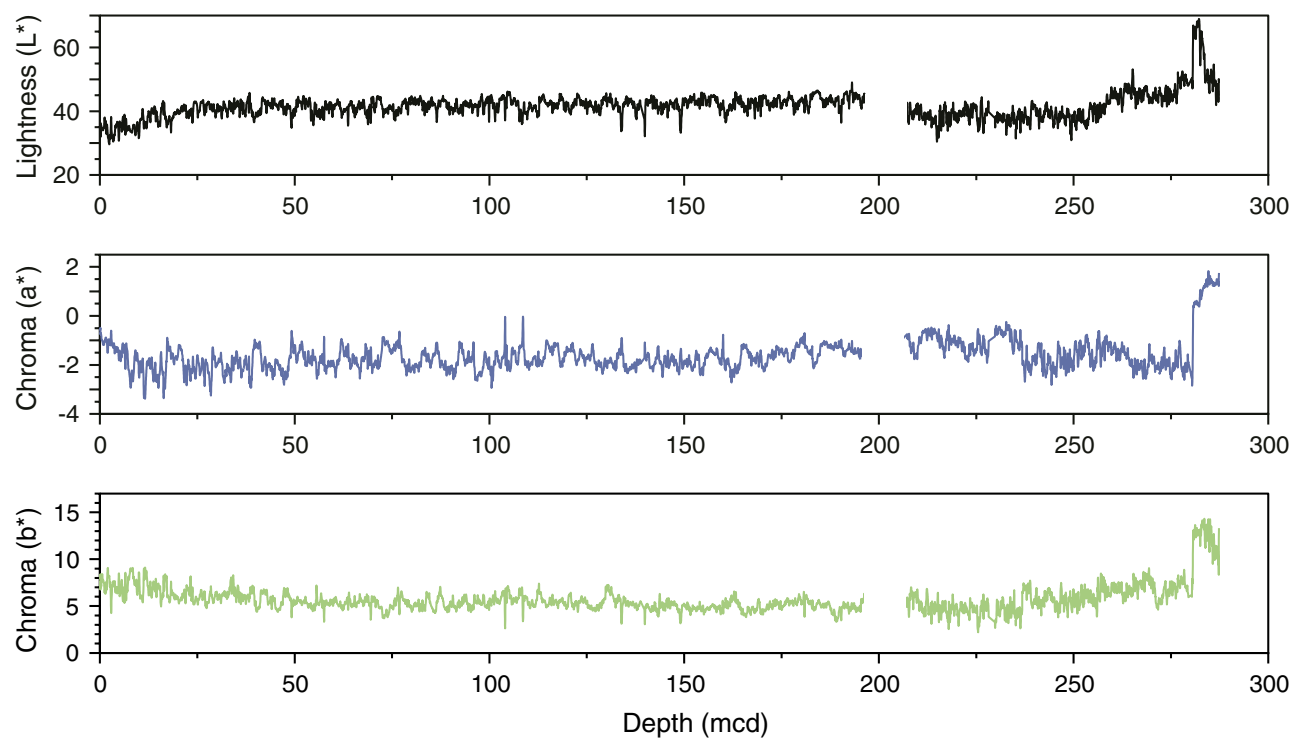
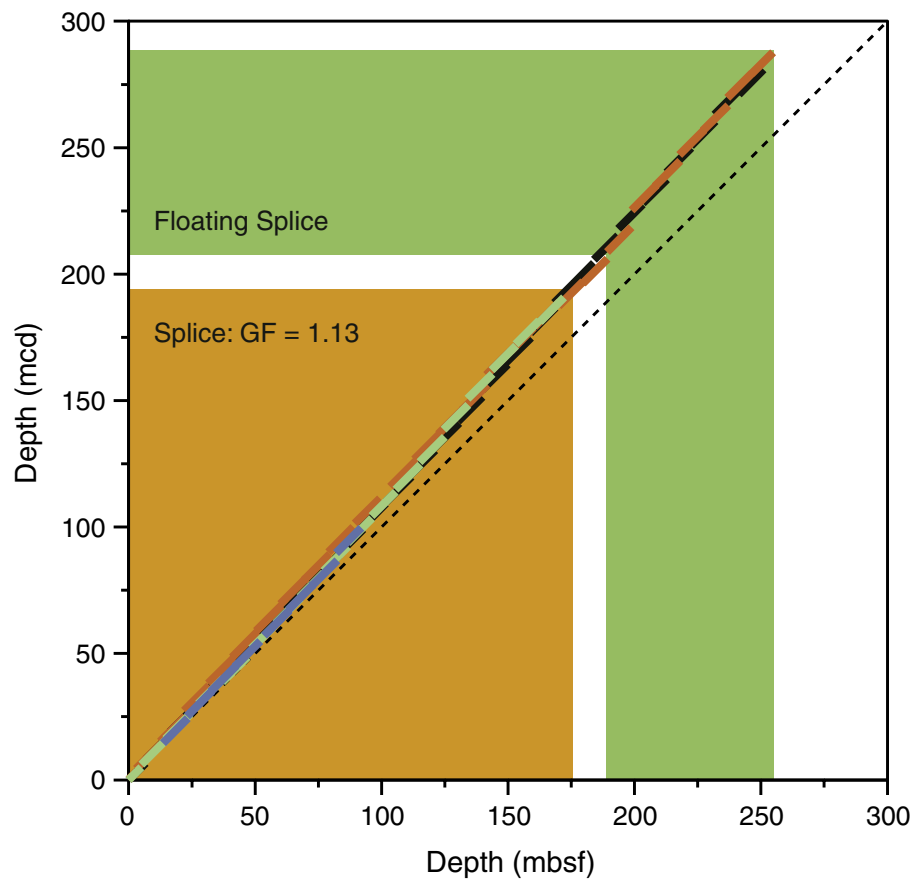


Figure F11. Smoothed (9-point Gaussian) spliced records of color reflectance from Site 1242: L\*, a\*, and b\*.



**Figure F12.** A comparison of the drillers depth (mbsf) and meters composite depth (mcd) scales in Holes 1242A through 1242C. On average, mcd is 13% greater than mbsf in the splice. The 1:1 (mbsf:mcd) line is also shown for comparison. The orange box shows the range of the splice and the green shading shows the range of the floating splice. GF = growth factor.



**Figure F13.** Core recovery, lithostratigraphic units, age, magnetic susceptibility, gamma ray attenuation (GRA) bulk density, natural gamma radiation (NGR), color reflectance ( $L^*$ ),  $\text{CaCO}_3$ , and total organic carbon (TOC) of sediments recovered from Site 1242. Gray lines = original data, black lines = 50-point smoothing averages of the original data.

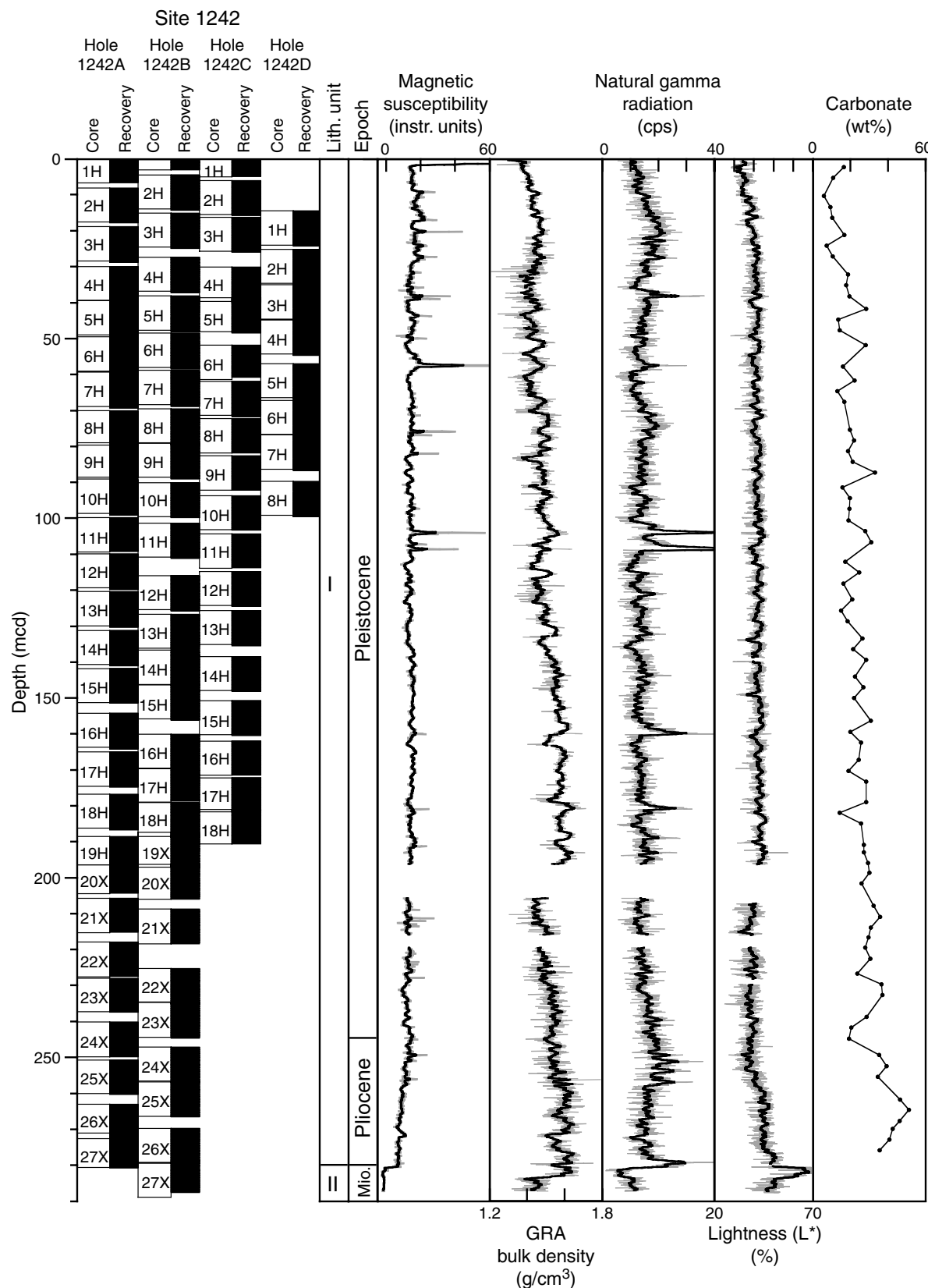


**Figure F14.** Major siliciclastic, volcaniclastic, and authigenic components observed in Hole 1242A smear slides (only dominant lithologies) vs. magnetic susceptibility and natural gamma radiation (NGR). Ash layers from Site 1242 are denoted by circles on the volcanic glass plot. Solid circles = ash layers observed in more than one hole, open circles = ash layers observed only in one hole.

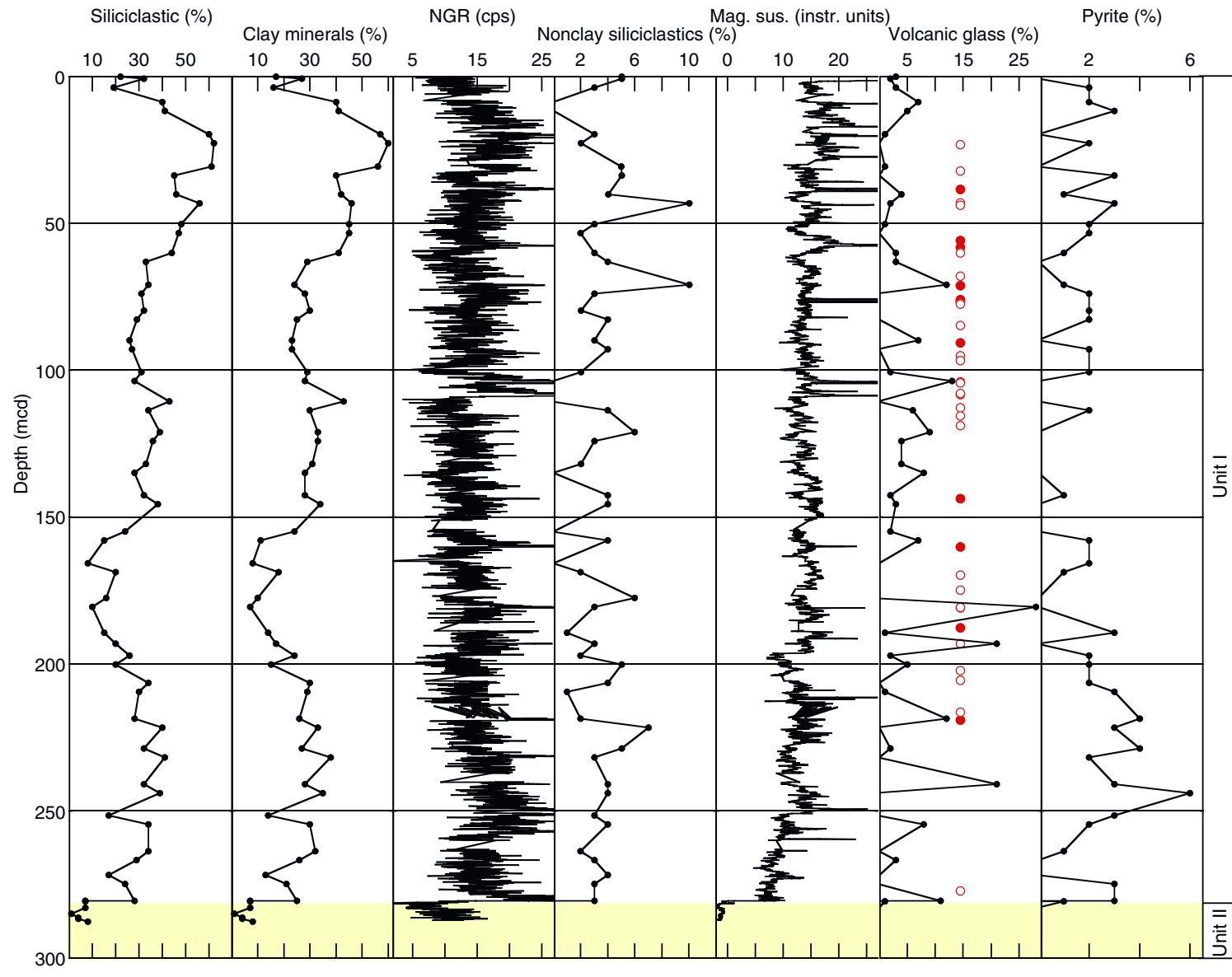


**Figure F15.** Major biogenic components observed in smear slides from Hole 1242A (only dominant lithologies) vs.  $\text{CaCO}_3$  concentrations. Rad. = radiolarians, Silicof. = silicoflagellates.

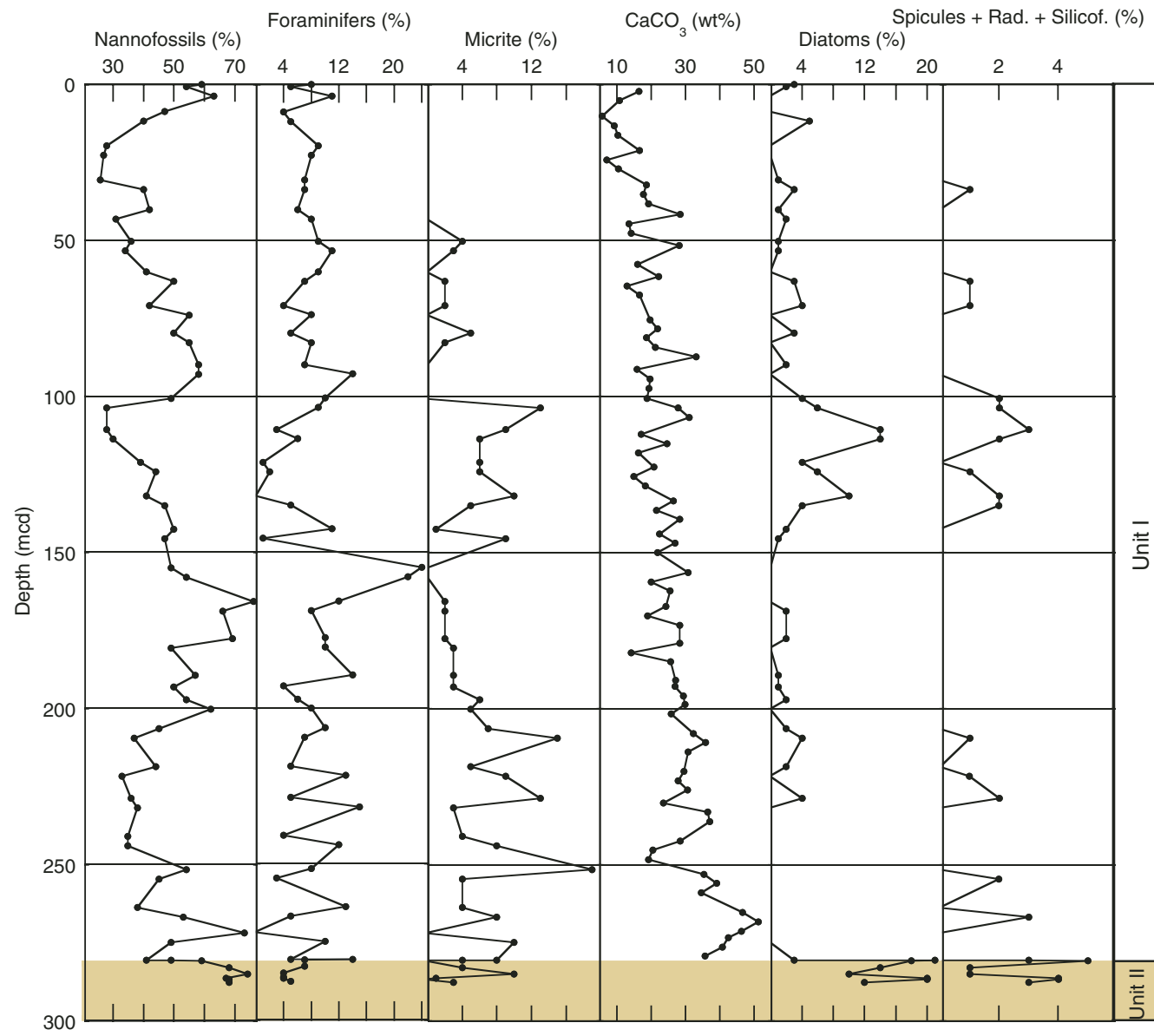


**Figure F16.** Close-up photograph of Unit I major lithology showing homogeneous grayish olive-green color, burrows, and spicule aggregates (interval 202-1242B-2H-6, 67–81 cm).



**Figure F17.** Close-up photograph of dark layer of the pennate diatom *Ethmodiscus* (interval 202-1242A-21X-5, 88-105 cm).

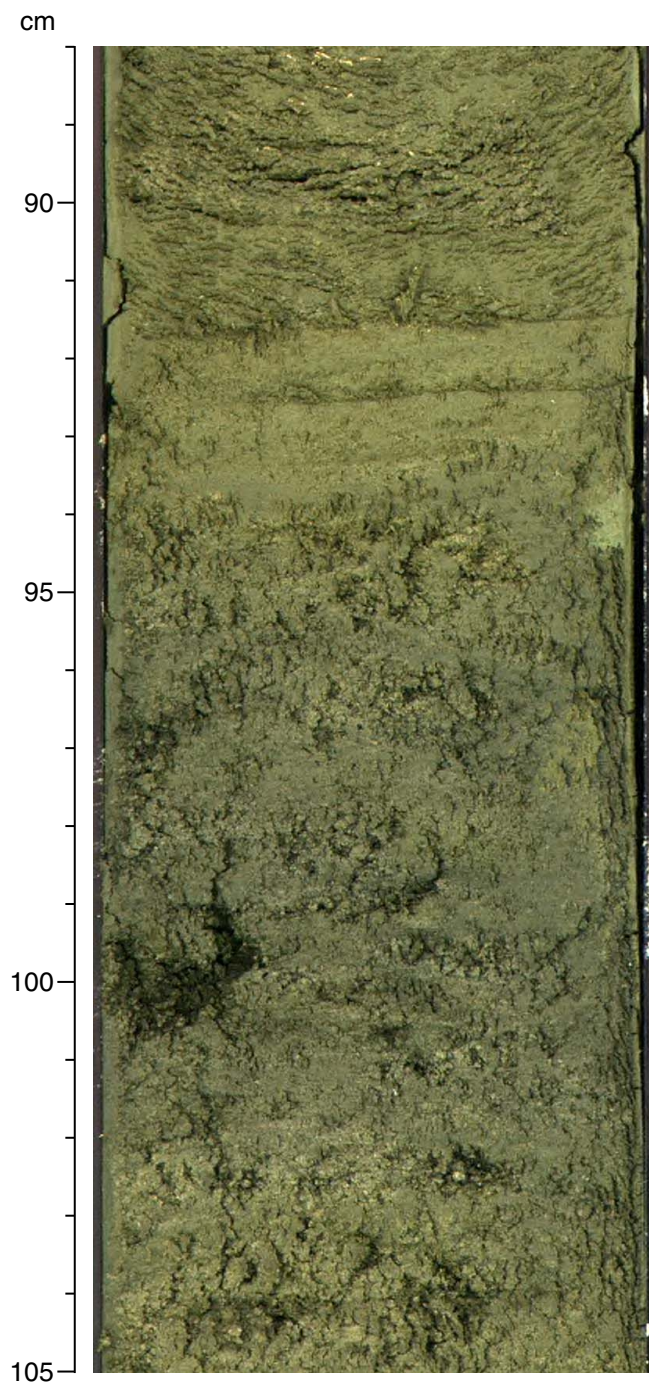


**Figure F18.** Close-up photograph of volcanic ash layer in Unit I showing sharp basal and diffuse upper contacts (interval 202-1242A-18H-3, 112–125 cm).

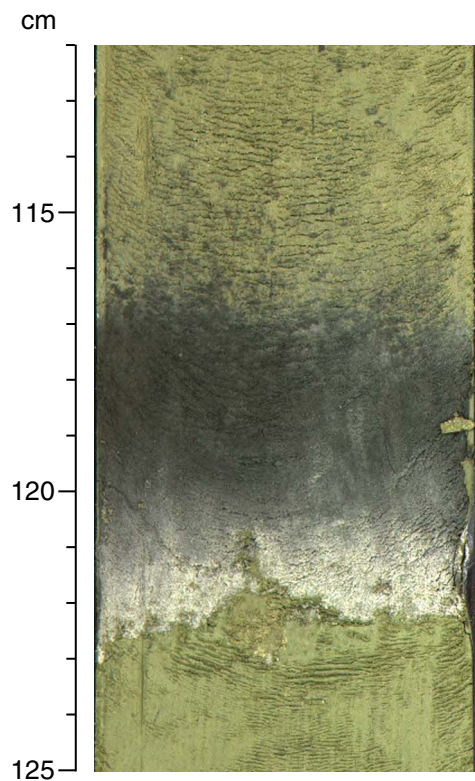


**Figure F19.** Color reflectance measurements at Site 1242 A. Measurements of  $a^*$  plotted with depth.  
B. Measurements of  $b^*$  plotted with depth. (Continued on next page.)

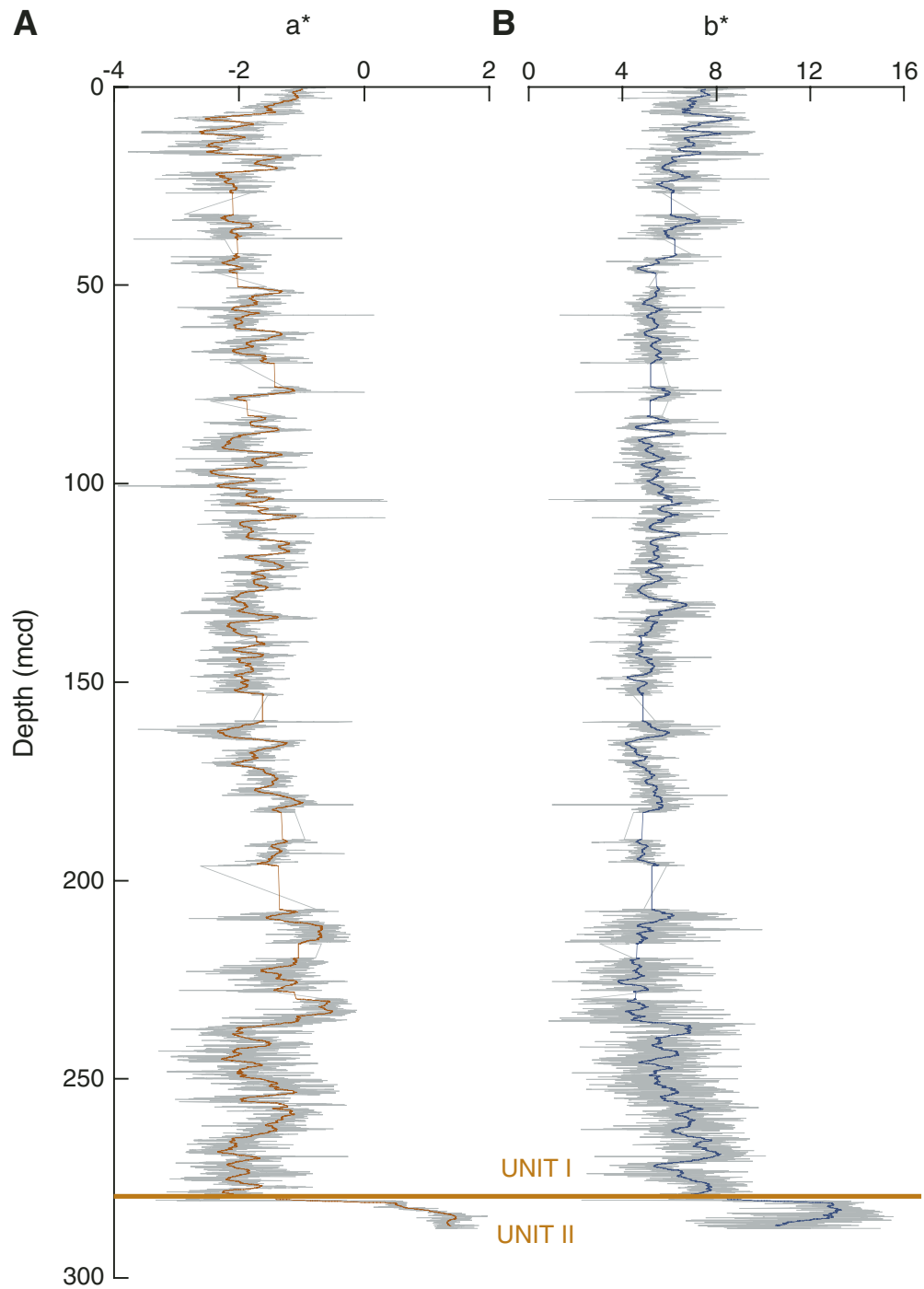


**Figure F19 (continued).** C. Unit I sediment plotted in the  $a^*$ - $b^*$  color plane. D. Unit II sediment plotted in the  $a^*$ - $b^*$  color plane.

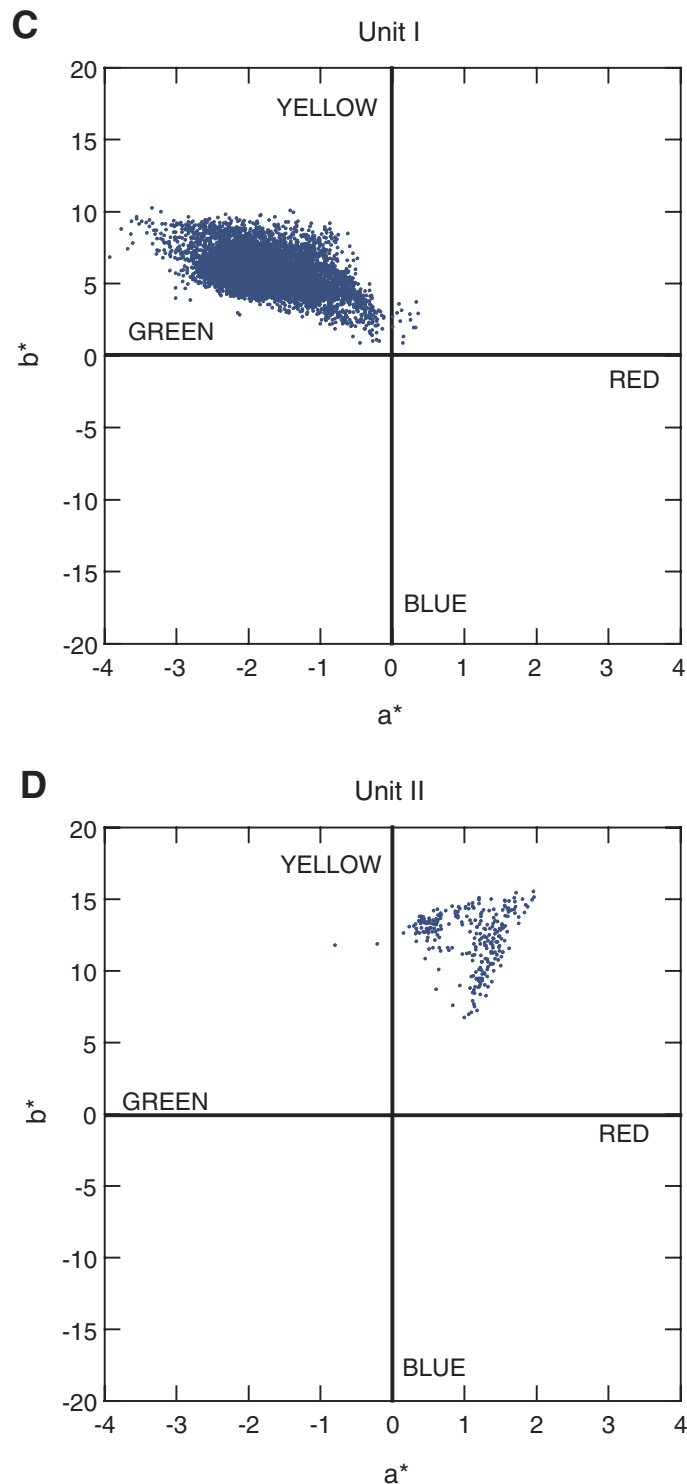


**Figure F20.** Physical properties measurements for Site 1242. A. Gamma ray attenuation (GRA) bulk density (line) and moisture and density (MAD) bulk density (symbols). Thin line = raw data, red line = smoothed record. B. Porosity. C. Grain density. D. Correlation between interpolated GRA and discrete MAD bulk density measurements. E. Correlation between MAD bulk density and porosity. F. Correlation between  $\text{CaCO}_3$  and grain density.

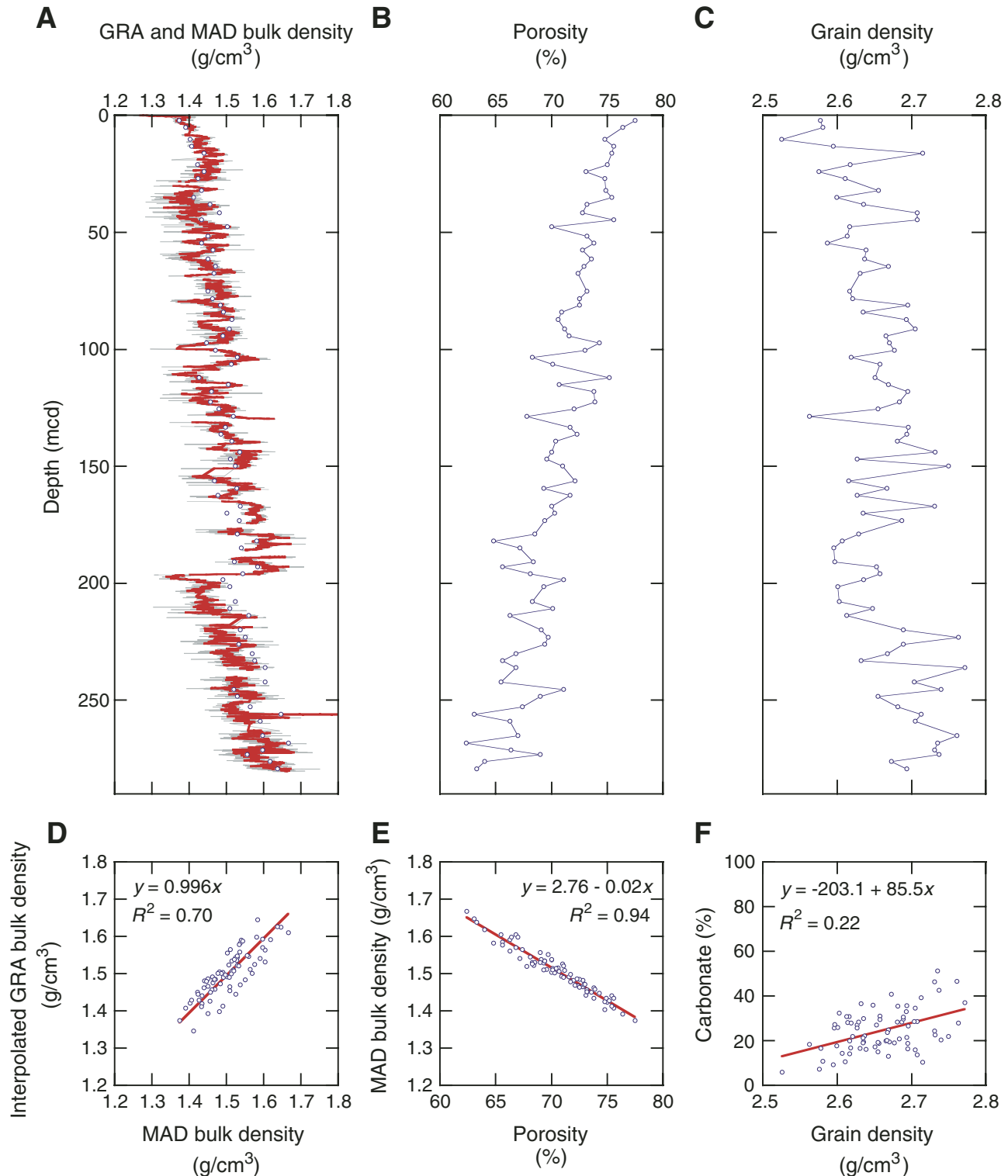


**Figure F21.** Close-up photograph showing lithologic unit boundary associated with 9.5-m.y. hiatus (Core 202-1242B-27X-2, 21–46 cm).

cm

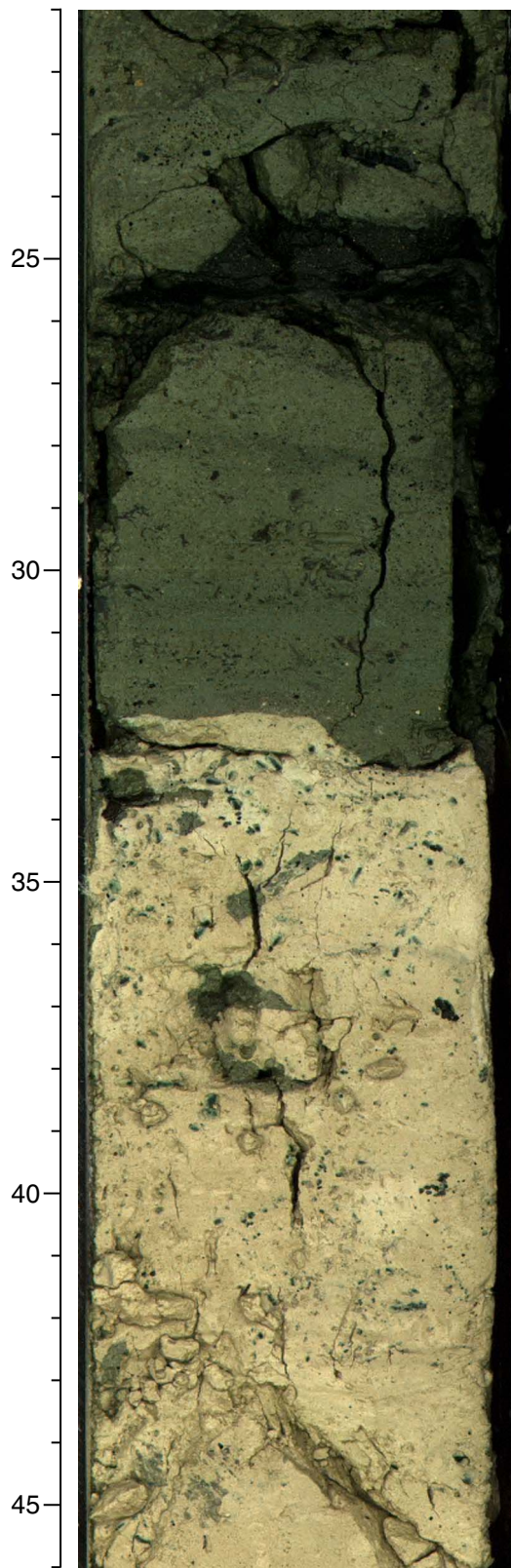


**Figure F22.** Core recovery, calcareous nannofossil and planktonic foraminifer abundance, benthic foraminifer percentage of total foraminifers, and diatom abundance at Site 1242. R = rare, F = few, C = common, A = abundant.

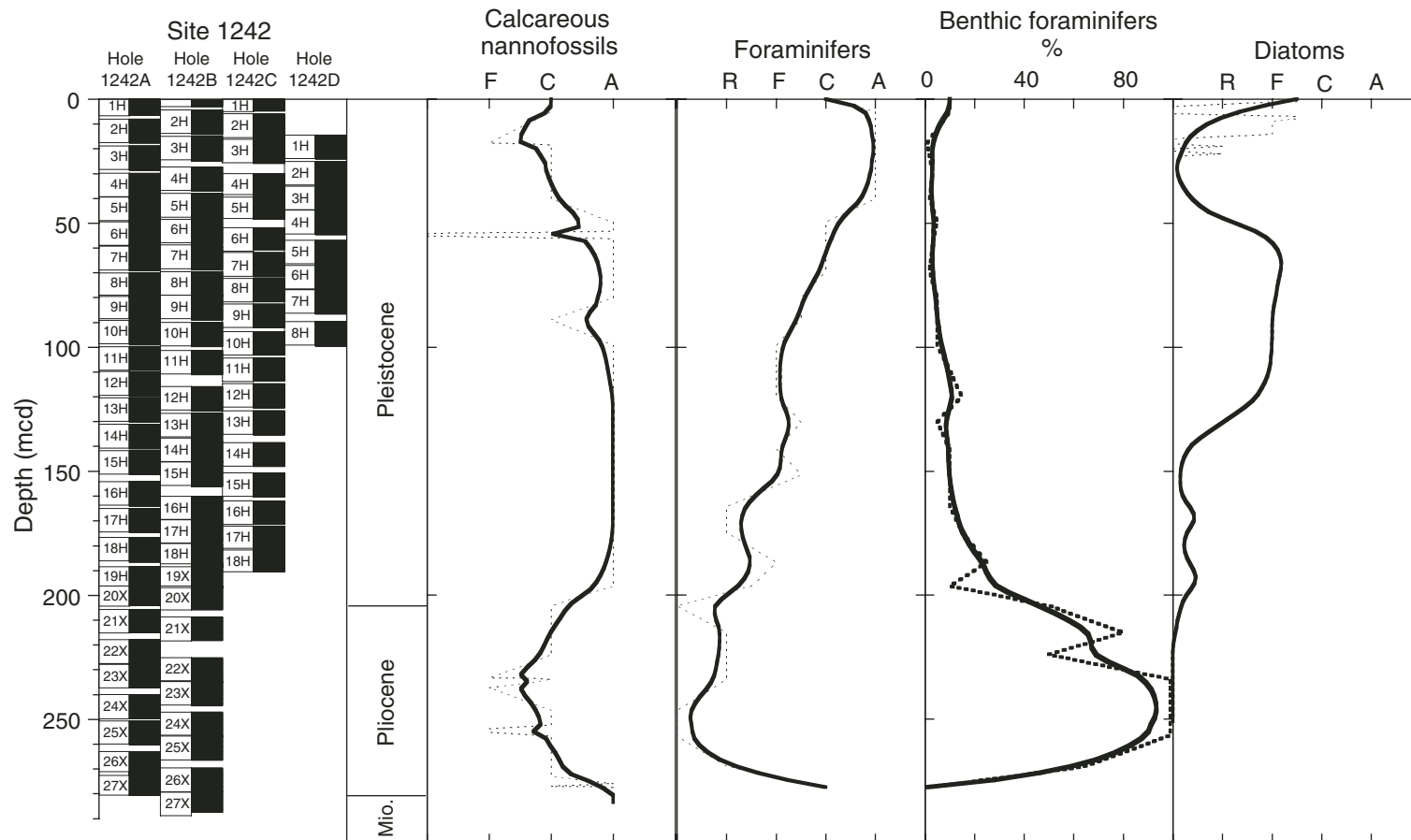


**Figure F23.** Site 1242 natural remanent magnetization (NRM) intensity before (black) and after (blue) AF demagnetization at peak fields of 20 mT vs. depth.

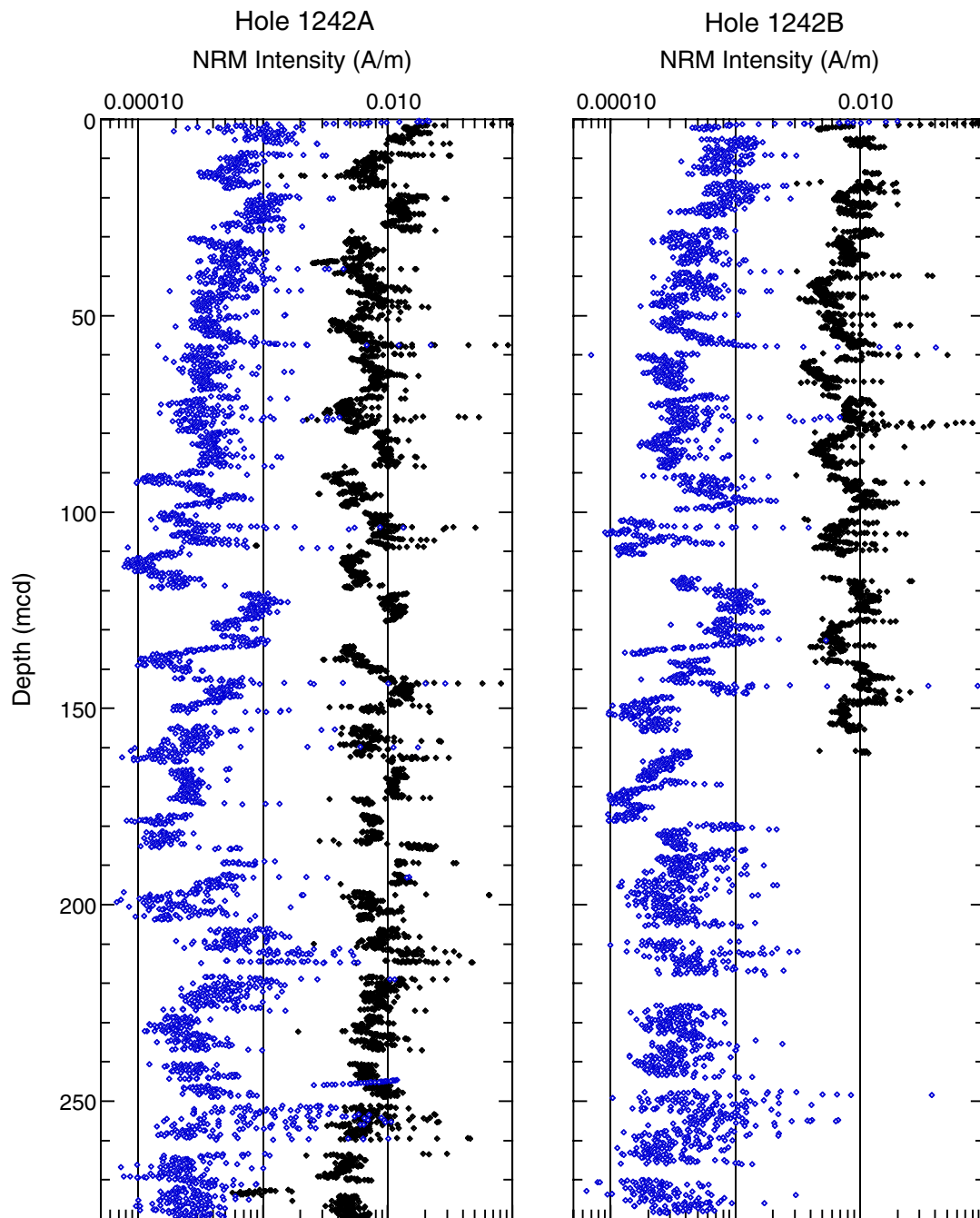


**Figure F24.** Site 1242 inclination after demagnetization at peak alternating fields of 20 mT vs. depth.

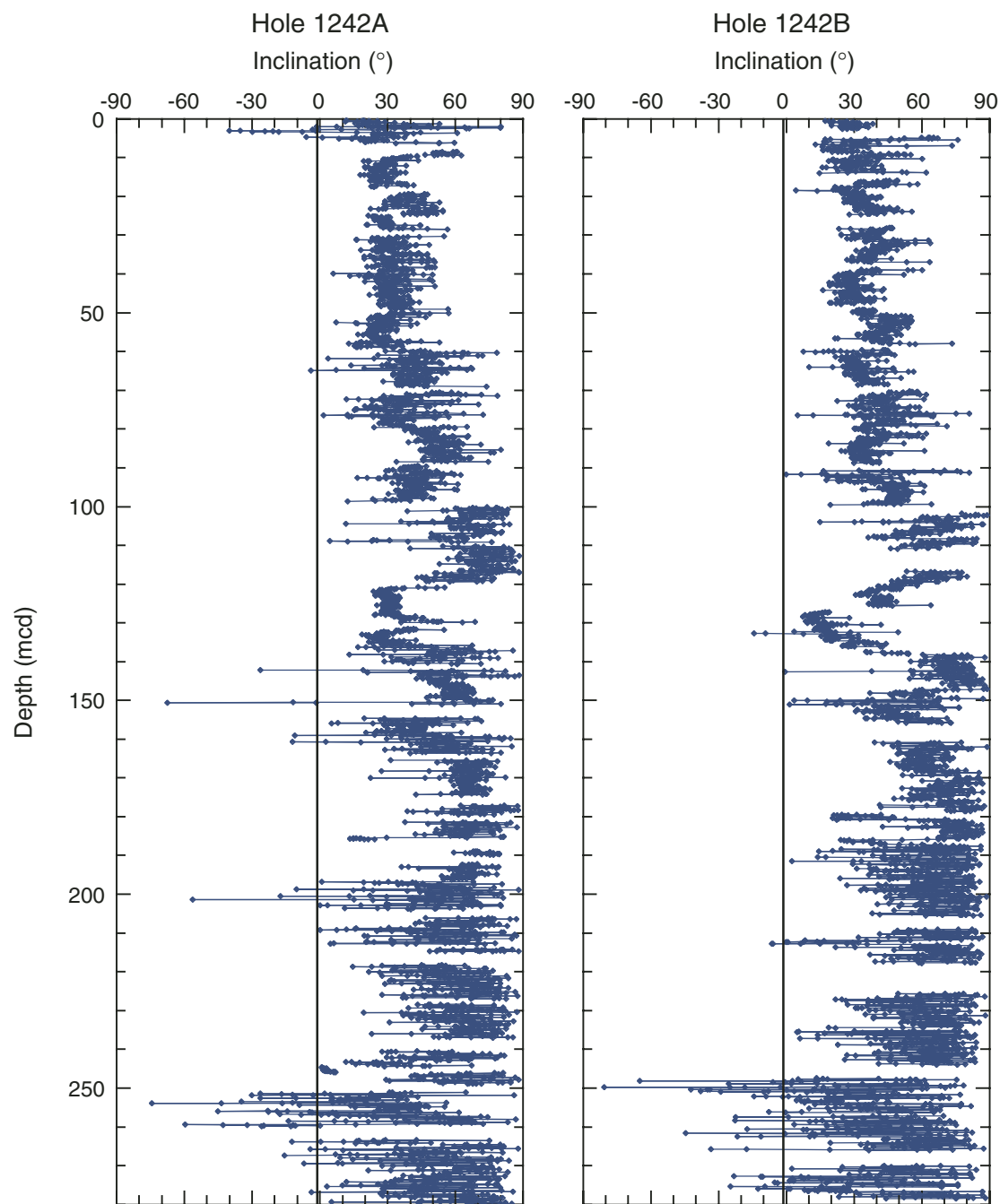


**Figure F25.** Site 1242 declination after demagnetization at peak alternating fields of 20 mT vs. depth.

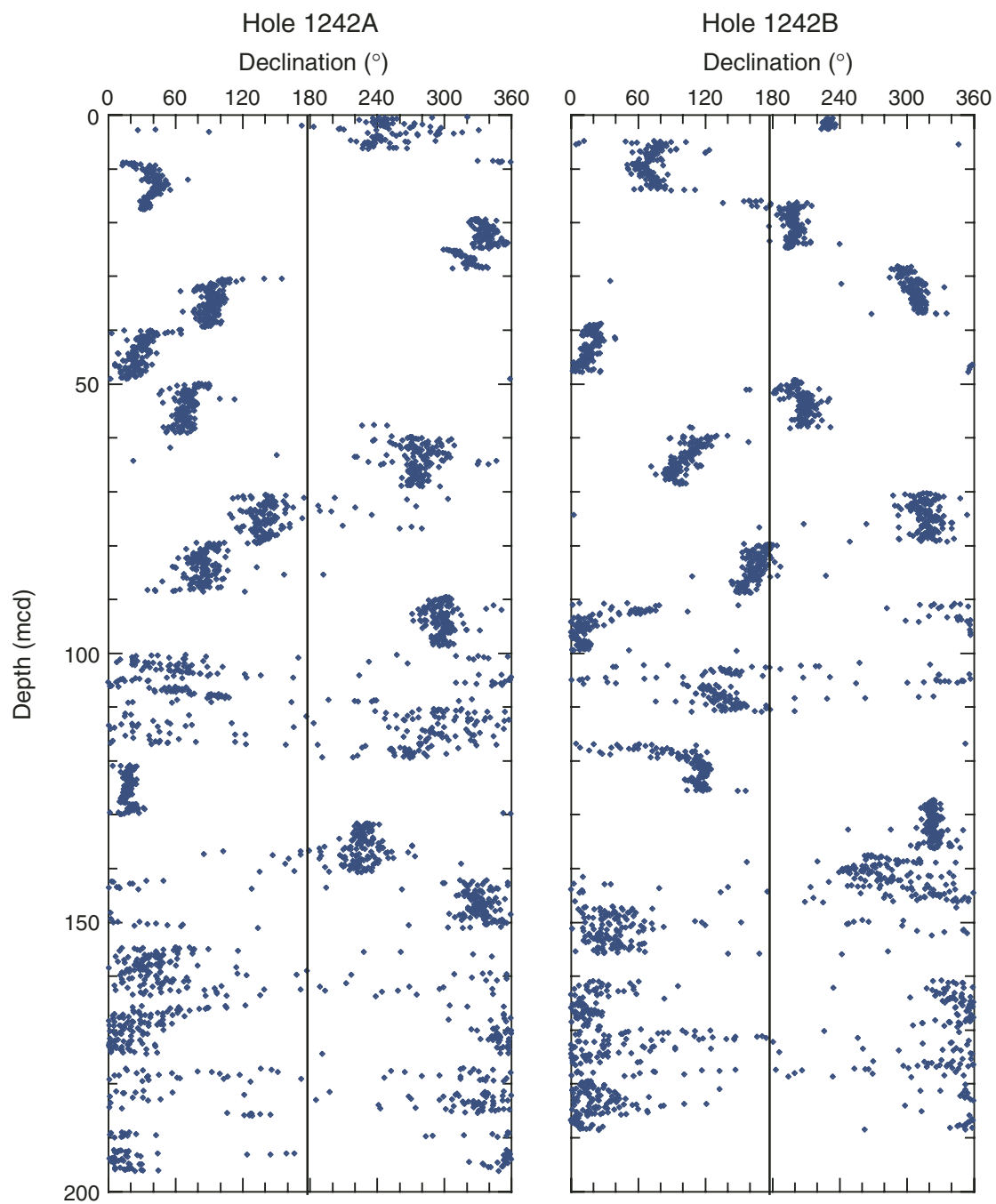


**Figure F26.** Headspace methane ( $C_1$ ) concentrations in sediments vs. depth for Hole 1242A.

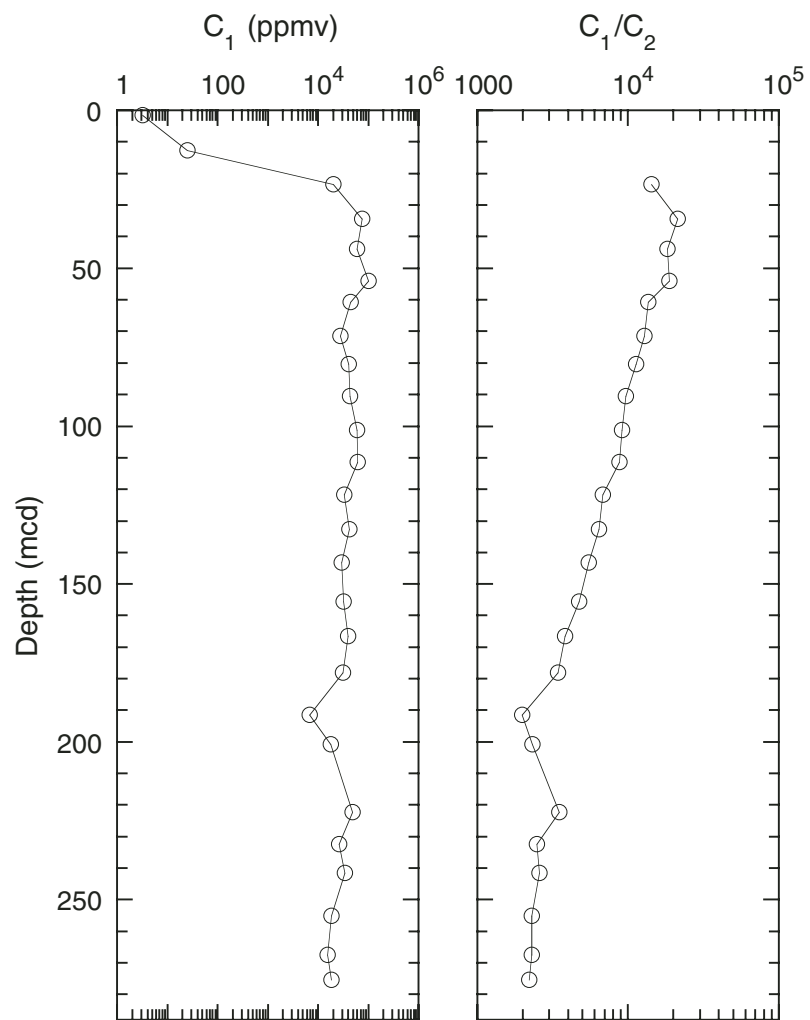


**Figure F27.** Interstitial water geochemical data for Site 1242. Open squares = calcium concentrations. Horizontal line indicates the lithologic unit boundary (see “[Description of Lithologic Units](#),” p. 6, in “Lithostratigraphy”). Values below the detection limits (sulfate = 0.6 mM, phosphate = 0.2 µM, ammonium = 0.42 mM, and barium = 0.1 µM) are plotted at zero.

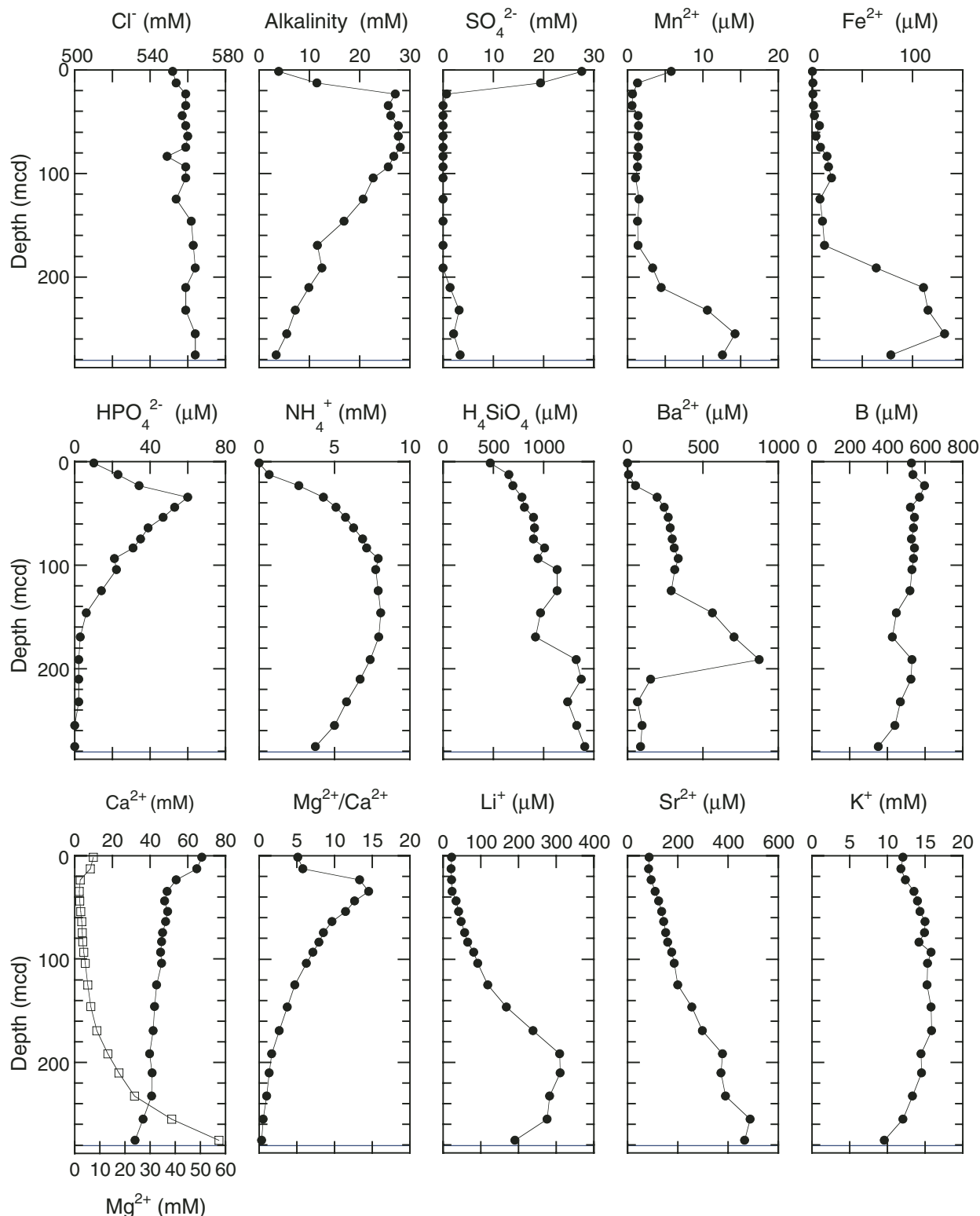


**Figure F28.** Calcium carbonate ( $\text{CaCO}_3$ ), total organic carbon (TOC), and total nitrogen (TN) concentrations, and TOC/TN ratio vs. depth in sediments from Hole 1242A.

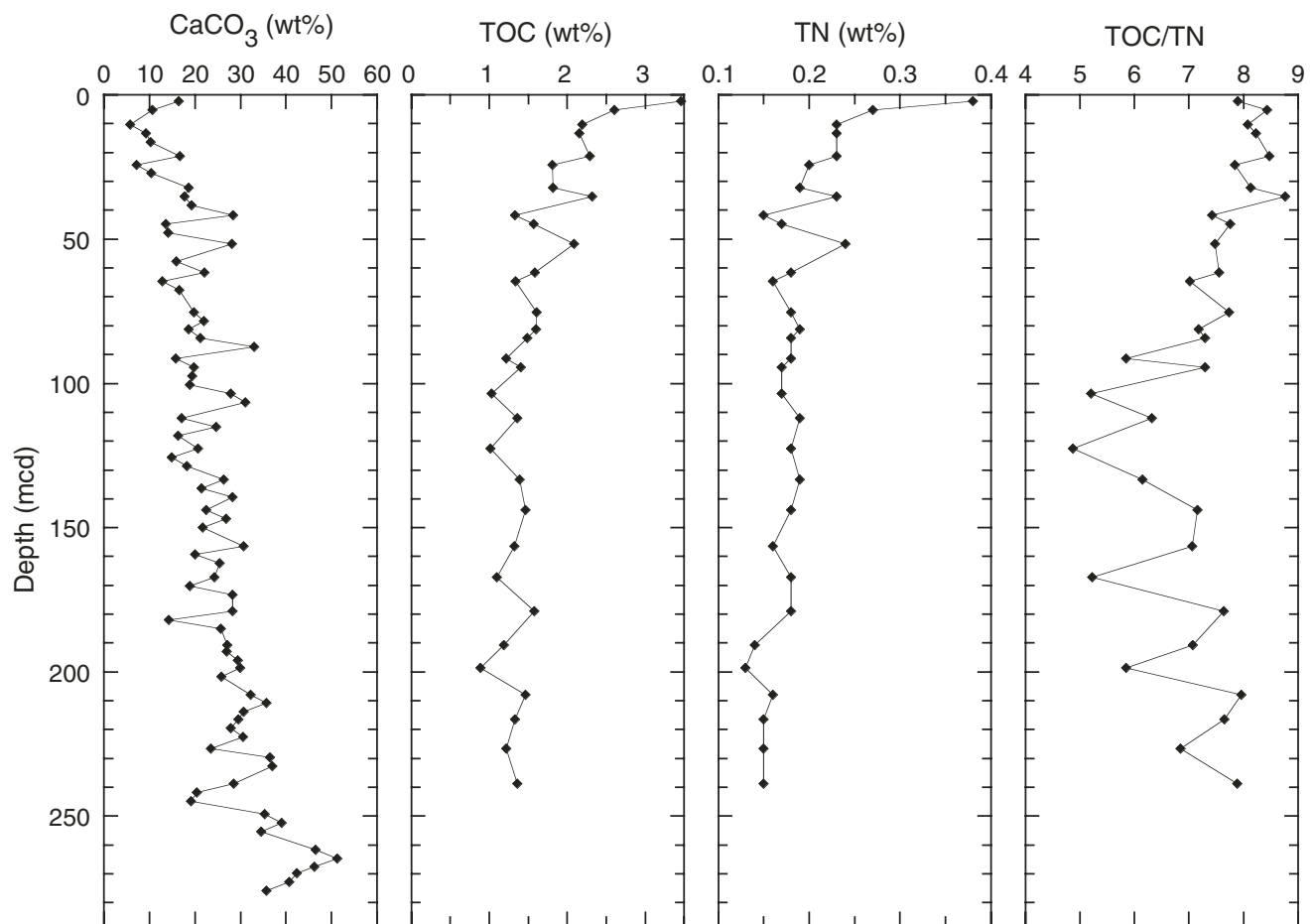
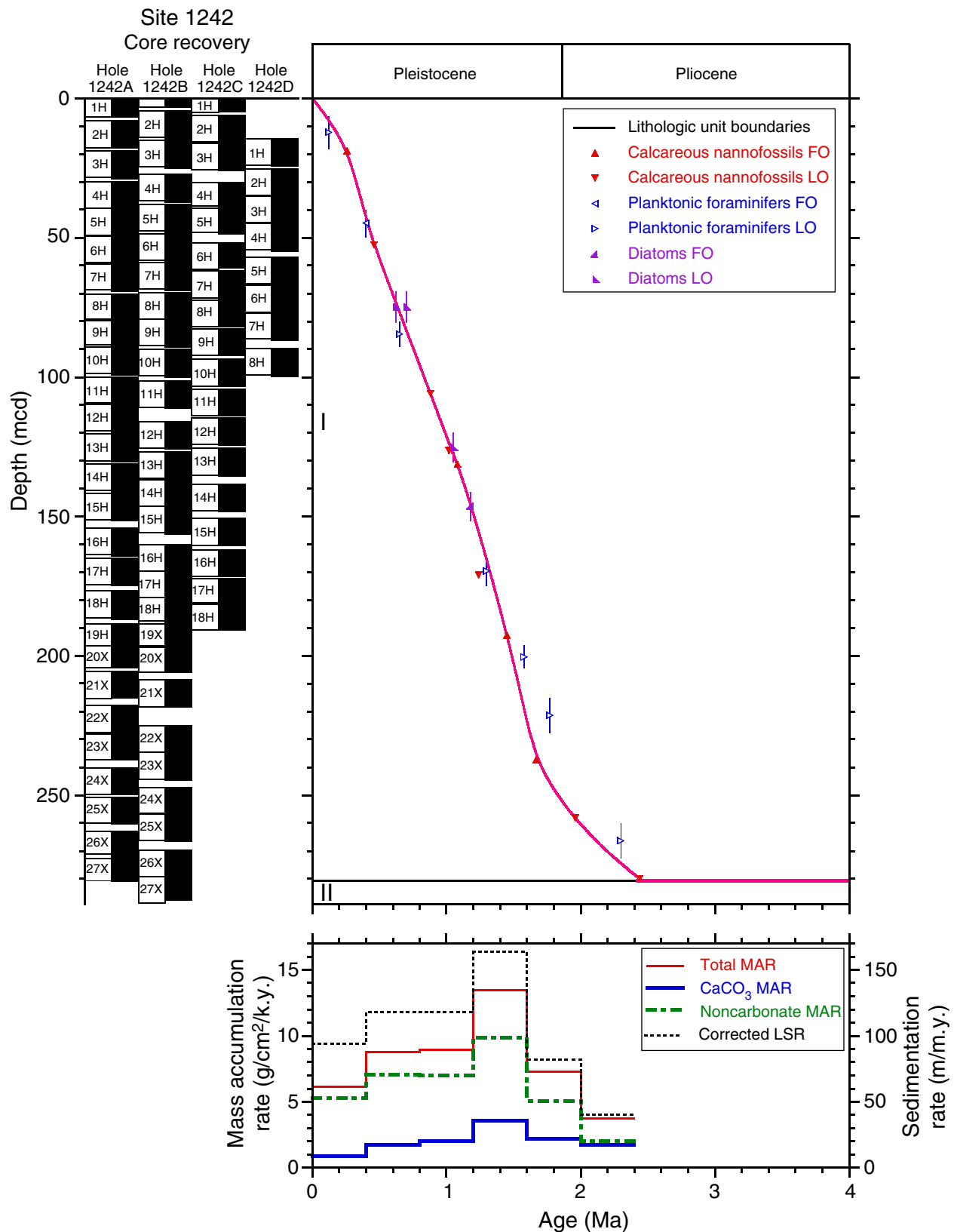


**Figure F29.** A. Shipboard biostratigraphic and magnetostratigraphic datums and age-depth model. B. Corrected linear sedimentation rates (LSRs), total mass accumulation rates (MARs), and carbonate mass accumulation rates calculated from the smooth age model, average dry density, and calcium carbonate concentrations at 0.4-m.y. intervals. FO = first occurrence, LO = last occurrence.



**SHIPBOARD SCIENTIFIC PARTY**  
**CHAPTER 13, SITE 1242**

**54**

**Table T1.** Operations summary, Site 1242. ([See table notes](#). Continued on next page.)

Core	Date (May 2002)	Local time (hr)	Depth (mbsf)		Length (m)		Recovery (%)	APCT	Orientation	NMCB
			Top	Bottom	Cored	Recovered				
<b>202-1242A-</b>										
1H	26	0720	0.0	6.7	6.7	6.70	100.0			
2H	26	0750	6.7	16.2	9.5	9.81	103.3		X	
3H	26	0825	16.2	25.7	9.5	9.97	105.0	Tensor		
4H	26	0925	25.7	35.2	9.5	10.00	105.3	X	Tensor	X
5H	26	0955	35.2	44.7	9.5	10.03	105.6	Tensor		
6H	26	1045	44.7	54.2	9.5	10.00	105.3	X	Tensor	X
7H	26	1120	54.2	63.7	9.5	10.23	107.7	Tensor		
8H	26	1215	63.7	73.2	9.5	10.04	105.7	X	Tensor	X
9H	26	1250	73.2	82.7	9.5	9.93	104.5	Tensor		
10H	26	1345	82.7	92.2	9.5	10.06	105.9	X	Tensor	X
11H	26	1430	92.2	101.7	9.5	9.54	100.4	Tensor		
12H	26	1530	101.7	111.2	9.5	10.10	106.3	X	Tensor	X
13H	26	1605	111.2	120.7	9.5	10.00	105.3			
14H	26	1700	120.7	130.2	9.5	10.00	105.3	X	Tensor	X
15H	26	1735	130.2	139.7	9.5	9.65	101.6	Tensor		
16H	26	1825	139.7	149.2	9.5	10.18	107.2	X	Tensor	X
17H	26	1900	149.2	158.7	9.5	9.88	104.0	Tensor		
18H	26	1955	158.7	168.2	9.5	10.07	106.0	X	Tensor	X
19H	26	2040	168.2	176.0	7.8	7.90	101.3	Tensor		
20X	26	2200	176.0	184.0	8.0	8.00	100.0			
21X	26	2245	184.0	193.6	9.6	9.58	99.8			
22X	26	2325	193.6	203.3	9.7	9.69	99.9			
23X	27	0010	203.3	212.6	9.3	9.54	102.6			
24X	27	0055	212.6	222.3	9.7	9.81	101.1			
25X	27	0135	222.3	231.6	9.3	9.74	104.7			
26X	27	0210	231.6	241.2	9.6	9.81	102.2			
27X	27	0255	241.2	250.8	9.6	9.85	102.6			
Cored totals:						250.8	260.11	103.7		
<b>202-1242B-</b>										
1H	27	0600	0.0	2.9	2.9	2.97	102.4	X		X
2H	27	0630	2.9	12.4	9.5	9.92	104.4			
3H	27	0700	12.4	21.9	9.5	10.02	105.5		X	
4H	27	0735	21.9	31.4	9.5	10.04	105.7	Tensor		
5H	27	0815	31.4	40.9	9.5	10.07	106.0	Tensor		X
6H	27	0850	40.9	50.4	9.5	10.03	105.6	Tensor		
7H	27	0925	50.4	59.9	9.5	10.08	106.1	Tensor		X
8H	27	1000	59.9	69.4	9.5	10.14	106.7	Tensor		
9H	27	1035	69.4	78.9	9.5	10.14	106.7	Tensor		X
10H	27	1110	78.9	88.4	9.5	9.92	104.4	Tensor		
11H	27	1145	89.4	98.9	9.5	9.96	104.8	Tensor		X
12H	27	1240	103.4	112.9	9.5	10.09	106.2	Tensor		
13H	27	1310	112.9	122.4	9.5	9.94	104.6	Tensor		X
14H	27	1345	122.4	131.9	9.5	9.93	104.5	Tensor		
15H	27	1420	131.9	141.4	9.5	10.00	105.3	Tensor		X
16H	27	1455	141.4	150.9	9.5	9.42	99.2	Tensor		
17H	27	1530	150.9	160.4	9.5	9.36	98.5	Tensor		X
18H	27	1600	160.4	169.9	9.5	9.93	104.5			
19X	27	1700	169.9	179.5	9.6	9.79	102.0			
20X	27	1735	179.5	189.1	9.6	9.79	102.0			
21X	27	1810	189.1	198.8	9.7	9.76	100.6			
22X	27	1850	198.8	208.1	9.3	9.95	107.0			
23X	27	1930	208.1	217.7	9.6	9.95	103.7			
24X	27	2010	217.7	227.1	9.4	9.93	105.6			
25X	27	2045	227.1	236.7	9.6	9.96	103.8			
26X	27	2115	236.7	246.4	9.7	9.73	100.3			
27X	27	2155	246.4	256.0	9.6	8.42	87.7			
Cored totals:						250.5	259.24	103.5		
<b>202-1242C-</b>										
1H	28	0040	0.0	5.0	5.0	5.06	101.2			
2H	28	0105	5.0	14.5	9.5	9.90	104.2		X	
3H	28	0145	14.5	24.0	9.5	9.91	104.3	Tensor		
4H	28	0230	27.5	37.0	9.5	10.01	105.4	Tensor		X
5H	28	0305	37.0	46.5	9.5	10.05	105.8	Tensor		
6H	28	0355	48.5	58.0	9.5	9.09	95.7	Tensor		X
7H	28	0430	58.0	67.5	9.5	9.92	104.4	Tensor		
8H	28	0510	67.5	77.0	9.5	9.69	102.0	Tensor		X

**Table T1 (continued).**

Core	Date (May 2002)	Local time (hr)	Depth (mbsf)		Length (m)		Recovery (%)	APCT	Orientation	NMCB
			Top	Bottom	Cored	Recovered				
9H	28	0540	77.0	86.5	9.5	9.69	102.0		Tensor	
10H	28	0620	86.5	96.0	9.5	9.75	102.6		Tensor	X
11H	28	0700	96.0	105.5	9.5	9.57	100.7		Tensor	
12H	28	0735	105.5	115.0	9.5	9.91	104.3		Tensor	X
13H	28	0805	115.0	124.5	9.5	9.97	105.0		Tensor	
14H	28	0840	124.5	134.0	9.5	9.84	103.6		Tensor	X
15H	28	0910	134.0	143.5	9.5	9.84	103.6			
16H	28	0945	143.5	153.0	9.5	9.69	102.0			X
17H	28	1015	153.0	162.5	9.5	9.37	98.6			
18H	28	1110	162.5	172.0	9.5	9.69	102.0			X
Cored totals:				166.5	170.95	102.7				
202-1242D-										
1H	28	1345	13.5	23.0	9.5	9.87	103.9		Tensor	X
2H	28	1415	23.0	32.5	9.5	9.93	104.5		Tensor	
3H	28	1500	32.5	42.0	9.5	10.06	105.9		Tensor	X
4H	28	1530	42.0	51.5	9.5	10.07	106.0		Tensor	
5H	28	1555	53.5	63.0	9.5	10.11	106.4		Tensor	X
6H	28	1630	63.0	72.5	9.5	10.05	105.8		Tensor	
7H	28	1700	72.5	82.0	9.5	10.01	105.4		Tensor	X
8H	28	1755	82.0	91.5	9.5	10.05	105.8		Tensor	
Cored totals:				76.0	80.15	105.5				
Site Totals:				743.8	770.57	103.6				

Notes: APCT = advanced piston corer temperature tool (stainless-steel housing is cutting shoe). NMCB = nonmagnetic core barrel, including cutting shoe (made from monel). X = APCT or NMCB was used. Tensor = brand name for core-barrel orientation tool.

**Table T2.** Composite depth scale, Site 1242. (See table notes. Continued on next page.)

Core	Depth of core top		Depth offset		Translation to cmcd	
	Drillers (mbsf)	Composite (mcd)	Cumulative (m)	Differential (m)	Growth factor*	Depth (cmcd)†
<b>202-1242A-</b>						
1H	0.0	0.00	0.00	0.00	1.13	0.00
2H	6.7	8.10	1.40	1.40	1.13	7.17
3H	16.2	18.90	2.70	1.30	1.13	16.73
4H	25.7	29.95	4.25	1.55	1.13	26.50
5H	35.2	39.50	4.30	0.05	1.13	34.96
6H	44.7	49.50	4.80	0.50	1.13	43.81
7H	54.2	59.35	5.15	0.35	1.13	52.52
8H	63.7	70.15	6.45	1.30	1.13	62.08
9H	73.2	79.05	5.85	-0.60	1.13	69.96
10H	82.7	89.15	6.45	0.60	1.13	78.89
11H	92.2	99.85	7.65	1.20	1.13	88.36
12H	101.7	109.88	8.18	0.53	1.13	97.24
13H	111.2	120.43	9.23	1.05	1.13	106.58
14H	120.7	131.18	10.48	1.25	1.13	116.09
15H	130.2	141.78	11.58	1.10	1.13	125.47
16H	139.7	154.18	14.48	2.90	1.13	136.44
17H	149.2	165.03	15.83	1.35	1.13	146.04
18H	158.7	176.73	18.03	2.20	1.13	156.40
19H	168.2	188.58	20.38	2.35	1.13	166.88
20X	176.0	196.38	20.38	0.00	1.13	173.79
21X	184.0	205.68	21.68	1.30	1.13	182.02
22X	193.6	217.88	24.28	2.60	1.13	192.81
23X	203.3	227.98	24.68	0.40	1.13	201.75
24X	212.6	240.13	27.53	2.85	1.13	212.50
25X	222.3	250.73	28.43	0.90	1.13	221.88
26X	231.6	263.03	31.43	3.00	1.13	232.77
27X	241.2	271.08	29.88	-1.55	1.13	239.89
<b>202-1242B-</b>						
1H	0.0	0.20	0.20	0.20	1.13	0.18
2H	2.9	4.40	1.50	1.30	1.13	3.89
3H	12.4	15.10	2.70	1.20	1.13	13.36
4H	21.9	27.35	5.45	2.75	1.13	24.20
5H	31.4	38.10	6.70	1.25	1.13	33.72
6H	40.9	48.50	7.60	0.90	1.13	42.92
7H	50.4	58.90	8.50	0.90	1.13	52.12
8H	59.9	69.55	9.65	1.15	1.13	61.55
9H	69.4	79.10	9.70	0.05	1.13	70.00
10H	78.9	90.05	11.15	1.45	1.13	79.69
11H	89.4	101.35	11.95	0.80	1.13	89.69
12H	103.4	115.93	12.53	0.58	1.13	102.59
13H	112.9	126.68	13.78	1.25	1.13	112.11
14H	122.4	136.73	14.33	0.55	1.13	121.00
15H	131.9	146.33	14.43	0.10	1.13	129.50
16H	141.4	160.08	18.68	4.25	1.13	141.66
17H	150.9	169.53	18.63	-0.05	1.13	150.03
18H	160.4	179.08	18.68	0.05	1.13	158.48
19X	169.9	187.38	17.48	-1.20	1.13	165.82
20X	179.5	196.34	16.84	-0.64	1.13	173.75
21X	189.1	208.73	19.63	2.79	1.13	184.72
22X	198.8	225.23	26.43	6.80	1.13	199.32
23X	208.1	234.78	26.68	0.25	1.13	207.77
24X	217.7	247.13	29.43	2.75	1.13	218.70
25X	227.1	256.78	29.68	0.25	1.13	227.24
26X	236.7	269.68	32.98	3.30	1.13	238.65
27X	246.4	279.28	32.88	-0.10	1.13	247.15
<b>202-1242C-</b>						
1H	0.0	0.00	0.00	0.00	1.13	0.00
2H	5.0	6.05	1.05	1.05	1.13	5.35
3H	14.5	16.20	1.70	0.65	1.13	14.34
4H	27.5	30.10	2.60	0.90	1.13	26.64
5H	37.0	38.60	1.60	-1.00	1.13	34.16
6H	48.5	51.90	3.40	1.80	1.13	45.93
7H	58.0	61.90	3.90	0.50	1.13	54.78
8H	67.5	72.30	4.80	0.90	1.13	63.98
9H	77.0	82.65	5.65	0.85	1.13	73.14

**Table T2 (continued).**

Core	Depth of core top		Depth offset		Translation to cmcd	
	Drillers (mbsf)	Composite (mcd)	Cumulative (m)	Differential (m)	Growth factor*	Depth (cmcd) <sup>†</sup>
10H	86.5	93.70	7.20	1.55	1.13	82.92
11H	96.0	104.38	8.38	1.18	1.13	92.37
12H	105.5	114.75	9.25	0.87	1.13	101.55
13H	115.0	125.68	10.68	1.43	1.13	111.22
14H	124.5	138.48	13.98	3.30	1.13	122.55
15H	134.0	150.73	16.73	2.75	1.13	133.39
16H	143.5	161.98	18.48	1.75	1.13	143.35
17H	153.0	172.23	19.23	0.75	1.13	152.42
18H	162.5	181.08	18.58	-0.65	1.13	160.25
<b>202-1242D-</b>						
1H	13.5	14.55	1.05	1.05	1.13	12.88
2H	23.0	25.20	2.20	1.15	1.13	22.30
3H	32.5	35.10	2.60	0.40	1.13	31.06
4H	42.0	44.85	2.85	0.25	1.13	39.69
5H	53.5	57.00	3.50	0.65	1.13	50.44
6H	63.0	67.15	4.15	0.65	1.13	59.42
7H	72.5	76.85	4.35	0.20	1.13	68.01
8H	82.0	89.70	7.70	3.35	1.13	79.38

Notes: \* = calculated based on mbsf-mcd relationship for splice shown in Figures F9, p. 27, F10, p. 33, and F12, p. 35. † = within the splice, the following equations apply: cmcd (mcd/growth factor); mcd = mbsf + cumulative depth offset; mcd = cmcd × growth factor; mbsf = cmcd × growth factor – cumulative offset. This table is also available in [ASCII](#).

**Table T3.** Splice tie points, Site 1242.

Hole, core, section, interval (cm)	Depth			Hole, core, section, interval (cm)	Depth			
	(mbsf)	(mcd)	(cmcd)		(mbsf)	(mcd)	(cmcd)	
<b>202-</b>								
1242A-1H-5, 5	6.06	6.06	5.35	Tie to	1242B-2H-2, 15.0	4.56	6.06	5.35
1242B-2H-4, 105	8.48	9.98	8.81	Tie to	1242A-2H-2, 37.0	8.58	9.98	8.81
1242A-2H-6, 65	14.88	16.28	14.38	Tie to	1242B-3H-1, 118.0	13.58	16.28	14.38
1242B-3H-5, 10	18.54	21.24	18.76	Tie to	1242A-3H-2, 83.0	18.54	21.24	18.76
1242A-3H-6, 35	24.11	26.81	23.67	Tie to	1242D-2H-2, 10.0	24.61	26.81	23.67
1242D-2H-5, 100	30.04	32.24	28.50	Tie to	1242C-4H-2, 63.0	29.64	32.24	28.50
1242C-4H-6, 85	35.89	38.49	34.03	Tie to	1242D-3H-3, 37.0	35.89	38.49	34.03
1242D-3H-5, 95	39.49	42.09	37.21	Tie to	1242A-5H-2, 108.0	37.79	42.09	37.21
1242A-5H-5, 145	42.68	46.98	41.55	Tie to	1242D-4H-2, 63.0	44.13	46.98	41.55
1242D-4H-4, 100	47.51	50.36	44.56	Tie to	1242A-6H-1, 86.0	45.56	50.36	44.56
1242A-6H-5, 5	50.77	55.57	49.16	Tie to	1242C-6H-3, 66.0	52.17	55.57	49.16
1242C-6H-6, 40	56.41	59.81	52.92	Tie to	1242B-7H-1, 91.0	51.31	59.81	52.92
1242B-7H-5, 55	56.95	65.45	57.92	Tie to	1242C-7H-3, 56.0	61.55	65.45	57.92
1242C-7H-6, 30	65.79	69.69	61.68	Tie to	1242D-6H-2, 104.0	65.54	69.69	61.68
1242D-6H-6, 85	71.37	75.52	66.81	Tie to	1242C-8H-3, 21.0	70.72	75.52	66.81
1242C-8H-5, 85	74.36	79.16	70.04	Tie to	1242D-7H-2, 81.0	74.81	79.16	70.04
1242D-7H-4, 145	78.45	82.80	73.27	Tie to	1242B-9H-3, 69.0	73.10	82.80	73.27
1242B-9H-5, 120	76.62	86.32	76.37	Tie to	1242C-9H-3, 69.0	80.67	86.32	76.37
1242C-9H-6, 60	85.07	90.72	80.31	Tie to	1242B-10H-1, 67.0	79.57	90.72	80.31
1242B-10H-5, 5	84.96	96.11	85.04	Tie to	1242C-10H-2, 91.0	88.91	96.11	85.04
1242C-10H-5, 80	93.31	100.51	88.94	Tie to	1242A-11H-1, 66.0	92.86	100.51	88.94
1242A-11H-6, 30	100.04	107.69	95.27	Tie to	1242C-11H-3, 30.0	99.32	107.69	95.27
1242C-11H-6, 90	104.42	112.80	99.81	Tie to	1242A-12H-2, 140.0	104.62	112.80	99.81
1242A-12H-6, 60	109.85	118.03	104.41	Tie to	1242B-12H-2, 60.0	105.50	118.03	104.41
1242B-12H-6, 10	111.01	123.54	109.32	Tie to	1242A-13H-3, 10.0	114.31	123.54	109.32
1242A-13H-6, 75	119.46	128.69	113.88	Tie to	1242B-13H-2, 51.0	114.91	128.69	113.88
1242B-13H-5, 5	118.96	132.74	117.46	Tie to	1242A-14H-2, 5.0	122.26	132.74	117.46
1242A-14H-6, 10	128.35	138.83	122.81	Tie to	1242B-14H-2, 59.0	124.50	138.83	122.81
1242B-14H-5, 85	129.28	143.61	127.06	Tie to	1242A-15H-2, 33.0	132.03	143.61	127.06
1242A-15H-5, 40	136.62	148.20	131.13	Tie to	1242B-15H-2, 37.0	133.77	148.20	131.13
1242B-15H-5, 95	138.85	153.28	135.65	Tie to	1242C-15H-2, 104.5	136.56	153.28	135.65
1242C-15H-7, 5	143.10	159.83	141.40	Tie to	1242A-16H-4, 115.0	145.35	159.83	141.40
1242A-16H-6, 140	148.61	163.09	144.32	Tie to	1242B-16H-2, 151.0	144.41	163.09	144.32
1242B-16H-5, 105	148.47	167.15	147.90	Tie to	1242A-17H-2, 62.0	151.32	167.15	147.90
1242A-17H-6, 40	157.10	172.93	153.04	Tie to	1242B-17H-3, 40.0	154.30	172.93	153.04
1242B-17H-6, 90	159.30	177.93	157.46	Tie to	1242A-18H-1, 121	159.91	177.93	157.46
1242A-18H-5, 15	164.87	182.90	161.84	Tie to	1242C-18H-2, 32.0	164.32	182.90	161.84
1242C-18H-6, 110	171.13	189.71	167.86	Tie to	1242A-19H-1, 113.0	169.33	189.71	167.86
1242A-19H-6, 105	175.93	196.31	173.73	Append	1242A-21X-1, 0.0	184.00	205.68	182.02
1242A-21X-6, 45	191.94	213.62	189.04	Tie to	1242B-21X-4, 39.0	193.99	213.62	189.04
1242B-21X-7, 70	198.32	217.95	192.88	Tie to	1242A-22X-2, 7.0	193.67	217.95	192.88
1242A-22X-6, 100	202.11	226.39	200.35	Tie to	1242B-22X-1, 116.5	199.97	226.39	200.35
1242B-22X-5, 115	205.96	232.39	205.65	Tie to	1242A-23X-3, 140.0	207.71	232.39	205.65
1242A-23X-7, 30	212.12	236.80	209.56	Tie to	1242B-23X-2, 52.0	210.12	236.80	209.56
1242B-23X-6, 20	215.75	242.43	214.54	Tie to	1242A-24X-2, 79.5	214.90	242.43	214.54
1242A-24X-5, 135	219.95	247.48	219.01	Tie to	1242B-24X-1, 35.0	218.05	247.48	219.01
1242B-24X-6, 145	226.67	256.10	226.64	Tie to	1242A-25X-4, 87.0	227.67	256.10	226.64
1242A-25X-5, 125	229.55	257.98	228.30	Tie to	1242B-25X-1, 120.0	228.30	257.98	228.30
1242B-25X-6, 105	235.65	265.33	234.81	Tie to	1242A-26X-2, 80.0	233.90	265.33	234.81
1242A-26X-6, 5	239.16	270.59	239.46	Tie to	1242B-26X-1, 89.0	237.61	270.59	239.46
1242B-26X-5, 90	243.60	276.58	244.76	Tie to	1242A-27X-4, 97.5	246.70	276.58	244.76
1242A-27X-6, 105	249.75	279.63	247.46	Tie to	1242B-27X-1, 35.0	246.75	279.63	247.46
1242B-27X-6, 100	254.43	287.31	254.26					

Note: This table is also available in [ASCII](#).

**Table T4.** OSUS-MS measurements, Hole 1242A.

Core, section, interval (cm)	Depth (mbsf)	Magnetic susceptibility (instrument units)	Run number	Depth from top of core (cm)
202-1242A-				
1H-1, 10	0.10	0.10	48.1	2578
1H-1, 15	0.15	0.15	47.3	2578
1H-1, 20	0.20	0.20	46.8	2578
1H-1, 25	0.25	0.25	48.5	2578
1H-1, 30	0.30	0.30	51.6	2578
1H-1, 35	0.35	0.35	54.3	2578
1H-1, 40	0.40	0.40	55.1	2578
1H-1, 45	0.45	0.45	54.9	2578
1H-1, 50	0.50	0.50	54.4	2578
1H-1, 55	0.55	0.55	55.2	2578
1H-1, 60	0.60	0.60	58.0	2578
1H-1, 65	0.65	0.65	60.7	2578
1H-1, 70	0.70	0.70	63.5	2578
1H-1, 75	0.75	0.75	64.7	2578
1H-1, 80	0.80	0.80	64.1	2578
1H-1, 85	0.85	0.85	61.8	2578
1H-1, 90	0.90	0.90	58.6	2578
1H-1, 95	0.95	0.95	53.6	2578
1H-1, 100	1.00	1.00	54.3	2578
1H-1, 105	1.05	1.05	54.0	2578
1H-1, 110	1.10	1.10	53.0	2578
1H-1, 115	1.15	1.15	44.8	2578
1H-1, 120	1.20	1.20	43.2	2578
1H-1, 125	1.25	1.25	39.8	2578
1H-1, 130	1.30	1.30	34.0	2578
1H-1, 135	1.35	1.35	28.3	2578
1H-1, 140	1.40	1.40	20.0	2578
1H-2, 5	1.55	1.55	13.5	2579
1H-2, 10	1.60	1.60	12.6	2579
1H-2, 15	1.65	1.65	11.4	2579
1H-2, 20	1.70	1.70	10.6	2579
1H-2, 25	1.75	1.75	10.0	2579
1H-2, 30	1.80	1.80	10.0	2579
1H-2, 35	1.85	1.85	9.8	2579
1H-2, 40	1.90	1.90	9.7	2579
1H-2, 45	1.95	1.95	9.3	2579
1H-2, 50	2.00	2.00	8.9	2579
1H-2, 55	2.05	2.05	8.7	2579
1H-2, 60	2.10	2.10	8.3	2579
1H-2, 65	2.15	2.15	8.2	2579
1H-2, 70	2.20	2.20	8.2	2579
1H-2, 75	2.25	2.25	8.3	2579
1H-2, 80	2.30	2.30	8.1	2579
1H-2, 85	2.35	2.35	8.0	2579
1H-2, 90	2.40	2.40	8.2	2579
1H-2, 95	2.45	2.45	8.1	2579
1H-2, 100	2.50	2.50	8.2	2579
1H-2, 105	2.55	2.55	8.3	2579
1H-2, 110	2.60	2.60	8.3	2579
1H-2, 115	2.65	2.65	8.2	2579
1H-2, 120	2.70	2.70	8.2	2579
1H-2, 125	2.75	2.75	8.2	2579
1H-2, 130	2.80	2.80	8.1	2579
1H-2, 135	2.85	2.85	8.0	2579
1H-2, 140	2.90	2.90	8.2	2579
1H-2, 145	2.95	2.95	7.4	2579
1H-3, 5	3.06	3.06	8.5	2580
1H-3, 10	3.11	3.11	8.9	2580
1H-3, 15	3.16	3.16	9.0	2580
1H-3, 20	3.21	3.21	9.3	2580
1H-3, 25	3.26	3.26	9.1	2580
1H-3, 30	3.31	3.31	9.0	2580
1H-3, 35	3.36	3.36	9.1	2580

Note: Only a portion of this table appears here. The complete table is available in [ASCII](#).

**Table T5.** OSUS-MS measurements, Hole 1242B.

Core, section, interval (cm)	Depth (mbsf)	Magnetic susceptibility (instrument units)	Run number	Depth from top of core (cm)
202-1242B-				
1H-1, 5	0.05	0.25	2653	5
1H-1, 10	0.10	0.30	2653	10
1H-1, 15	0.15	0.35	2653	15
1H-1, 20	0.20	0.40	2653	20
1H-1, 25	0.25	0.45	2653	25
1H-1, 30	0.30	0.50	2653	30
1H-1, 35	0.35	0.55	2653	35
1H-1, 40	0.40	0.60	2653	40
1H-1, 45	0.45	0.65	2653	45
1H-1, 50	0.50	0.70	2653	50
1H-1, 55	0.55	0.75	2653	55
1H-1, 60	0.60	0.80	2653	60
1H-1, 65	0.65	0.85	2653	65
1H-1, 70	0.70	0.90	2653	70
1H-1, 75	0.75	0.95	2653	75
1H-1, 80	0.80	1.00	2653	80
1H-1, 85	0.85	1.05	2653	85
1H-1, 90	0.90	1.10	2653	90
1H-1, 95	0.95	1.15	2653	95
1H-1, 100	1.00	1.20	2653	100
1H-1, 105	1.05	1.25	2653	105
1H-1, 110	1.10	1.30	2653	110
1H-1, 115	1.15	1.35	2653	115
1H-1, 120	1.20	1.40	2653	120
1H-1, 125	1.25	1.45	2653	125
1H-1, 130	1.30	1.50	2653	130
1H-1, 135	1.35	1.55	2653	135
1H-1, 140	1.40	1.60	2653	140
1H-1, 145	1.45	1.65	2653	145
1H-2, 5	1.56	1.76	2654	155
1H-2, 10	1.61	1.81	2654	160
1H-2, 15	1.66	1.86	2654	165
1H-2, 20	1.71	1.91	2654	170
1H-2, 25	1.76	1.96	2654	175
1H-2, 30	1.81	2.01	2654	180
1H-2, 35	1.86	2.06	2654	185
1H-2, 40	1.91	2.11	2654	190
1H-2, 45	1.96	2.16	2654	195
1H-2, 50	2.01	2.21	2654	200
1H-2, 55	2.06	2.26	2654	205
1H-2, 60	2.11	2.31	2654	210
1H-2, 65	2.16	2.36	2654	215
1H-2, 70	2.21	2.41	2654	220
1H-2, 75	2.26	2.46	2654	225
1H-2, 80	2.31	2.51	2654	230
1H-2, 85	2.36	2.56	2654	235
1H-2, 90	2.41	2.61	2654	240
1H-2, 95	2.46	2.66	2654	245
1H-2, 100	2.51	2.71	2654	250
1H-2, 105	2.56	2.76	2654	255
2H-1, 5	2.95	4.45	2655	5
2H-1, 10	3.00	4.50	2655	10
2H-1, 15	3.05	4.55	2655	15
2H-1, 20	3.10	4.60	2655	20
2H-1, 25	3.15	4.65	2655	25
2H-1, 30	3.20	4.70	2655	30
2H-1, 35	3.25	4.75	2655	35
2H-1, 40	3.30	4.80	2655	40
2H-1, 45	3.35	4.85	2655	45
2H-1, 50	3.40	4.90	2655	50
2H-1, 55	3.45	4.95	2655	55
2H-1, 60	3.50	5.00	2655	60
2H-1, 65	3.55	5.05	2655	65

Note: Only a portion of this table appears here. The complete table is available in [ASCII](#).

**Table T6.** OSUS-MS measurements, Hole 1242C.

Core, section, interval (cm)	Depth (mbsf)	Depth (mcd)	Magnetic susceptibility (instrument units)	Run number	Depth from top of core (cm)
202-1242C-					
1H-1, 5	0.05	0.05	888.1	2690	5
1H-1, 10	0.10	0.10	412.9	2690	10
1H-1, 15	0.15	0.15	70.6	2690	15
1H-1, 20	0.20	0.20	51.1	2690	20
1H-1, 25	0.25	0.25	46.8	2690	25
1H-1, 30	0.30	0.30	43.3	2690	30
1H-1, 35	0.35	0.35	40.9	2690	35
1H-1, 40	0.40	0.40	42.2	2690	40
1H-1, 45	0.45	0.45	47.2	2690	45
1H-1, 50	0.50	0.50	48.7	2690	50
1H-1, 55	0.55	0.55	50.4	2690	55
1H-1, 60	0.60	0.60	46.5	2690	60
1H-1, 65	0.65	0.65	48.5	2690	65
1H-1, 70	0.70	0.70	50.5	2690	70
1H-1, 75	0.75	0.75	52.4	2690	75
1H-1, 80	0.80	0.80	56.2	2690	80
1H-1, 85	0.85	0.85	54.4	2690	85
1H-1, 90	0.90	0.90	51.7	2690	90
1H-1, 95	0.95	0.95	49.5	2690	95
1H-1, 100	1.00	1.00	50.5	2690	100
1H-1, 105	1.05	1.05	46.3	2690	105
1H-1, 110	1.10	1.10	43.3	2690	110
1H-1, 115	1.15	1.15	38.7	2690	115
1H-1, 120	1.20	1.20	35.7	2690	120
1H-1, 125	1.25	1.25	31.8	2690	125
1H-1, 130	1.30	1.30	24.8	2690	130
1H-1, 135	1.35	1.35	20.6	2690	135
1H-1, 140	1.40	1.40	17.3	2690	140
1H-1, 145	1.45	1.45	13.3	2690	145
1H-2, 5	1.54	1.54	12.2	2691	155
1H-2, 10	1.59	1.59	12.0	2691	160
1H-2, 15	1.64	1.64	11.4	2691	165
1H-2, 20	1.69	1.69	10.5	2691	170
1H-2, 25	1.74	1.74	10.1	2691	175
1H-2, 30	1.79	1.79	9.9	2691	180
1H-2, 35	1.84	1.84	10.0	2691	185
1H-2, 40	1.89	1.89	9.7	2691	190
1H-2, 45	1.94	1.94	9.4	2691	195
1H-2, 50	1.99	1.99	9.0	2691	200
1H-2, 55	2.04	2.04	8.7	2691	205
1H-2, 60	2.09	2.09	8.6	2691	210
1H-2, 65	2.14	2.14	8.5	2691	215
1H-2, 70	2.19	2.19	8.5	2691	220
1H-2, 75	2.24	2.24	8.4	2691	225
1H-2, 80	2.29	2.29	8.4	2691	230
1H-2, 85	2.34	2.34	8.5	2691	235
1H-2, 90	2.39	2.39	8.6	2691	240
1H-2, 95	2.44	2.44	8.6	2691	245
1H-2, 100	2.49	2.49	8.6	2691	250
1H-2, 105	2.54	2.54	8.7	2691	255
1H-2, 110	2.59	2.59	8.6	2691	260
1H-2, 115	2.64	2.64	8.6	2691	265
1H-2, 120	2.69	2.69	8.4	2691	270
1H-2, 125	2.74	2.74	8.3	2691	275
1H-2, 130	2.79	2.79	8.2	2691	280
1H-2, 135	2.84	2.84	8.5	2691	285
1H-2, 140	2.89	2.89	8.4	2691	290
1H-2, 145	2.94	2.94	7.4	2691	295
1H-3, 5	3.04	3.04	8.0	2692	305
1H-3, 10	3.09	3.09	8.2	2692	310
1H-3, 15	3.14	3.14	8.2	2692	315
1H-3, 20	3.19	3.19	8.2	2692	320
1H-3, 25	3.24	3.24	8.2	2692	325

Note: Only a portion of this table appears here. The complete table is available in [ASCII](#).

**Table T7.** OSUS-MS measurements, Hole 1242D.

Core, section, interval (cm)	Depth (mbsf)	Magnetic susceptibility (instrument units)	Run number	Depth from top of core (cm)
202-1242D-				
1H-1, 5	13.55	14.60	9.1	2761
1H-1, 10	13.60	14.65	9.7	2761
1H-1, 15	13.65	14.70	9.5	2761
1H-1, 20	13.70	14.75	9.1	2761
1H-1, 25	13.75	14.80	9.3	2761
1H-1, 30	13.80	14.85	9.3	2761
1H-1, 35	13.85	14.90	8.9	2761
1H-1, 40	13.90	14.95	8.7	2761
1H-1, 45	13.95	15.00	8.6	2761
1H-1, 50	14.00	15.05	8.6	2761
1H-1, 55	14.05	15.10	8.6	2761
1H-1, 60	14.10	15.15	8.4	2761
1H-1, 65	14.15	15.20	8.2	2761
1H-1, 70	14.20	15.25	8.1	2761
1H-1, 75	14.25	15.30	7.8	2761
1H-1, 80	14.30	15.35	8.1	2761
1H-1, 85	14.35	15.40	7.9	2761
1H-1, 90	14.40	15.45	8.4	2761
1H-1, 95	14.45	15.50	8.9	2761
1H-1, 100	14.50	15.55	9.1	2761
1H-1, 105	14.55	15.60	9.6	2761
1H-1, 110	14.60	15.65	10.3	2761
1H-1, 115	14.65	15.70	10.5	2761
1H-1, 120	14.70	15.75	10.4	2761
1H-1, 125	14.75	15.80	10.2	2761
1H-1, 130	14.80	15.85	10.0	2761
1H-1, 135	14.85	15.90	10.0	2761
1H-1, 140	14.90	15.95	10.2	2761
1H-1, 145	14.95	16.00	9.9	2761
1H-2, 5	15.06	16.11	11.7	2767
1H-2, 5	15.06	16.11	11.9	2762
1H-2, 10	15.11	16.16	12.4	2762
1H-2, 10	15.11	16.16	12.4	2767
1H-2, 15	15.16	16.21	12.7	2762
1H-2, 15	15.16	16.21	12.7	2767
1H-2, 20	15.21	16.26	12.8	2762
1H-2, 20	15.21	16.26	12.8	2767
1H-2, 25	15.26	16.31	12.2	2762
1H-2, 25	15.26	16.31	12.2	2767
1H-2, 30	15.31	16.36	11.7	2762
1H-2, 30	15.31	16.36	11.8	2767
1H-2, 35	15.36	16.41	11.5	2762
1H-2, 35	15.36	16.41	11.6	2767
1H-2, 40	15.41	16.46	11.2	2762
1H-2, 40	15.41	16.46	11.4	2767
1H-2, 45	15.46	16.51	11.3	2762
1H-2, 45	15.46	16.51	11.4	2767
1H-2, 50	15.51	16.56	11.5	2762
1H-2, 50	15.51	16.56	11.7	2767
1H-2, 55	15.56	16.61	11.3	2762
1H-2, 55	15.56	16.61	11.5	2767
1H-2, 60	15.61	16.66	11.2	2762
1H-2, 60	15.61	16.66	11.4	2767
1H-2, 65	15.66	16.71	11.2	2762
1H-2, 65	15.66	16.71	11.4	2767
1H-2, 70	15.71	16.76	11.2	2762
1H-2, 70	15.71	16.76	11.4	2767
1H-2, 75	15.76	16.81	11.0	2762
1H-2, 75	15.76	16.81	11.2	2767
1H-2, 80	15.81	16.86	11.1	2762
1H-2, 80	15.81	16.86	11.4	2767
1H-2, 85	15.86	16.91	11.4	2762
1H-2, 85	15.86	16.91	11.6	2767
				235

Note: Only a portion of this table appears here. The complete table is available in [ASCII](#).

**Table T8.** Lithologic units, Site 1242.

Unit	Top			Base			Description	Interpretation
	Core, section, interval (cm)	Depth (mbsf)	(mcd)	Core, section, interval (cm)	Depth (mbsf)	(mcd)		
I	202-			202-				
	1242A-1H-1, 0	0.00	0.00	1242A-27X-7, 51	250.71	280.59	Clayey nannofossil ooze and nannofossil clay	Hemipelagic sedimentation
	1242B-1H-1, 0	0.00	0.20	1242B-27X-2, 33	247.75	280.63		
	1242C-1H-1, 0	0.00	0.00	1242C-18H-CC, 24	172.23	190.81		
II	1242D-1H-1, 0	13.50	14.55	1242D-8H-CC, 32	92.06	99.76		
	1242A-27X-CC, 0	250.71	280.59	1242A-27X-CC, 34	251.05	280.93	Diatom-bearing nannofossil ooze	Pelagic sedimentation
	1242B-27X-2, 33	247.75	280.63	1242B-27X-CC, 36	254.86	287.74		

**Table T9.** Ash layers, Site 1242.

Number	Core, section, interval (cm)	Depth (mcd)		Core, section, interval (cm)	Depth (mcd)		Core, section, interval (cm)	Depth (mcd)		Core, section, interval (cm)	Depth (mcd)		Glass color
		Top	Bottom										
<b>202-1242A-</b>													
1	NF			3H-6, 59-64	23.24	23.29	2H-3, 35		9.40	ND			?
2	4H-2, 74		32.20	NF			3H-5, 102-103	23.22	23.23	1H-6, 104-105	23.09	23.10	Clear
3	4H-6, 75-82	38.24	38.31	5H-1, 21-30	38.31	38.40	NF			2H-5, 100-108	32.20	32.28	Clear >> brown
4	NF			NF			4H-6, 64-67	38.24	38.27	3H-3, 13-20	38.23	38.30	Clear >> brown
5	5H-3, 46-47	42.98	42.99	NF			4H-6, 104-106	38.64	38.66	NF			?
6	5H-3, 123-126	43.75	43.78	NF			NF			NF			Clear
7	6H-5, 13-15	55.65	55.67	6H-5, 142-143	55.95	55.96	NF			NF			Clear > brown
8	6H-6, 54-59	57.57	57.62	6H-7, 54-63	58.09	58.18	NF			NF			Clear
9	7H-1, 71-72	60.06	60.07	NF			6H-4, 115-117	57.55	57.57	5H-1, 50-60	57.50	57.60	Clear > brown
10	7H-6, 120-121	68.08	68.09	NF			NF			NF			Clear
11	8H-1, 100-106	71.15	71.21	8H-2, 22-25	71.27	71.30	NF			NF			Clear
12	NF			NF			7H-7, 49-52	71.39	71.42	6H-3, 120-125	71.35	71.40	Clear
13	8H-4, 126-129	75.90	75.93	8H-5, 41-43	75.96	75.98	8H-2, 67-70	74.47	74.50	NF			?
14	8H-5, 32-37	76.46	76.51	8H-5, 100-103	76.55	76.58	8H-3, 60-62	75.90	75.92	NF			Clear >> brown
15	8H-5, 63-68	76.77	76.82	8H-5, 135-138	76.90	76.93	8H-3, 124-126	76.54	76.56	6H-7, 39-50	76.54	76.65	Clear
16	8H-5, 128-131	77.42	77.45	NF			8H-4, 7-10	76.87	76.90	NF			Clear
17	9H-4, 121-122	84.76	84.77	NF			8H-4, 82-83	77.62	77.63	NF			Clear
18	10H-1, 142-143	90.57	90.58	10H-1, 54-55	90.59	90.60	NF			NF			Clear
19	NF			10H-4, 50-51	95.05	95.06	NF			8H-1, 92-94	90.62	90.64	Clear
20	NF			10H-5, 69-70	96.74	96.75	NF						Clear
21	11H-3, 112-126	103.99	104.13	11H-2, 113-127	103.98	104.12	NF						Clear
22	11H-4, 0-9	104.37	104.46	NF			<b>Core gap</b>						Clear >> brown
23	NF			NF			Core gap			ND			Clear >> brown
24	NF			NF			11H-1, 47-48	104.85	104.86	ND			?
25	NF			11H-5, 60-61	107.95	107.96	11H-1, 77-78	105.15	105.16	ND			?
26	11H-7, 6-20	108.59	108.73	11H-5, 75-87	108.10	108.22	NF			ND			Clear
27	12H-2, 136-137	112.76	112.77	Core gap			11H-3, 118-132	108.56	108.70	ND			Clear >> brown
28	12H-4, 107-109	115.48	115.50	Core gap			NF			ND			Clear
29	Core gap			12H-2, 141-142	118.84	118.85	12H-1, 68-70	115.43	115.45	ND			Clear
30	NF			NF			12H-3, 113-116	118.86	118.89	ND			Clear
31	15H-2, 48-49	143.76	143.77	14H-6, 8-10	144.31	144.33	13H-4, 103-105	131.21	131.23	ND			?
32	16H-4, 133-137	160.01	160.05	16H-1, 23-26	160.31	160.34	NF			ND			Clear
33	NF			17H-1, 25		169.78	15H-7, 25-29	159.98	160.02	ND			Clear >> brown
34	NF			17H-4, 74		174.77	NF			ND			Pumice (4 mm)
35	1242A-18H-3, 101-105	180.75	180.79	NF			NF			ND			Clear
36	18H-3, 117-123	180.91	180.97	18H-2, 30-35	180.88	180.93	NF			ND			Clear
37	19H-1, 31-32	188.89	188.90	19X-1, 21-23	187.59	187.61	NF			ND			Clear
38	19H-4, 85-89	193.09	193.13	NF			18H-6, 0-3	188.58	188.61	ND			Clear
39	NF			20X-5, 104-105	202.27	202.28	ND			ND			Clear
40	NF			20X-8, 42-43	205.65	205.66	ND			ND			Clear
41	NF			21X-6, 14-15	216.37	216.38	ND			ND			Clear
42	22X-1, 116-121	219.04	219.09	21X-CC, 15-18	218.14	218.17	ND			ND			Clear
43	NF			26X-4, 137-140	275.55	275.58	ND			ND			Clear
44	NF			27X-2, 25-26	277.15	277.16	ND			ND			?

Notes: Ash layers that could be correlated between holes are located in the same row and printed in bold type. ND = not drilled, NF = not found, ? = unknown.

**Table T10.** Age-depth control points, Holes 1242A and 1242B.

Datum	Source	Age (Ma)		Top sample (FO presence/LO absence)		Bottom sample (LO presence/FO absence)		Age (Ma)		Depth		
		Minimum	Maximum	Core, section, interval (cm)	Depth (mbsf)	Core, section, interval (cm)	Depth (mbsf)	Average	Uncertainty (±)	Average (mbsf)	Average (mcd)	Uncertainty (±m)
				202-1242A-		202-1242A-						
LO <i>Globigerinoides ruber</i> pink	PF	0.12	0.12	1H-CC, 5	6.55	2H-CC, 16	16.46	0.12	0.00	11.51	12.21	4.95
FO <i>Emiliania huxleyi</i>	CN	0.26	0.26	2H-CC, 16	16.46	3H-1, 75	16.95	0.26	0.00	16.71	18.76	0.24
FO <i>Globigerinoides ruber</i> pink	PF	0.40	0.40	4H-CC, 33	35.65	5H-CC, 20	45.18	0.40	0.00	40.42	44.76	4.77
LO <i>Pseudoemiliana lacunosa</i>	CN	0.46	0.46	6H-2, 75	46.95	6H-3, 75	48.45	0.46	0.00	47.70	52.52	0.75
LO <i>Nitzschia reinholdii</i>	D	0.62	0.62	7H-CC, 20	64.32	8H-CC, 37	73.69	0.62	0.00	69.04	74.71	4.66
LO <i>Stilostomella</i> spp.	PF	0.65	0.65	8H-CC, 37	73.69	9H-CC, 19	83.08	0.65	0.00	78.39	84.54	4.69
LO <i>Nitzschia fossilis</i>	D	0.70	0.70	7H-CC, 20	64.32	8H-CC, 37	73.69	0.70	0.00	69.04	74.71	4.66
LO <i>Reticulofenestra asanoi</i>	CN	0.88	0.88	11H-4, 75	97.45	11H-5, 75	98.95	0.88	0.00	98.20	105.88	0.75
Reentry <i>Gephyrocapsa</i> (medium)	CN	1.02	1.02	13H-4, 75	116.45	13H-5, 75	117.95	1.02	0.00	117.20	126.44	0.75
LO <i>Rhizosolenia matuyamai</i>	D	1.05	1.05	12H-CC, 42	111.75	13H-CC, 26	121.15	1.05	0.00	116.45	125.20	4.70
FO <i>Reticulofenestra asanoi</i>	CN	1.08	1.08	13H-CC, 26	121.15	14H-1, 75	121.45	1.08	0.00	121.30	131.16	0.15
FO <i>Rhizosolenia matuyamai</i>	D	1.18	1.18	14H-CC, 33	130.65	15H-CC, 20	139.80	1.18	0.00	135.23	146.32	4.58
LO <i>Gephyrocapsa</i> (large)	CN	1.24	1.24	17H-4, 74	154.44	17H-5, 75	155.95	1.24	0.00	155.20	171.03	0.75
LO <i>Globigerinoides obliquus</i>	PF	1.30	1.30	16H-CC, 45	149.83	17H-CC, 17	158.93	1.30	0.00	154.38	169.55	4.55
FO <i>Gephyrocapsa</i> (large)	CN	1.45	1.45	19H-3, 40	171.60	19H-4, 75	172.60	1.45	0.00	172.10	192.49	0.50
LO <i>Neogloboquadrina acostaensis</i>	PF	1.58	1.58	19H-CC, 1	175.96	20X-CC, 24	183.95	1.58	0.00	179.96	200.36	3.99
FO <i>Gephyrocapsa</i> (medium)	CN	1.67	1.67	23X-7, 40	212.20	23X-CC, 20	212.79	1.67	0.00	212.50	237.20	0.30
LO <i>Globigerinoides extremus</i>	PF	1.77	1.77	21X-CC, 28	193.53	22X-CC, 27	203.24	1.77	0.00	198.39	221.39	4.85
LO <i>Discoaster brouweri</i>	CN	1.96	1.96	25X-5, 75	229.05	25X-6, 75	230.55	1.96	0.00	229.80	258.23	0.75
LO <i>Globorotalia pseudomicenica</i>	PF	2.30	2.30	25X-CC, 28	231.89	26X-CC, 1	241.09	2.30	0.00	236.49	266.45	4.60
LO <i>Discoaster pentaradiatus</i>	CN	2.44	2.44	27X-6, 75	249.45	27X-7, 40	250.60	2.44	0.00	250.03	279.91	0.57
LO <i>Globorotalia foehsi</i> s.l.	PF	11.68	11.68	26X-CC, 1	241.09	27X-CC, 30	251.00	11.68	0.00	246.05	269.97	4.96
LO <i>Globorotalia panda</i>	PF	11.80	11.80	26X-CC, 1	241.09	27X-CC, 30	251.00	11.80	0.00	246.05	276.72	4.96
LO <i>Globorotalia praescitula</i>	PF	11.90	11.90	26X-CC, 1	241.09	27X-CC, 30	251.00	11.90	0.00	246.05	276.72	4.96
				202-1242B-		202-1242B-						
LO <i>Coronocyclus nitescens</i>	CN	12.43	12.43	27X-3, 75	249.70	27X-4, 75	251.20	12.43	0.00	250.45	283.30	0.75
FO <i>Triquetrorhabdulus rugosus</i>	CN	12.62	12.62	27X-3, 75	249.70	27X-4, 75	251.20	12.62	0.00	250.45	283.30	0.75

Notes: FO = first occurrence, LO = last occurrence. CN = calcareous nannofossils, PF = planktonic foraminifers, D = diatoms.

**Table T11.** Distribution of calcareous nannofossils, Holes 1242A, 1242B, and 1242C. (See table notes. Continued on next page.)

Core, section, interval (cm)	Depth (mbsf)	Depth (mcd)	Preservation	Abundance	<i>Calcidiscus macintyrei</i>	<i>Coccolithus miopelagicus</i>	<i>Coronocyclus nitescens</i>	<i>Cyclargolithus floridanus</i>	<i>Discoaster brouweri</i>	<i>Discoaster pentaradiatus</i>	<i>Emiliana huxleyi</i>	<i>Gephyrocapsa</i> spp. (large)	<i>Gephyrocapsa</i> spp. (medium)	<i>Gephyrocapsa</i> spp. (small)	<i>Helicosphaera sellii</i>	<i>Pseudomiliaria lacunosa</i>	<i>Reticulofenestra asanoi</i>	<i>Reticulofenestra pseudounbiliclus</i>	<i>Reticulofenestra</i> (small)	<i>Sphenolithus abies</i>	<i>Triquetrorhabdulus rugosus</i>
202-1242C-1H-1, 0	0.00	0.00	M G	C C						F	C	C									
1H-CC, 16	4.98	4.98	M G	C C						R	C	C									
202-1242A-2H-CC, 16	16.46	17.87	M F							R	F	F									
3H-1, 75	16.95	19.65	M C								C	C									
202-1242C-3H-2, 75	16.74	18.44	M C								C	C									
202-1242A-3H-CC, 20	26.21	28.91	M C								C	C									
4H-CC, 33	35.75	40.00	G C								F	A									
5H-CC, 20	45.22	49.52	M A								F	A									
6H-2, 75	46.95	51.76	M A								C	A									
6H-3, 75	48.45	53.27	M A								C	A									
6H-4, 75	49.95	54.77	B																		
6H-5, 75	51.45	56.27	M A								C	A									
6H-CC, 29	54.70	59.50	M A								C	A									
7H-CC, 20	64.33	69.47	G A								C	C									
8H-CC, 37	73.69	80.13	M A								C	C									
9H-CC, 19	83.08	88.94	M C								C	C									
10H-CC, 36	92.75	99.20	M A								A	C									
11H-2, 75	94.45	102.12	M A								F	C									
11H-3, 75	95.95	103.62	M A								F	C									
11H-4, 75	97.45	105.12	M A								F	C									
11H-5, 75	98.95	106.63	M A								F	C									
11H-7, 40	101.23	108.93	M A								F	C									
11H-CC, 1	101.74	109.40	M A								F	C									
12H-CC, 42	111.82	120.00	M A								F	C									
13H-3, 75	114.95	124.19	M A								C	A									
13H-4, 75	116.45	125.69	M A								R	A									
13H-5, 75	117.95	127.19	M A									A									
13H-CC, 26	121.16	130.39	M A									D									
14H-1, 75	121.45	131.93	M A									A									
14H-2, 75	122.95	133.44	M A									A									
14H-3, 75	124.45	134.95	M A									A									
14H-CC, 33	130.72	141.20	M A									A									
15H-CC, 20	139.86	151.44	M A									A									
16H-CC, 45	149.85	164.33	M A									D									
17H-4, 75	154.45	170.28	M A									A									
17H-5, 75	155.95	171.78	M A									F	A								
17H-6, 75	157.45	173.28	M A									F	A								
17H-CC, 17	158.93	174.77	M A									F	A								
18H-CC, 68	168.78	186.81	M A									R	F	D							
19H-2, 40	170.10	190.49	M A									R	F	D							
19H-3, 40	171.60	191.99	M A									R	F	D							
19H-4, 40	172.25	192.64	M A										F	D							
19H-CC, 1	176.00	196.38	M A										R	A							
20X-CC, 24	183.96	204.34	M C										F	C		R					
21X-CC, 28	193.55	215.23	M C										R	C	F	F					
22X-CC, 27	203.27	227.55	M C										F	C	F	R					
23X-7, 40	212.20	236.90	M F										R	F	F	F					
23X-CC, 20	212.82	237.50	M C										R	C	R	F					
24X-1, 75	213.35	240.88	M F										F	F	F						
24X-CC, 29	222.39	249.92	M C										C		R						
25X-4, 75	227.55	255.98	M C										C		R						
25X-5, 75	229.05	257.48	M F										C		R						
25X-6, 75	230.55	258.98	M F										F		C	R					

**Table T11 (continued).**

Core, section, interval (cm)	Depth (mbsf)	Depth (mcd)	Preservation	Abundance	<i>Calcidicus macintyrei</i>	<i>Coccolithus miopelagicus</i>	<i>Coronocyclus nitescens</i>	<i>Cyclaragolithus floridanus</i>	<i>Discoaster brouweri</i>	<i>Discoaster pentadiscatus</i>	<i>Emiliania huxleyi</i>	<i>Gephyrocapsa</i> spp. (large)	<i>Gephyrocapsa</i> spp. (medium)	<i>Gephyrocapsa</i> spp. (small)	<i>Helicosphaera sellii</i>	<i>Pseudomiliaria lacunosa</i>	<i>Reticulofenestra asanoi</i>	<i>Reticulofenestra pseudumbilicus</i>	<i>Reticulofenestra</i> (small)	<i>Sphenolithus abies</i>	<i>Triquetorabdulus rugosus</i>
25X-CC, 28	231.89	260.35	M	C						R											
26X-CC, 1	241.11	272.54	M	C						F											
27X-4, 75	246.45	276.33	M	A						F											
27X-6, 75	249.45	279.33	M	C						F											
27X-7, 40	250.60	280.48	M	C						F											
27X-CC, 1	250.71	280.60	M	C						F											
27X-CC, 30	251.00	280.89	M	A	R			C		R											
202-1242B-																					
27X-2, 75	248.15	281.05	M	A	R														A	R	
27X-3, 75	249.65	282.55	M	A	R														A	R	
27X-4, 75	251.15	284.05	M	A	R	R													A		
27X-6, 75	254.15	287.06	M	A	R	R													A		

Notes: Preservation: G = good, M = moderate. Abundance: A = abundance, C = common, F = few, R = rare.

Table T12. Distribution of planktonic foraminifers, Hole 1242A.

Core, section, interval (cm)	Depth (mbsf)	Depth (mcd)	Preparation	Preservation	Abundance	Planktonic foraminifers (%)	Remarks	<i>Dentoglobigerina altispina</i>	<i>Globigerinella aquiloideris</i>	<i>Globigerinoides extremus</i>	<i>Globigerinoides obliquus</i>	<i>Globigerinoides ruber</i>	<i>Globigerinoides ruber pink</i>	<i>Globigerinoides trilobus</i>	<i>Globiquadrina barremensis</i>	<i>Globorotalia crassula</i>	<i>Globorotalia dehiscens</i>	<i>Globorotalia flexuosa</i>	<i>Globorotalia fohsi s.l.</i>	<i>Globorotalia inflata</i>	<i>Globorotalia menardii</i>	<i>Globorotalia panda</i>	<i>Globorotalia praeminentii</i>	<i>Globorotalia praescitula</i>	<i>Globorotalia pseudomiocenica</i>	<i>Globorotalia sacculifer</i>	<i>Globorotalia scitula</i>	<i>Globorotalia thayeri</i>	<i>Globorotalia tosaensis</i>	<i>Globorotalia turnida</i>	<i>Globorotalia ungulata</i>	<i>Neogloboquadrina acostaensis</i>	<i>Orbulina universa</i>	<i>Pulenia obliquiloculata</i>	<i>Sphaerodinella dehiscens</i>	<i>Stilostomella spp.</i>
202-1242A-Mudline, 0	0.00	0.00	S	M/G	C	10	Radiolarians: C																													
1H-CC, 16	6.66	6.66	S	M/G	A	10	Radiolarians: R	F	F	F	R																									
2H-CC, 16	16.47	17.87	S	M/G	A	1	Radiolarians: R	F	F	F	F																									
3H-CC, 20	26.21	28.91	S	M/G	A	3	Radiolarians: R; Glauconite: F	F	F	F	F																									
4H-CC, 33	35.75	40.00	S	G	A	2																														
5H-CC, 20	45.22	49.52	S	M	C	5	Wood fragments	R	F	F	F																									
6H-CC, 29	54.70	59.50	S	M/G	C	3	Radiolarians: C	R	F/C	F	R																									
7H-CC, 20	64.32	69.47	S	M	C	2	Radiolarians: R; Diatoms: R																													
8H-CC, 37	73.69	80.13	S	M	F/C	5	Radiolarians: R; Diatoms: R; Glauconite: R																													
9H-CC, 19	83.09	88.94	S	M	F/C	5	Radiolarians: F; Diatoms: R; Glauconite: R	R	F	F																										
10H-CC, 36	92.75	99.20	S	M	F	5	Radiolarians: C; Diatoms: F	F	F	F																										
11H-CC, 1	101.74	109.40	S	P/M	F	10	Radiolarians: C; Diatoms: F																													
12H-CC, 42	111.82	120.00	S	M	F	15	Radiolarians: F; Diatoms: C; Glauconite: C																													
13H-CC, 26	121.16	130.39	S	P/M	F/C	5	Radiolarians: F; Diatoms: F; Glauconite: F																													
14H-CC, 33	130.72	141.20	S	P/M	F	10	Radiolarians: R																													
15H-CC, 20	139.86	151.44	S	M	F/C	10	Radiolarians: R																													
16H-CC, 45	149.85	164.33	C	P/M	R	10	Radiolarians: R; Diatoms: R; Glauconite: R	R	F	F																										
17H-CC, 17	158.93	174.77	C	P/M	R	15	Radiolarians: R; Diatoms: F		R	F	F																									
18H-CC, 68	168.78	186.81	C	M	F	25	Radiolarians: R; Diatoms: F	F	F	F																										
19H-CC, 1	176.00	196.38	C	M	R/F	10	Radiolarians: F; Diatoms: C; Glauconite: C	R	C	R																										
20X-CC, 24	183.96	204.34	C	P/M	VR	50	Radiolarians: F; Glauconite: R		R	R	R																									
21X-CC, 28	193.55	215.23	C	P	R	80	Radiolarians: A; Glauconite: F		R	R	R																									
22X-CC, 27	203.27	227.55	C	P	R	50	Radiolarians: F; Diatoms: F; Glauconite: F	R	R	R	R																									
23X-CC, 20	212.82	237.50	C	P	R	99	Radiolarians: F; Glauconite: C	R	R	R	R																									
24X-CC, 29	222.39	249.92	C	P	VR	99	Radiolarians: F; Glauconite: A	R	R	R	R																									
25X-CC, 28	231.92	260.35	C	P	VR	99	Radiolarians: F; Glauconite: F	R	R	R	R																									
26X-CC, 1	241.11	272.54	C	P	R	65	Radiolarians: F; Glauconite: A	R	R	R	R																									
27X-CC, 30	251.01	280.89	S	M/G	C	1	Radiolarians: C	C	F	F	F																									

Notes: Preparation: S = sieve, C = Calgon. Preservation: G = good, M = moderate, P = poor. Abundance: A = abundance, C = common, F = few, R = rare.

**Table T13.** Distribution of diatoms, Hole 1242A.

Core, section, interval (cm)	Depth (mbsf)	Depth (mcd)	Identification	Method	Abundance	Preservation	<i>Actinocyclus ellipticus</i>	<i>Actinocyclus spp.</i>	<i>Actinopychus senarius</i>	<i>Asteromphalus spp.</i>	<i>Azpeitia nodulifera</i>	<i>Chaetoceros spp. (resting spores)</i>	<i>Coscinodiscus spp.</i>	<i>Denticulopsis simonsenii</i> s.l.	<i>Fragilaropsis dolulus</i>	<i>Hemidiscus curviformis</i>	<i>Nitzschia fossilis</i>	<i>Nitzschia marinna</i>	<i>Nitzschia reitholdii</i>	<i>Rhizosolenia matuyamai</i>	<i>Rhizosolenia spp.</i>	<i>Rossiella paleacea</i> s.l.	<i>Stephanopyxis spp.</i>	<i>Thalassionema spp.</i>	<i>Thalassiosira oestruppii</i>	<i>Thalassiosira yabei</i>	<i>Thalassiosira spp.</i>	<i>Thalassiothrix</i> dds.	Remarks
202-1242A																													
Mudline	0.00	0.00	PAL	S	F-C	M-G																							
1H-CC, 16	6.65	6.66	PAL	S	R	P-M																							
2H-CC, 16	16.46	17.87	PAL	S	T	P																							
3H-CC, 20	26.12	28.91	PAL	S	T	P																							
4H-CC, 33	35.65	40.00	PAL	S	T	P																							
5H-CC, 20	45.18	49.52	PAL	S	T	P																							
6H-CC, 29	54.65	59.50	PAL	S	F-C	M																							
7H-CC, 1	64.38	69.48	PAL	S	F-C	M																							
8H-CC, 37	73.69	80.13	PAL	S	F	M																							
9H-CC, 19	83.08	88.94	PAL	S	F	M																							
10H-CC, 36	92.71	99.20	PAL	S	F	M																							
11H-CC, 0	101.69	109.39	PAL	S	F	M																							
12H-CC, 42	111.75	120.00	PAL	S	F	M																							
13H-CC, 26	121.15	130.39	PAL	S	F	M																							
14H-CC, 33	130.65	141.20	PAL	S	R	P																							
15H-CC, 20	139.80	151.44	PAL	S	T	P																							
16H-CC, 45	149.83	164.33	PAL	S	T	P																							
17H-CC, 27	159.03	174.87	PAL	S	T	P																							
18H-CC, 68	168.72	186.81	PAL	S	R	P																							
19H-CC, 0	175.95	196.37	PAL	S	T	P																							
20X-CC, 24	183.95	204.34	PAL	S	T	P																							
21X-CC, 28	193.53	215.23	PAL	S	R	P																							
22X-CC, 27	203.24	227.55	PAL	S	T	P																							
23X-CC, 20	212.79	237.50	PAL	S	T	P																							
24X-CC, 29	222.36	249.92	PAL	S	T	P																							
25X-CC, 28	231.89	260.35	PAL	S	T	P																							
26X-CC, 0	241.08	272.53	PAL	S	T	P																							
27X-CC, 30	251.00	280.89	PAL	S	T	P																							
27X-CC, 30	251.00	280.89	PAL	S	F	P																							

Notes: PAL = paleontology sample. S = smear slide. Abundance: C = common, F = few, R = rare, T = trace. Preservation: G = good, M = moderate, P = poor.

**Table T14.** Headspace gas concentrations and C<sub>1</sub>/C<sub>2</sub> ratio in sediments, Hole 1242A.

Core, section, interval (cm)	Depth (mbsf) (mcd)		C <sub>1</sub> (ppmv)	C <sub>2</sub> (ppmv)	C <sub>1</sub> /C <sub>2</sub>	C <sub>2</sub> = (ppmv)	C <sub>3</sub> (ppmv)
<b>202-1242A-</b>							
1H-2, 0-5	1.50	1.50	3	0.0		0.0	0.0
2H-4, 0-5	11.22	12.62	25	0.0		0.0	0.0
3H-4, 0-5	20.73	23.43	20,036	1.4	14,311	0.0	0.0
4H-4, 0-5	30.23	34.48	75,083	3.5	21,452	0.0	0.0
5H-4, 0-5	39.72	44.02	60,272	3.3	18,264	0.0	0.6
6H-4, 0-5	49.22	54.02	101,288	5.4	18,757	0.0	4.8
7H-2, 0-5	55.71	60.86	45,113	3.3	13,670	0.0	3.0
8H-2, 0-5	65.20	71.65	28,176	2.2	12,807	0.0	0.0
9H-2, 0-5	74.70	80.55	40,841	3.6	11,345	0.0	4.7
10H-2, 0-5	84.20	90.65	43,555	4.5	9,679	0.5	6.0
11H-2, 0-5	93.72	101.37	60,409	6.6	9,153	0.0	11.2
12H-2, 0-5	103.22	111.40	61,285	7.0	8,755	0.0	11.5
13H-2, 0-5	112.71	121.94	32,850	4.8	6,844	0.3	7.7
14H-2, 0-5	122.21	132.69	42,361	6.6	6,418	0.0	12.8
15H-2, 0-5	131.70	143.28	29,770	5.4	5,513	0.4	10.5
16H-2, 0-5	141.20	155.68	32,356	6.8	4,758	0.0	14.9
17H-2, 0-5	150.70	166.53	39,807	10.4	3,828	0.8	24.8
18H-2, 0-5	160.20	178.23	31,554	9.2	3,430	1.0	25.5
19H-3, 0-5	171.21	191.59	6,735	3.4	1,981	0.9	12.3
20X-4, 0-5	180.48	200.86	17,926	7.7	2,328	0.8	31.1
22X-4, 0-5	198.11	222.39	48,990	14.0	3,499	0.7	42.1
23X-4, 0-5	207.81	232.49	26,033	10.4	2,503	0.8	43.7
24X-2, 0-5	214.10	241.63	34,753	13.4	2,593	1.0	53.2
25X-4, 0-5	226.80	255.23	18,659	8.1	2,303	0.6	27.3
26X-4, 0-5	236.11	267.54	15,399	6.7	2,298	0.4	19.3
27X-4, 0-5	245.70	275.58	18,671	8.4	2,223	0.0	19.4

**Table T15.** Interstitial water geochemical data, Hole 1242A.

Core, section, interval (cm)	Depth		Alkalinity (mM)	Salinity	Cl <sup>-</sup> (mM)	Na <sup>+</sup> (mM)	SO <sub>4</sub> <sup>2-</sup> (mM)	HPO <sub>4</sub> <sup>2-</sup> (μM)	NH <sub>4</sub> <sup>+</sup> (mM)	H <sub>4</sub> SiO <sub>4</sub> (μM)	Mn <sup>2+</sup> (μM)	Fe <sup>2+</sup> (μM)	Ca <sup>2+</sup> (mM)	Mg <sup>2+</sup> (mM)	B (μM)	Sr <sup>2+</sup> (μM)	Ba <sup>2+</sup> (μM)	Li <sup>+</sup> (μM)	K <sup>+</sup> (mM)	
	(mbsf)	(mcd)																		
202-1242A-																				
1H-1, 145–150	1.45	1.45	7.69	3.9	35.0	552	478	27.6	10	BDL	468	5.8	0.3	9.9	50.7	529	85	BDL	23	12.0
2H-3, 145–150	11.17	12.57	7.91	11.5	34.0	554	479	19.4	23	0.65	653	1.4	0.8	8.4	48.7	536	84	5	21	11.8
3H-3, 145–150	20.67	23.37	7.92	27.1	33.0	559	488	0.7	34	2.63	696	0.7	1.1	3.0	40.4	598	94	52	22	12.4
4H-3, 145–150	30.18	34.43	7.46	25.7	33.0	559	493	BDL	60	4.26	783	0.6	1.5	2.5	36.8	570	109	196	24	13.5
5H-3, 145–150	39.67	43.97	7.52	26.2	33.0	557	492	BDL	53	5.11	810	1.4	2.5	2.8	35.8	523	124	244	34	14.0
6H-3, 145–150	49.17	53.97	7.54	27.7	33.0	559	492	BDL	47	5.73	897	1.4	7.4	3.2	37.0	544	136	271	42	14.3
7H-3, 145–150	58.67	63.82	7.52	27.7	33.0	560	493	BDL	39	6.26	908	1.4	4.0	3.7	36.2	538	143	283	47	15.0
8H-3, 145–150	68.15	74.60	7.34	28.1	34.0	559	494	BDL	35	6.86	897	1.5	8.6	4.1	35.0	529	151	296	57	14.9
9H-3, 145–150	77.65	83.50	7.34	26.8	32.0	549	484	BDL	31	7.13	1011	1.4	14.9	4.4	34.6	544	160	310	65	14.2
10H-3, 145–150	87.15	93.60	7.20	25.7	33.0	559	491	BDL	21	7.88	946	1.3	16.6	4.8	34.2	540	175	338	82	15.8
11H-3, 145–150	96.67	104.32	7.08	22.7	33.0	559	486	BDL	22	7.73	1136	1.1	19.3	5.5	34.6	531	185	312	92	15.3
13H-3, 145–150	115.66	124.89	8.04	20.7	32.0	554	481	BDL	14	7.90	1136	1.5	8.0	6.9	32.5	519	199	290	118	15.3
15H-3, 145–150	134.66	146.24	7.68	16.9	33.0	562	482	BDL	6	8.07	968	1.3	10.5	8.5	31.9	448	255	563	167	15.8
17H-3, 145–150	153.65	169.48	7.35	11.5	32.0	563	473	BDL	3	7.92	919	1.4	12.4	11.8	31.2	426	298	707	239	15.9
19H-2, 145–150	171.16	191.54	6.88	12.5	32.0	564	468	BDL	2	7.35	1321	3.3	64.2	17.6	29.7	531	378	872	310	14.4
21X-3, 145–150	188.45	210.13	6.95	9.9	33.0	559	449	1.4	2	6.70	1376	4.5	110.9	23.5	30.7	525	373	151	310	14.5
23X-3, 140–150	207.71	232.39	6.83	7.2	33.0	559	435	3.2	2	5.80	1240	10.6	115.5	31.7	30.7	470	390	65	283	13.3
25X-3, 140–150	226.70	255.13	6.85	5.5	33.0	564	404	2.1	BDL	4.99	1327	14.3	131.9	51.6	27.3	439	488	96	276	12.1
27X-3, 140–150	245.60	275.48	6.69	3.3	34.0	564	363	3.3	BDL	3.73	1408	12.6	78.3	76.6	23.9	351	466	88	191	9.6

Note: BDL = below detection limit (SO<sub>4</sub><sup>2-</sup> = 0.6 mM, HPO<sub>4</sub><sup>2-</sup> = 1 μM, NH<sub>4</sub><sup>+</sup> = 0.42 mM, Ba<sup>2+</sup> = 0.1 μM).

**Table T16.** Inorganic carbon, calcium carbonate, total carbon, total organic carbon, and total nitrogen concentrations, and TOC/TN ratio in sediments, Hole 1242A. ([See table note](#). Continued on next page.)

Core, section, interval (cm)	Depth		IC (wt%)	CaCO <sub>3</sub> (wt%)	TC (wt%)	TOC (wt%)	TN (wt%)	TOC/TN (atomic)
	(mbsf)	(mcd)						
<b>202-1242A-</b>								
1H-2, 74-75	2.24	2.24	1.97	16.4	5.43	3.46	0.38	7.90
1H-4, 74-75	5.25	5.25	1.29	10.7	3.90	2.61	0.27	8.43
2H-2, 74-75	8.95	10.35	0.69	5.7	2.88	2.19	0.23	8.08
2H-4, 74-75	11.96	13.36	1.11	9.2	3.27	2.16	0.23	8.23
2H-6, 74-75	14.97	16.37	1.24	10.3				
3H-2, 74-75	18.45	21.15	2.00	16.7	4.29	2.29	0.23	8.47
3H-4, 74-75	21.47	24.17	0.86	7.1	2.67	1.81	0.20	7.84
3H-6, 74-75	24.50	27.20	1.25	10.4				
4H-2, 74-75	27.95	32.20	2.24	18.6	4.06	1.82	0.19	8.13
4H-4, 74-75	30.97	35.22	2.12	17.6	4.44	2.32	0.23	8.76
4H-6, 74-75	33.98	38.23	2.31	19.3				
5H-2, 74-75	37.45	41.75	3.41	28.4	4.74	1.33	0.15	7.42
5H-4, 74-75	40.46	44.76	1.63	13.5	3.20	1.57	0.17	7.76
5H-6, 74-75	43.47	47.77	1.69	14.1				
6H-2, 74-75	46.95	51.75	3.38	28.1	5.47	2.09	0.24	7.48
6H-6, 74-75	52.97	57.77	1.92	16.0				
7H-2, 74-75	56.45	61.60	2.65	22.1	4.24	1.59	0.18	7.55
7H-4, 74-75	59.46	64.61	1.54	12.8	2.88	1.34	0.16	7.02
7H-6, 74-75	62.47	67.62	1.99	16.6				
8H-4, 74-75	68.93	75.38	2.37	19.7	3.98	1.61	0.18	7.73
8H-6, 74-75	71.93	78.38	2.63	21.9				
9H-2, 74-75	75.44	81.29	2.23	18.6	3.83	1.60	0.19	7.18
9H-4, 74-75	78.44	84.29	2.54	21.1	4.03	1.49	0.18	7.29
9H-6, 74-75	81.44	87.29	3.96	33.0				
10H-2, 74-75	84.94	91.39	1.89	15.8	3.11	1.22	0.18	5.85
10H-4, 74-75	87.94	94.39	2.37	19.7	3.78	1.41	0.17	7.29
10H-6, 74-75	90.96	97.41	2.33	19.4				
11H-1, 74-75	92.94	100.59	2.26	18.8				
11H-3, 74-75	95.96	103.61	3.34	27.8	4.37	1.03	0.17	5.21
11H-5, 74-75	98.97	106.62	3.73	31.0				
12H-2, 74-75	103.96	112.14	2.06	17.1	3.42	1.36	0.19	6.32
12H-4, 74-75	106.97	115.15	2.96	24.6				
12H-6, 74-75	109.99	118.17	1.95	16.3				
13H-2, 74-75	113.45	122.68	2.49	20.7	3.51	1.02	0.18	4.87
13H-4, 74-75	116.45	125.68	1.79	14.9				
13H-6, 74-75	119.45	128.68	2.20	18.3				
14H-2, 74-75	122.95	133.43	3.16	26.4	4.55	1.39	0.19	6.15
14H-4, 74-75	125.97	136.45	2.57	21.4				
14H-6, 74-75	128.99	139.47	3.39	28.3				
15H-2, 74-75	132.44	144.02	2.69	22.4	4.16	1.47	0.18	7.16
15H-4, 74-75	135.45	147.03	3.23	26.9				
15H-6, 74-75	138.47	150.05	2.61	21.7				
16H-2, 74-75	141.94	156.42	3.68	30.7	5.00	1.32	0.16	7.06
16H-4, 74-75	144.94	159.42	2.40	20.0				
16H-6, 74-75	147.95	162.43	3.06	25.5				
17H-2, 74-75	151.44	167.27	2.92	24.3	4.02	1.10	0.18	5.23
17H-4, 74-75	154.44	170.27	2.27	18.9				
17H-6, 74-75	157.44	173.27	3.39	28.2				
18H-2, 74-75	160.94	178.97	3.39	28.3	4.97	1.58	0.18	7.64
18H-4, 74-75	163.96	181.99	1.71	14.2				
18H-6, 74-75	166.97	185.00	3.08	25.7				
19H-2, 74-75	170.45	190.83	3.25	27.1	4.44	1.19	0.14	7.07
19H-4, 74-75	172.60	192.98	3.23	26.9				
19H-6, 74-75	175.62	196.00	3.53	29.4				
20X-2, 74-75	178.22	198.60	3.59	29.9	4.48	0.89	0.13	5.85
20X-4, 74-75	181.22	201.60	3.11	25.9				
21X-2, 74-75	186.24	207.92	3.87	32.3	5.34	1.47	0.16	7.96
21X-4, 74-75	189.24	210.92	4.29	35.8				
21X-6, 74-75	192.23	213.91	3.68	30.7				
22X-2, 74-75	195.85	220.13	3.54	29.5	4.87	1.33	0.15	7.65
22X-4, 74-75	198.85	223.13	3.34	27.8				
22X-6, 74-75	201.85	226.13	3.66	30.5				
23X-2, 74-75	205.55	230.23	2.83	23.6	4.05	1.22	0.15	6.85
23X-4, 74-75	208.55	233.23	4.38	36.5				

**Table T16 (continued).**

Core, section, interval (cm)	Depth		IC (wt%)	CaCO <sub>3</sub> (wt%)	TC (wt%)	TOC (wt%)	TN (wt%)	TOC/TN (atomic)
	(mbsf)	(mcd)						
23X-6, 74-75	211.55	236.23	4.44	37.0				
24X-2, 74-75	214.84	242.37	3.42	28.5	4.78	1.36	0.15	7.89
24X-4, 74-75	217.84	245.37	2.44	20.4				
24X-6, 74-75	220.85	248.38	2.30	19.1				
25X-2, 74-75	224.54	252.97	4.24	35.3				
25X-4, 74-75	227.54	255.97	4.69	39.1				
25X-6, 74-75	230.54	258.97	4.15	34.5				
26X-2, 74-75	233.84	265.27	5.58	46.5				
26X-4, 74-75	236.85	268.28	6.15	51.2				
26X-6, 74-75	239.85	271.28	5.55	46.2				
27X-2, 74-75	243.44	273.32	5.09	42.4				
27X-4, 74-75	246.44	276.32	4.89	40.7				
27X-6, 74-75	249.44	279.32	4.28	35.7				

Note: IC = inorganic carbon, TC = total carbon, TOC = total organic carbon, TN = total nitrogen.

**Table T17.** Age-depth model, linear sedimentation rates, and mass accumulation rates, Site 1242.

Age (Ma)	Depth (mcd)	LSR (mcd/m.y.)	mcd growth factor	Corrected LSR (m/m.y.)	Dry density (g/cm <sup>3</sup> )	CaCO <sub>3</sub> average concentration (wt%)	TOC average concentration (wt%)	Total MAR (g/cm <sup>2</sup> /k.y.)	CaCO <sub>3</sub> MAR (g/cm <sup>2</sup> /k.y.)	TOC MAR (g/cm <sup>2</sup> /k.y.)	Noncarbonate MAR (g/cm <sup>2</sup> /k.y.)
0.0	0.0										
0.4	42.4	106	1.13	94	0.66	14.2	1.67	6.2	0.9	0.103	5.3
0.8	95.8	133	1.13	118	0.74	19.5	0.99	8.7	1.7	0.087	7.0
1.2	149.2	134	1.13	118	0.76	22.3	0.42	9.0	2.0	0.037	7.0
1.6	223.2	185	1.13	164	0.82	26.6	0.44	13.4	3.6	0.060	9.9
2.0	260.4	93	1.13	82	0.89	30.4	0.26	7.3	2.2	0.019	5.1
2.4	278.4	45	1.13	40	0.93	45.4	0.00	3.7	1.7	0.000	2.0

Notes: LSR = linear sedimentation rate, MAR = mass accumulation rate. TOC = total organic carbon. This table is also available in [ASCII](#).